2019-07-27

Proceedings of the 4th Rocky Mountain Muscle Symposium

Joumaa, Venus

rMMs - 2019

4th Rocky Mountain Muscle Symposium

Canmore Nordic Centre, Alberta, Canada
July 27 - 29, 2019

Acknowledgements

We would like to acknowledge the following for their generous contributions to the muscle symposium

UNIVERSITY OF CALGARY
FACULTY OF KINESIOLOGY

UNIVERSITY OF CALGARY
Biomedical Engineering

UNIVERSITY OF CALGARY
Office of the Vice-President (Research)

aurora
SCIENTIFIC

Performance.
Precision.
Progress.

www.AuroraScientific.com

Welcome to Canmore

The symposium on skeletal muscles in Canmore is the fourth Rocky Mountain Symposium of its kind. The first was held in 1999 in Canmore, the second and third in 2002 and 2006 in Banff. The goal of this fourth symposium is the same as that of the previous meetings: we would like to promote a scientific exchange of ideas on the highest level in a small setting with ample time for discussion and informal interaction. The opportunity presented itself to meet just prior to the ISB/ASB conference 2019 (July 31 – August 4, 2019) in Calgary, so you can combine your travels.

Scientifically, skeletal muscle contraction and function will be addressed at all structural levels, varying from single actin-myosin interactions to the function and control of muscles during voluntary contractions in humans. This program will require some tolerance, as biophysicists working on the molecular level have a different view of muscles than physiologists working on the single fibre level, or biomechanists working in a clinical rehabilitation setting with human patients. Nevertheless, the success of the first three symposia instills confidence that there is a desire, and maybe even a need, to discuss muscle contraction and function at all scales and all structural levels.

Socially, the Canmore Nordic Centre is a fantastic and unique facility for small scale symposia. Built for the 1988 Winter Olympics and set in a Provincial Park just at the eastern edge of the Rocky Mountains, it is a destination for thousands of tourists each year and hosts world-class competitions for cross-country skiing, biathlon and Nordic combined. In the summer, you can enjoy, hiking, mountain biking and Frisbee Golf – a perfect location to discuss and use muscles!

The preliminary program shows that we have organized sessions in such a way that you can enjoy the outdoors each day and socialize in an informal way.

We have tried very hard to make this 4th Rocky Mountain Muscle Symposium an unforgettable scientific and social experience. We hope that you take the opportunity to present, discuss, interact, and explore in the scientific sessions, and that you will make new friendships and renew old ones.

Walter Herzog
Scientific Organizer and Program Chair
4th Rocky Mountain Muscle Symposium

Maps
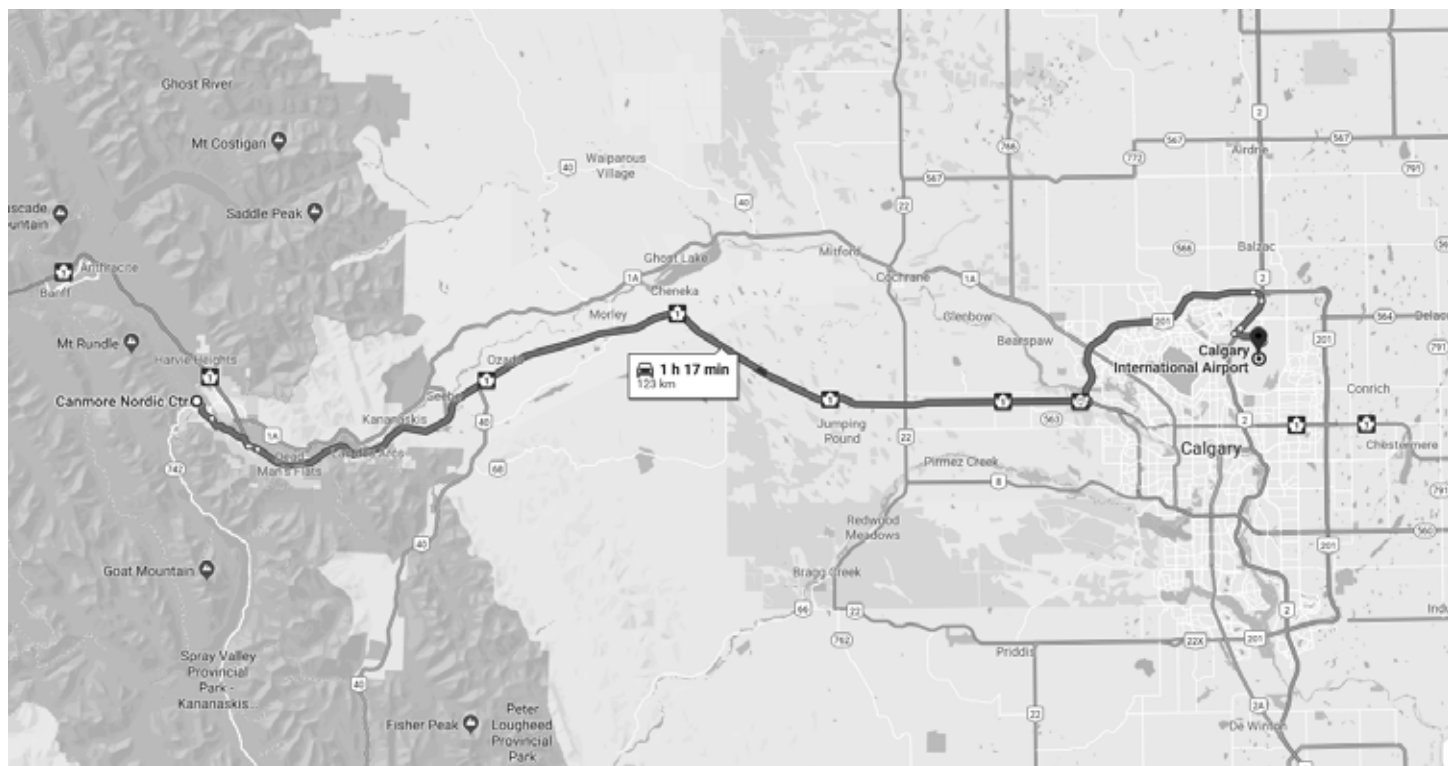
Muscle Symposium - Program		
Saturday, July 27		
14:00 - 14:30	Registration Pre-function Area 14:00 - 20:00	Disc Golf at Canmore Nordic Centre / Free Time
14:30 - 15:00		
15:00 - 15:30		
15:30 - 16:00		
16:00 - 16:30		
16:30 - 17:00		
17:00 - 17:30		Welcome Reception - Pre-Function Area
17:30 - 18:00		Keynote Lecture 1 - Rick Lieber: The mystery of human skeletal muscle contracture
18:00 - 18:30		
18:30 - 19:00		Social - Pre-Function Area
19:00 - 19:30		
19:30 - 20:00		
20:00 - 20:30	Shuttle bus leaves at 20:00 return Canmore loop	
20:30 - 21:00		

rMMs

			Muscle Symposium - Program
			Sunday, July 28
8:00 - 8:24			8:00-8:24 Coffee - Prefunction Area
8:24 - 8:48	Molecular Muscle Mechanics / Physiology Banquet Room	Invited 1	*Venus Joumaa:* **Towards a better understanding of muscle contraction**
8:48 - 9:00		Oral 1.1	*Anthony Hessel:* X-ray diffraction analysis before and after active and passive stretch in skinned muscle fiber bundles from wild type and mdm mice
9:00 - 9:12		Oral 1.2	*Kiisa Nishikawa:* Calcium-dependent titin – thin filament interactions in muscle: observations and theory
9:12 - 9:24		Oral 1.3	*Matthew Millard:* A three filament muscle model based on a titin-myosin interaction
9:24 - 9:36		Oral 1.4	*Seong-won Han:* Residual force enhancement in cardiac myofibrils on the ascending limb of the force-length relationship
9:36 - 9:48		Oral 1.5	*Kaylyn Bell:* The muscle mechanical basis of Freeman-Sheldon Syndrome
9:48 - 10:00		Oral 1.6	*Tim Leonard:* Adductor longus myofibrillar passive stiffness is reduced in cerebral palsy
10:00 - 10:30			**Coffee Break with Snacks - Prefunction Area**
10:30 - 11:30			**Keynote Lecture 2 - Motoshi Kaya: Reverse stroke of cardiac myosin is essential for heart function: lessons from skeletal myosin**
11:30 - 11:42	Cellular Muscle Mechanics / Physiology Banquet Room	Oral 2.1	*David Corr:* History-dependent behaviour in drosophila jump muscle: do myosin kinetics influence force-depression?
11:42 - 11:54		Oral 2.2	*Douglas Swank:* A myosin based mechanism for stretch activation and its possible purpose revealed by varying phosphate concentration in mammalian skeletal muscle fibers
11:54 - 12:06		Oral 2.3	*Marlies Corvelyn:* Skeletal muscle stem cell properties from young children with cerebral palsy
12:06 - 12:18		Oral 2.4	*Ridhi Sahani:* Collagen preferred direction relative to muscle fiber direction in three and six-month-old Mdx mice
12:18 - 12:30		Oral 2.5	*Nicole Mazara:* The effect of Ca2+ on rate of force redevelopment of single muscle fibres in young and older adults
12:30 - 12:42		Oral 2.6	*Eng Kuan Moo:* The influence of muscle architecture on sarcomere force-length relationship in intact muscle
12:42 - 14:00			**Lunch - Meeting Room B, some reserved seating/tables downstairs in main space or enjoy outdoors**
14:00 - 14:30 / 14:30 - 15:00			**Keynote Lecture 3 - Henk Granzier, Titin determines passive stiffness and the sarcomere length working range of skeletal muscle**
15:00 - 15:30 / 15:30 - 16:00 / 16:00 - 16:30			**15:00 - 16:30 Poster Session 1** **Meeting Room B**
16:30 - 17:00 / 17:00 - 17:30 / 17:30 - 18:00 / 18:00 - 18:30 / 18:30 - 19:00			**Grassi Lakes Hike** **Shuttle bus to trail head leaves at 16:45** **Pick up after hike at 19:00 to return Canmore loop**
19:00 - 19:30 / 19:30 - 20:00 / 20:00 - 20:30 / 20:30 - 21:00	**Dinner for Keynote Presenters (downtown Canmore)**		**Dinner on your own**

Poster Session 1	Poster 1.1	*Matthew Millard:* Is titin actively preloaded?
	Poster 1.2	*Ashley Oldshue:* Modeling muscle cross-bridge dynamics for movement simulations
	Poster 1.3	*Amy Adkins:* The paretic biceps brachii contains fewer sarcomeres in series than the contralateral biceps brachii following stroke
	Poster 1.4	*Amy Loya:* Characterizing shortening deactivation in drosophila and lethocerus muscle types
	Poster 1.5	*Kevin Boldt:* Residual and passive force enhancement in skinned cardiac fibre bundles
	Poster 1.6	*Kaat Desloovere:* Are pre-treatment assessments of muscle morphology related to the effects of treatment with Botulinum NeuroToxin-A and lower leg casting in children with cerebral palsy?
	Poster 1.7	*Atsuki Fukutani:* Effect of stretch-shortening cycle is prominent in the reduced force condition
	Poster 1.8	*Giovanni Martino:* Simulating the pendulum test to understand mechanisms of Parkinsonian rigidity
	Poster 1.9	*Nathalie De Beukelaer:* Relationship between spasticity phenotypes and muscle morphology is different in children with spastic cerebral palsy and children with hereditary spastic paraplegia
	Poster 1.10	*Brian Horslen:* Acto-myosin cross-bridge stretch mechanics underlie history-dependent changes in muscle spindle sensory feedback: a multi-scale experimental and simulation study
	Poster 1.11	*Anouk Agten:* Muscle fibre type characteristics of the lumbar multifidus and erector spinae in persons with non-specific chronic low back pain and healthy controls
	Poster 1.12	*Domiziana Costamagna:* IL4 counteracts cancer-induced skeletal muscle atrophy: one cytokine for multiple effects

6

rMMs

4th Rocky Mountain Muscle Symposium - Canmore Nordic Centre - July 27-29, 2019

			Monday, July 29
8:00 - 8:24			8:00-8:24 Coffee - Prefunction Area
8:24 - 8:48	In vivo Animal Muscle Function Banquet Room	Invited 2	*Sabrina Lee:* **Musculoskeletal changes and adaptions - from aging to pathology in humans**
8:48 - 9:00		Oral 3.1	*Marie Janneke Schwaner:* Muscle dynamics of the vastus lateralis in jumping kangaroo rats (D. deserti)
9:00 - 9:12		Oral 3.2	*Emily Abbott:* Examining in situ changes to muscle spindle signals with increased muscle-tendon compliance
9:12 - 9:24		Oral 3.3	*Benjamin Binder-Markey:* Intramuscular Anatomy drives muscle collagen content variation, likely impacting passive muscle stiffness
9:24 - 9:36		Oral 3.4	*Tobias Siebert:* Uniaxial transverse loading decreases muscle force
9:36 - 9:48		Oral 3.5	*David Lin:* How do the contractile properties of individual muscles within a synergistic group combine?
9:48 - 10:00		Oral 3.6	*Heiliane de Brito Fontana:* Loss in agonistic muscle torque during simultaneous (submaximal) activation
10:00 - 10:30			**Coffee Break - Meeting Room B**
10:30 - 11:30			**Keynote Lecture 4 - Monica Daley: In vivo muscle dynamics in steady and non-steady bipedal locomotion in guinea fowl**
11:30 - 11:42	In vivo Human Muscle Function Banquet Room	Oral 4.1	*Daniel Hahn:* History dependence of in vivo muscle force production: the role of muscle-tendon unit compliance
11:42 - 11:54		Oral 4.2	*Amy Adkins:* Quantifying in vivo variability in sarcomere length along the length of the long head of the biceps brachii
11:54 - 12:06		Oral 4.3	*Pavlos Evangelidis:* Fatigue-induced changes in hamstrings shear modulus and load distribution depend on contraction type
12:06 - 12:18		Oral 4.4	*Katherine Knaus:* 3D representation of complex soleus aponeurosis geometry and muscle fiber architecture based on magnetic resonance imaging and Laplacian flow simulation
12:18 - 12:30		Oral 4.5	*Ian Smith:* Summation properties are improved by a preceding contraction and intervening rest period
12:30 - 12:42		Oral 4.6	*Kaat Desloovere:* Macroscopic morphological muscle properties to feature spasticity phenotypes in children with cerebral palsy
12:42 - 14:00			**Lunch - Meeting Room B, some reserved seating/tables downstairs in main space or enjoy outdoors**
14:00 - 14:30 / 14:30 - 15:00			**Keynote Lecture 5 - Yasuo Kawakami: Muscle-tendon-fascia system as a fibre-reinforced entity of actuators and springs: *in vivo* and *ex situ* evidence**
15:00 - 15:30 / 15:30 - 16:00			**15:00 - 16:30 Poster Session 2**
16:00 - 16:30			**Meeting Room B**
16:30 - 17:00 / 17:00 - 17:30 / 17:30 - 18:00 / 18:00 - 18:30 / 18:30 - 19:00			**Mountain Biking at Canmore Nordic Centre / Free Time**
19:00 - 19:30			**Social - Prefunction Area**
19:30 - 20:00 / 20:00 - 20:30 / 20:30 - 21:00			**Banquet Dinner - Banquet Room** / **Shuttle bus leaves at 21:00 return Canmore loop**

Poster Session 2	Poster 2.1	*Emma Hodson-Tole:* Ultrasound Derived in vivo Measures of Skeletal Muscle Vibration during Locomotion in Humans
	Poster 2.2	*Liliam Oliveira:* Shear modulus of the resting agonist/antagonist muscles
	Poster 2.3	*Hoshizora Ichinose:* Contractile and non-contractile tissues in the midthigh of the elderly and younger athletes: Inter-individual differences and relationships with body composition and muscle function
	Poster 2.4	*Neale Tillin:* The influence of residual force depression on torque during shortening contractions without - relative to with - pre-load
	Poster 2.5	*Brent Raiteri:* Eccentric hamstring fascicle behavior occurs during the Nordic hamstring exercise
	Poster 2.6	*Wolfgang Seiberl:* Electrically versus voluntarily activated stretch-contractions: is there a true non-responder?
	Poster 2.7	*Marco Vaz:* Influence of NMES frequency and waveform on torque production, stimulation efficiency and discomfort in healthy subjects
	Poster 2.8	*Carlos Cruz-Montecinos:* Adaptations in intermuscular coordination of the triceps surae muscles in people with haemophilic arthropathy
	Poster 2.9	*Robert Griffiths:* Muscular and non-muscular contraction in the mammalian diaphragm
	Poster 2.10	*Brian MacIntosh:* Force-frequency relationship during fatiguing contractions of rat medial gastrognemius muscle
	Poster 2.11	*Jaqueline Lourdes Rios:* Protective effect of moderate exercise and prebiotic fibre supplementation on vastus lateralis muscle in a rat model of obesity
	Poster 2.12	*Fransiska Bossuyt:* Supraspinatus tendon changes with repetitive wheelchair propulsion are associated with fatigue, sex, and body weight

7

4th Rocky Mountain Muscle Symposium - Canmore Nordic Centre - July 27-29, 2019

rMMs

Instructions for Presenters

Oral Presentations:

- Oral presentations are assigned a 12-minute time slot (divided into a 1-minute introduction, an **8-minute presentation**, and 3 minutes for questions)
    - o The 8-minute **presentation length** will be **strictly enforced**, so we ask that you please stay within your allotted time.
- The exact date and time for your presentation is in the schedule on pages 5-7 and the event website.
- We have a speaker ready area in the foyer / pre-function area at the symposium where speakers **must** upload their presenations from a USB **on the day before** their presentation. As an alternative you can email your presentation and ancillary files p to 24 h ahead. A link has been provided via email to all delegates.

Poster Presentations:

- Posters must be **no more than 0.9 m wide (3') and 1.1 m high (3' 7")**
- Poster sessions will be held July on 28 and 29 from 15:00 to 16:30
    - o The exact date and poster number for your specific poster is in the schedule on pages 5-7 and the event website.
- Pins will be provided for attaching posters to the boards.
- Posters may be **mounted between 12:45 and 14:00** (during lunch break) on the day of your session. Please **remove** your poster **promptly after** the session.

Keynote and Invited Speakers

Monica Daley

Henk Granzier

Venus Joumaa

Yasuo Kawakami

Motoshi Kaya

Sabrina Lee

Rick Lieber

rMMs

MONIKA DALEY

Monica Daley is a Reader in Locomotor Biomechanics in the Comparative Biomedical Sciences department at the Royal Veterinary College (RVC) in London, UK. Daley trained in Biology (HBSc) at the University of Utah, and earned her PhD at Harvard University, supported by a Predoctoral Fellowship from the Howard Hughes Medical Institute. Daley's PhD research developed novel approaches to investigate in vivo muscle-tendon dynamics and sensorimotor control of locomotion, using ground birds as a bipedal animal model. Daley was awarded a Postdoctoral Fellowship by the U.S. National Science Foundation to develop neuromechanical models of bipedal locomotion with Dan Ferris at the University of Michigan. Daley joined the RVC in 2008, where her team investigates neuromuscular function from an integrative perspective, with a particular focus on how intrinsic mechanical properties of muscle are integrated with neural control to meet the rapidly changing mechanical demands of non-steady locomotion. Daley serves on the Scientific Board of the conferences Dynamic Walking and Adaptive Motion in Animals and Machines, and the Editorial Boards of the Journal of Experimental Biology, Royal Society Open Science and Physiological and Biochemical Zoology. Daley is a co-founding member of the Comparative Neuromuscular Biomechanics 'seed group' of the International Society for Biomechanics, which aims to increase collaboration and dialogue among researchers in human and comparative animal biomechanics.

HENK GRANZIER

Henk Granzier holds a Ph.D. in Bioengineering from the University of Washington and did postdoctoral research in Biochemistry at the University of Texas at Austin. In 1993 he joined the faculty at Washington State University where he rose through the ranks to become Full Professor in 2002. He was a Helmholtz-Humboldt visiting Professor at Max Delbrück Center for Molecular Medicine in Berlin, Germany in 2006. In 2007 he moved to the University of Arizona (Tucson) where he is a Professor of Cellular and Molecular Medicine, Physiology and Bioengineering. He also holds the Norville Endowed chair for heart disease research. His laboratory is focused on defining the roles of titin and nebulin in muscle function and disease. The research is multi-disciplinary and ranges from the single molecule, single cell, isolated muscle, and whole animal levels. Highlights include the discovery that titin's I-band region functions as a molecular spring that can be tuned through post-transcriptional and post-translational mechanism. Furthermore, the work on nebulin has shown that nebulin affects stiffness in the thin filament and is critically important in regulating force of skeletal muscle via its effect on thin filament length and actomyosin interaction. Granzier has a long record of creative and rigorous research.

VENUS JOUMAA

Venus Joumaa is an Adjunct Assistant Professor in the Faculty of Kinesiology at the University of Calgary since 2009. She received her PhD in Biomechanics and Biomedical Engineering from the University of Technology of Compiegne, France in 2005 and has become an expert in single muscle fibre research. Currently, Dr. Joumaa's research focuses on understanding the role of titin in active force regulation and to potentially use this knowledge for diagnostic and treatment purposes. Dr. Joumaa regularly teaches classes in biomechanics, human physiology, and biomedical engineering and supervises and mentors undergraduate, summer, visiting and graduate students in the Human Performance Laboratory. She is a reviewer for Royal Society Open Science and Acta Physiologica and a member of CSB, ASB, ISB, APS and the Biophysical Society.

YASUO KAWAKAMI

Yasuo Kawakami is a professor of biodynamics, Faculty of Sport Sciences, Waseda University, Japan. He received Bachelor of Education, Master of Science, and Ph.D. from the University of Tokyo (1988-1995). After his career as an assistant professor, University of Tokyo, 1991-1999, associate professor, University of Tokyo, 1999-2003, and associate professor, Waseda University, School of Sport Sciences, 2003-2005, he is a professor of Waseda University. His expertise is in biomechanics and exercise physiology with the main research interest in the area of muscle mechanics, particularly on the in vivo skeletal muscle behavior during various human movements. Effects of exercise training, growth, aging, and fatigue on the human musculoskeletal system are also in the scope of his research. He has published more than 200 articles in international journals (>6500 citations, h-index=44 as of February 2019). He has been a member of the societies and organizations including International Society of Biomechanics, Japanese Society of Biomechanics, Japanese Society of Physical Fitness and Sports Medicine, Tokyo Society of Physical Education, Health and Sport Science, Japan Society of Training Science for Exercise and Sport, the Japanese Society of Bone and Muscle Ultrasound, Japan Society of Golf Sciences, and Science Council of Japan. He is a director of Human Performance Laboratory, Organization for University Research Initiatives, Waseda University (https://www.waseda.jp/prj-hpl/eng/).

MOTOSHI KAYA

Motoshi Kaya is an Assistant Professor in the Department of Physics at the University of Tokyo and a PRESTO Research Fellow at the Japan Science and Technology Agency. He received his PhD in Mechanical Engineering from the University of Calgary, Canada. His research program investigates how myosin molecules interact with actin filaments during muscle contraction. One of his group's primary goals is to understand how myosin force generation contributes to efficiency of muscle contraction. They address mechanistic questions by combining optical laser trapping with high spatiotemporal resolution microscopy, for the measurement of single molecule myosin interactions with actin. This enables them to reveal unique mechanical properties of skeletal and cardiac muscle myosin molecules. Kaya's group has applied this technology to quantify the nonlinear elasticity of myosin molecules, which dramatically reduces intermolecular friction when multiple myosin molecules interact to slide an actin filament (Science 329, 2010; Biophysics 51, 2011; Cell Mol Life Sci 70, 2013)). More recently, they showed that high mechanical loads on myosin filaments result in coordinated force generation among myosin molecules within the filament (Nature Comm 8, 2017).

SABRINA LEE

Sabrina Lee is an assistant professor in the Department of Physical Therapy and Human Movement Sciences (PTHMS) at Northwestern University in the Feinberg School of Medicine. She trained in Physiology (BSc) at McGill University and Kinesiology (PhD) at Pennsylvania State University. Her doctoral research focused on developing ultrasound methods to investigate changes in ankle and muscle architecture in sprinters. Her postdoctoral work with James Wakeling (Simon Fraser University) and Andrew Biewener (Harvard University) involved developing muscle models with independent components of slow and fast muscle fibers based on experimental measures of goat locomotion. She was awarded a Postdoctoral Fellowship by the National Institute on Disability and Rehabilitation Research to investigate muscle material properties of individuals post-stroke with Zev Rymer at the Rehabilitation Institute of Chicago. She joined PTHMS at Northwestern University in 2014, where her research is focused on investigating the underlying mechanisms that contribute to impaired movement in individuals with decreased mobility such as older adults and those with neurological impairments such as stroke, cerebral palsy, or spinal cord injury. Specifically, she is interested in changes in musculoskeletal architecture, muscle material properties and composition, as well as recruitment patterns of different motor unit types. Knowing the influence of these changes on impaired movement forms the basis for proposing clinical tools used to aid in diagnosing and assessment and for developing novel interventions for rehabilitation.

RICK LIEBER

Rick Lieber is a scientist who earned his Ph.D. in Biophysics from U.C. Davis developing a theory of light diffraction that was applied to mechanical studies of single muscle cells. He joined the faculty at the University of California, San Diego in 1985 where he spent the first 30 years of his academic career, achieving the rank of Professor and Vice-Chair of the Department of Orthopaedic Surgery. He received his M.B.A. in 2013 and is currently Chief Scientific Officer and Senior Vice President at the Shirley Ryan AbilityLab and Professor of Physical Medicine & Rehabilitation at Northwestern University in Chicago, IL.

Dr. Lieber's work represents a translational approach, applying basic scientific principles to help patients who have experienced spinal cord injury, stroke, musculoskeletal trauma and cerebral palsy. —an approach that is relevant to those who study biomechanics, rehabilitation and orthopaedic surgery. He has published almost 300 articles in journals ranging from the very basic such as The Biophysical Journal and The Journal of Cell Biology to clinical journals such as The Journal of Hand Surgery and Clinical Orthopaedics and Related Research. Dr. Lieber's research focuses on design and plasticity of skeletal muscle. Currently, he is developing state-of-the-art approaches to understanding muscle contractures that result from cerebral palsy, stroke and spinal cord injury.

In recognition of the clinical impact of his basic science studies, Dr. Lieber has been honored by the American Academy of Orthopaedic Surgeons (Kappa Delta Award; twice), the American Bone and Joint Surgeons (Nicolas Andry Award) the American College of Sports Medicine (Fellow), the Council for the International Exchange of Scholars (Fulbright Fellowship) and the American Society for Biomechanics (Borelli Award; Hay Award). He was also named a Senior Research Career Scientist from the Department of Veterans Affairs from which he has received continuous support since 1985.

rMMs

Saturday, July 28

Keynote Lecture 1: Rick Lieber   **17:30-18:30**

The mystery of human skeletal muscle contracture

Sunday, July 28
Molecular Muscle Mechanics / Physiology   8:24-10:00

Towards a better understanding of muscle contraction
Venus Joumaa - Invited Lecture

X-ray diffraction analysis before and after active and passive stretch in skinned muscle fiber bundles from wild type and mdm mice
Anthony Hessel

Calcium-dependent titin – thin filament interactions in muscle: observations and theory
Kiisa Nishikawa

A three filament muscle model based on a titin-myosin interaction
Matthew Millard

Residual force enhancement in cardiac myofibrils on the ascending limb of the force-length relationship
Seong-won Han

The muscle mechanical basis of Freeman-Sheldon Syndrome
Kaylyn Bell

Adductor longus myofibrillar passive stiffness is reduced in cerebral palsy
Tim Leonard

Keynote Lecture 2: Motoshi Kaya   10:30-11:30

Reverse stroke of cardiac myosin is essential for heart function: lessons from skeletal myosin

Cellular Muscle Mechanics / Physiology   11:30-12:42

History-dependent behaviour in drosophila jump muscle: do myosin kinetics influence force-depression?
David Corr

A myosin based mechanism for stretch activation and its possible purpose revealed by varying phosphate concentration in mammalian skeletal muscle fibers
Douglas Swank

Skeletal muscle stem cell properties from young children with cerebral palsy
Marlies Corvelyn

Collagen preferred direction relative to muscle fiber direction in three and six-month-old Mdx mice
Ridhi Sahani

The effect of Ca2+ on rate of force redevelopment of single muscle fibres in young and older adults
Nicole Mazara

The influence of muscle architecture on sarcomere force-length relationship in intact muscle
Eng Kuan Moo

Keynote Lecture 3: Henk Granzier   14:00-15:00

Titin determines passive stiffness and the sarcomere length working range of skeletal muscle

Monday, July 29
In vivo Animal Muscle Function   8:24 - 10:00

Musculoskeletal changes and adaptions - from aging to pathology in humans
Sabrina Lee - Invited Lecture

Muscle dynamics of the vastus lateralis in jumping kangaroo rats (D. deserti)
Marie Janneke Schwaner

Examining in situ changes to muscle spindle signals with increased muscle-tendon compliance
Emily Abbott

Intramuscular Anatomy drives muscle collagen content variation, likely impacting passive muscle stiffness
Benjamin Binder-Markey

Uniaxial transverse loading decreases muscle force
Tobias Siebert

How do the contractile properties of individual muscles within a synergistic group combine?
David Lin

Loss in agonistic muscle torque during simultaneous (submaximal) activation
Heiliane de Brito Fontana

Keynote Lecture 4: Monica Daley   10:30-11:30

In vivo muscle dynamics in steady and non-steady bipedal locomotion in guinea fowl

In vivo Human Muscle Function   11:30-12:42

History dependence of in vivo muscle force production: the role of muscle-tendon unit compliance
Daniel Hahn

Quantifying in vivo variability in sarcomere length along the length of the long head of the biceps brachii
Amy Adkins

Fatigue-induced changes in hamstrings shear modulus and load distribution depend oncontraction type
Pavlos Evangelidis

3D representation of complex soleus aponeurosis geometry and muscle fiber architecture based on magnetic resonance imaging and Laplacian flow simulation
Katherine Knaus

Summation properties are improved by a preceeding contraction and intervening rest period
Ian Smith

Macroscopic morphological muscle properties to feature spasticity phenotypes in children with cerebral palsy
Kaat Desloovere

Keynote Lecture 5: Yasuo Kawakami   14:00-15:00

Muscle-tendon-fascia system as a fibre-reinforced entity of actuators and springs: *in vivo* and *ex situ* evidence

Is titin actively preloaded?
Matthew Millard

Modeling muscle cross-bridge dynamics for movement simulations
Ashley Oldshue

The paretic biceps brachii contains fewer sarcomeres in series than the contralateral biceps brachii following stroke
Amy Adkins

Characterizing shortening deactivation in drosophila and lethocerus muscle types
Amy Loya

Residual and passive force enhancement in skinned cardiac fibre bundles
Kevin Boldt

Are pre-treatment assessments of muscle morphology related to the effects of treatment with Botulinum NeuroToxin-A and lower leg casting in children with cerebral palsy?
Kaat Desloovere

Effect of stretch-shortening cycle is prominent in the reduced force condition
Atsuki Fukutani

Simulating the pendulum test to understand mechanisms of Parkinsonian rigidity
Giovanni Martino

Relationship between spasticity phenotypes and muscle morphology is different in children with spastic cerebral palsy and children with hereditary spastic paraplegia
Nathalie De Beukelaer

Acto-myosin cross-bridge stretch mechanics underlie history-dependent changes in muscle spindle sensory feedback: a multi-scale experimental and simulation study
Brian Horslen

Muscle fibre type characteristics of the lumbar multifidus and erector spinae in persons with non-specific chronic low back pain and healthy controls
Anouk Agten

IL4 counteracts cancer-induced skeletal muscle atrophy: one cytokine for multiple effects
Domiziana Costamagna

Poster Session 2   15:00 - 16:30

Ultrasound Derived in vivo Measures of Skeletal Muscle Vibration during Locomotion in Humans
   Emma Hodson-Tole

Shear modulus of the resting agonist/antagonist muscles
   Liliam Oliveira

Contractile and non-contractile tissues in the midthigh of the elderly and younger athletes: Inter-individual differences and relationships with body composition and muscle function
   Hoshizora Ichinose

The influence of residual force depression on torque during shortening contractions without - relative to with - pre-load
   Neale Tillin

Eccentric hamstring fascicle behavior occurs during the Nordic hamstring exercise
   Brent Raiteri

Electricaly versus voluntarily activated stretch-contractions: is there a true non-responder?
   Wolfgang Seiberl

Influence of NMES frequency and waveform on torque production, stimulation efficiency and discomfort in healthy subjects
   Marco Vaz

Adaptations in intermuscular coordination of the triceps surae muscles in people with haemophilic arthropathy
   Carlos Cruz-Montecinos

Muscular and non-muscular contraction in the mammalian diaphragm
   Robert Griffiths

Force-frequency relationship during fatiguing contractions of rat medial gastrognemius muscle
   Brian MacIntosh

Protective effect of moderate exercise and prebiotic fibre supplementation on vastus lateralis muscle in a rat model of obesity
   Jaqueline Lourdes Rios

Supraspinatus tendon changes with repetitive wheelchair propulsion are associated with fatigue, sex, and body weight

Keynote Presentations

Rick Lieber

Motoshi Kaya

Henk Granzier

Monica Daley

Yasuo Kawakami

The Mystery of the Human Skeletal Muscle Contracture

[1,2]**Richard L. Lieber**
[1]Departments of Physiology and Biomedical Engineering, Northwestern University, Chicago, IL, USA
[2]Shirley Ryan AbilityLab, Chicago, IL USA
corresponding author: rlieber@sralab.org

INTRODUCTION

Skeletal muscle contractures, which are often painful, affect about a third of children with cerebral palsy (CP) and limit their involvement in daily activities, school, and sports. A variety of long-established treatment methods—splinting, stretching, neurotoxin injection, exercise, serial casting, and even surgery—do not resolve the underlying contracture. Since our fortuitous finding that muscle contractures had dramatically altered structure (1), we have studied their biology and mechanics at a variety of scales.

CONTRACTURES HAVE LONG SARCOMERES

The first and most paradoxical observation made during surgery on contractured muscles was that, although significantly shortened, wrist flexors were composed of sarcomeres that were highly stretched (1) sometimes even beyond their normal *in vivo* operating range. We have since made similar observations for the soleus (2), gracilis (3), and semitendinosus (3) muscles. We believe this result suggests that contractured muscle has a defect in its abilty to grow longitudinally, i.e., add serial sarcomeres.

CONTRACTURES HAVE FEWER SATELLITE CELLS

Skeletal muscle ECM contains satellite cells (SC), named as such because they are located at the periphery of the muscle cell, sandwiched between the sarcolemma and the basal lamina (4). Sophisticated experiments using transgenic mouse models have conclusively demonstrated that SCs are required for muscle regeneration from a toxin-induced degeneration injury (5). In the absence of SCs, other cells such as fibroblasts and fibroadipogenic progenitors (FAPs) proliferate unchecked to create stiff, fibrotic, and fat-infiltrated tissue (6). Using both cell sorting (7) and immunohistochemistry (8), we showed that satellite cell number was dramatically reduced in contractures. Is it possible that SCs are necessary for longitudinal growth in muscle? In support of this idea is our recent study that demonstrated the inability of mouse muscles with decreased SC content to add sarcomeres serially (9).

SATELLITE CELLS IN CONTRACTURES ARE EPIGENETICALLY MODIFIED

In an attempt to understand the decreased satellite cell number, we isolated and grew these cells from human muscle biopsies. Interestingly, SCs proliferated more rapidly than muscle from typically developing (TD) muscle, but failed to develop into mature muscle as shown by decreased myosin heavy chain and integrin β1-D expression and hypermethylation of the promotor region of these genes (10). Thus, not only is the contracture hampered from growth due to loss of SCs but the remaining SCs are not able to develop into normal muscle, which makes their rehabilitation ability questionable.

DEFECTIVE SATELLITE CELLS CAN BE RESCUED BY DEMETHYLATING AGENTS

The hyperproliferative, immature state of the SCs led to the idea that these cells were epigenetically modified similar to some cancers (10). We thus performed an experiment in which a single 24-hour pre-treatment of CP myoblasts with 5 μM of cytidine analog 5-Azacytidine (AZA), an FDA-approved DNA methyl-transferase (DNMT) inhibitor restored methylation levels to control levels (measured in TD cells) and rescued the expression of pro-myogenic genes and led to a significant increase in myotube formation during differentiation (Fig. 1).
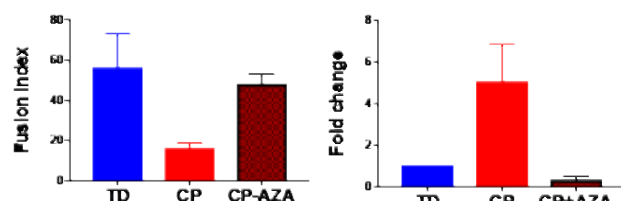

Figure 1: Fusion index (left, percentage of myotubes with 3+ myonuclei) and degree of promoter methylation (right) in TD, CP and CP cells treated with AZA. Note that AZA rescues the CP cells to be more like the TD cells and thus, may be used to treat contractures. (Data replotted from reference 10.)

POSSIBLE TREATMENT OF CONTRACTURES BY DRUG REPURPOSING

Based on these findings, we are planning a clinical trial of AZA in children with contractures. Current studies are defining dosing magnitudes and strategies for use of this compound. This requires the development of dosing strategies (route of administration, dose, frequency) as well as the determination adjuvant physical therapy treatments that will accompany the drug treatment. Because the compound is already FDA-approved (albeit for cancer, not for cerebral palsy) the pathway to approval for these studies is relatively fast. Our vision is to develop a permanent, nonsurgical cure for skeletal muscle contractures.

ACKNOWLEDGEMENTS

REFERENCES

1. Lieber *et al.* Muscle & Nerve. 2002;**25**:265-70.
2. Mathewson *et al.* J Orthop Res. 2015;**33**:33-9.
3. Smith *et al.* J Physiol. 2011;**589**:2625-39.
4. Mauro J. Biophys. Biochem. Cytol. 1961;**9**:493-5.
5. Lepper *et al.* Develop. 2011;**138**:3639-46.
6. Joe *et al.* Nature. 2010;**12**:153-63.
7. Smith *et al.* Dev Med Child Neurol. 2013;**55**:264-70.
8. Dayanidhi *et al.* J Orthop Res. 2015;**33**:1039-45.
9. Kinney *et al.* Muscle Nerve. 2017;**55**:384-92.
10. Domenighetti *et al.* Am J Physiol 2018;**315**:C247-C57.

Reverse stroke of cardiac myosin is essential for heart function: lessons from skeletal myosin

[1]Yongtae Hwang, [2]Takumi Washio, [2]Toshiaki Hisada, [1]Hideo Higuchi and [1]**Motoshi Kaya**
[1]Department of Physics, The University of Tokyo, Tokyo, Japan
[2]Department of Human and Engineered Environmental Studies, The University of Tokyo, Tokyo, Japan
corresponding author: kaya@nanobio.phys.s.u-tokyo.ac.jp

INTRODUCTION

Numerous studies have investigated molecular properties of cardiac myosin and its modulation by a small molecule agent, since mutation in cardiac myosin was found to be a major cause of hypertrophic cardiomyopathy, the most frequently occurring inherited cardiovascular disease. Since ß-myosin heavy chain is found in both cardiac and in type I skeletal muscle fibers, one can expect that dynamic behaviours of cardiac myosins are similar to but slower than fast skeletal myosins. We previously performed the force measurements on fast skeletal myosins using optical tweezers and proposed the molecular properties of skeletal myosins designed for efficient muscle contractions [1, 2]. In this study, in order to understand the unique properties of cardiac myosin that distinctively differ from those in skeletal myosins, we measured forces generated by synthetic ß-cardiac myosin filaments and analysed data combined with a Monte Carlo-based simulation model. We further performed single molecule observation of ß-cardiac myosin dynamics under various loads and elucidated its molecular mechanisms essential for heart contractions.

METHODS

For the force measurement on synthetic cardiac myosin filament, ß-cardiac myosins purified from porcine ventricle were mixed with florescence-labelled myosin rods at the ratio of 4:1 and rapidly diluted by low ionic strength solution. In synthetic myofilaments, we estimated that ~14 myosin molecules are maximally accessible to single actin filament. An actin-bead complex was trapped by optical tweezers and placed near a myosin-rod cofilament fixed on a glass surface such that it can be overlapped with myosin-rod cofilament. Forces driven by cardiac myosins at either 10 µM or 1 mM ATP were calculated by multiplying the bead displacement by the trap stiffness. For the detection of single cardiac myosin dynamics, ß-cardiac myosins were mixed with rods at the ration of 1:1500. Once myosin interacted with actin filament, an actin-bead complex was pulled backward such that dynamic responses of single myosin molecule can be evaluated against loads in either 1 mM ADP or 1 mM ADP and 10 mM Pi.

RESULTS AND DISCUSSION

Forces driven by cardiac myosins were generated much more slowly than those driven by skeletal myosins (Fig. 1). Stepwise actin displacements were generated by either single or coordinated power stroke execution of cardiac myosins [2]. In contrast to skeletal myosins, data showed frequent backward movements (Fig. 1, arrow heads). Such frequent backward displacements can be reproduced by increasing the rate for reverse stroke of the force-generating myosin in our simulation model designed originally for skeletal myosins. Thus, these results imply that frequent reverse stroke execution is essential for cardiac myosin function.
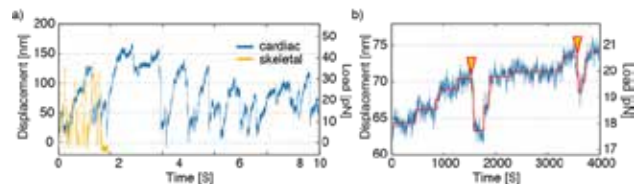

Figure 1: Force generation of ß-cardiac myosin-rod cofilament measured by optical tweezers was compared to those of skeletal myosin in a) and was expanded in a narrower range of time in b).
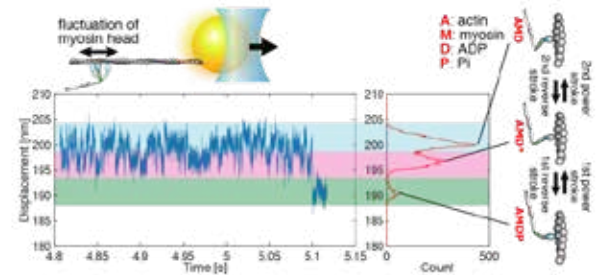

Figure 2: Dynamic behaviour of cardiac myosin head in response to stretching of actin filament. Histgram shows three stable bead positions (peaks), which correspond to three force-generating states (AMDP, AMD*, AMD) associated with power and reverse strokes.

In order to test this idea, dynamics of single cardiac myosin molecule was measured under various loads (Fig. 2). Bead displacements show fluctuations of myosin molecule, which are repeatedly located at one of three stable positions (Fig. 2). These stable positions potentially indicate three stable conformations (AMDP, AMD* and AMD) of myosin head in force-generating states associated with first and second power / reverse stroke. We also confirmed that these reversible actions between force-generating states are rarely observed from skeletal myosins, suggesting that these properties are inherent to cardiac myosins.

In summary, we observed frequent backward movements of actin driven by cardiac myosins. Such movements are likely caused by frequent reverse stroke execution during force generation. Our simulation model suggests that such a molecular property is advantage to maintain high tension for a long period of time in systolic phase of heart cycle by remaining many myosin molecules bound to actin filaments with a small amount of ATP consumption.

REFERENCES

[1] Kaya M. and Higuchi H. (2010). *Science*, **329**: 686-689.
[2] Kaya M et al. (2017) *Nat Commun*, **8**: 16036.

23

rMMs

TITIN DETERMINES PASSIVE STIFFNESS AND THE SARCOMERE LENGTH WORKING RANGE OF SKELETAL MUSCLE.

Ambjorn Brynnel, Yaeren Hernandez, Balazs Kiss, Johan Lindqvist, Maya Adler, Robbert van der Pijl, and **Henk Granzier**.
Department of Cellular and Molecular Medicine, University of Arizona, Tucson, USA; Email: granzier@email.arizona.edu

INTRODUCTION

The focus of this study is on titin, the largest known protein that forms the third myofilament type of striated muscle, spanning the half-sarcomere from Z-disk to M-band [1]. The I-band region of titin functions as a molecular spring that extends and generates passive force when muscles are stretched [1]. Titin's molecular spring consists of two main sub-segments, the tandem Ig segment (serially-linked immunoglobulin (Ig)-like domains) and the PEVK (proline, glutamate, valine, and lysine-rich) segment. These segments have different biophysical properties and therefore their extensibilities dominate at different physiological sarcomere length ranges [1]. While the contribution of titin to sarcomere passive stiffness in single fibers is widely accepted, there are conflicting views on the relevance of titin to passive stiffness at the whole skeletal muscle level. It has been proposed that the extracellular matrix (ECM) dominates whole muscle passive stiffness and that titin is less relevant at the whole muscle level [2]. This contrasts with studies that concluded that the passive stiffness of whole muscle fully resides in single fibers (titin) and also with work on cardiac muscle, where titin's stiffness exceeds ECM-stiffness [3]. An important goal of the present study was to directly address the role of titin in passive stiffness of whole skeletal muscle.

A mouse model was created for this work in which titin's stiffness was increased by shortening titin's molecular spring region [4]. We targeted for deletion 46 PEVK exons (Ttn exon 112-158), creating a model referred to as the TtnΔ112-158 model. The TtnΔ112-158 model also provides a unique opportunity to test the effects of altered titin-based tension on active muscle function. Recently, several novel mechanisms have been proposed that link titin-based tension to active tension. For example, titin might store elastic energy by unfolding Ig domains in passive muscle. Through their refolding during contraction, titin might generate forces that add to the active force [5].

METHODS

Transcript, protein and functional studies (muscle mechanics, exercise testing) were performed, to determine the effects of the deletion on the single muscle fiber, whole muscle, and organismal levels. We focused on the diaphragm, included because of its critical importance for the vital breathing function, and two contrasting peripheral muscle types, the slow-twitch soleus and fast-twitch EDL muscles.

Titin is not the only source of muscle passive tension, the extracellular matrix (ECM) also contributes. To determine how much each contributes to total passive muscle tension, the EDL fifth toe muscle was studied because it is thin enough to: 1) measure sarcomere length with laser diffraction in intact muscle, 2) fully demembranate the muscle with detergent, and 3) extract the skinned muscle with KCl/KI solutions that remove titin's anchors in the sarcomere, leaving the ECM intact but abolishing titin-based tension.

RESULTS AND DISCUSSION

To evaluate the effects of the shortened PEVK segment on titin-based stiffness the extension of the PEVK segment was measured in sarcomeres stretched by varying degrees. The obtained values were used in the worm-like chain equation and the force per titin molecule was calculated. The results reveal that compared to WT, the titin-based stiffness of TtnΔ112-158 mice is predicted to be greatly increased. To investigate the effect of shortening titin's PEVK segment on passive muscle stiffness, the passive tension - sarcomere length relation was studied at the level of the whole muscle. All studied muscle types showed a several-fold increased passive stiffness in TtnΔ112-158 mice.

The titin-based and ECM-based tensions were functionally dissected. The titin-based passive stiffness was increased ~5-fold; the ECM stiffness was increased as well but its magnitude remained below the stiffness of titin. Thus, passive TtnΔ112-158 skeletal muscles are much stiffer, which largely can be accounted for by increased titin stiffness.

To determine whether the increased titin-based tension of TtnΔ112-158 muscles affected active tension, the active tension-frequency relation was measured. Overall, the studies on activated muscles support that force development is faster in TtnΔ112-158 mice, but that maximal active tension levels are unaffected.

We also found that the diaphragm muscle of TtnΔ112-158 mice had a significantly reduced sarcomere length both during expiration and inspiration; the physiological sarcomere length range of the diaphragm was 2.85 μm to 2.22 μm in WT mice but only 2.37 μm to 1.88 μm in TtnΔ112-158 mice. Additional experiments showed that a shift in the physiological sarcomere lengths to shorter lengths occurred in peripheral muscles as well. The shift in the working sarcomere length range in TtnΔ112-158 mice can be explained by the increase in the number of sarcomeres in series that was found.

In summary, this study supports that titin is the main determinant of passive stiffness of skeletal muscle and that an increase in titin-based stiffness carries through to the whole muscle level. Findings also show that increasing the stiffness of titin does not influence the final level of active force that is reached. The functional lowering of passive stiffness through the serial addition of sarcomeres that shortens the sarcomere length working range requires multiple major adaptations, indicating that increased passive stiffness is functionally detrimental and has to be avoided.

REFERENCES

[1] Granzier HL, Labeit S (2005). Adv Protein Chem.,**71**:89-119.
[2] Tirrell TF, et al. (2012). J Exp Biol.,**215**:2551-9.
[3] Wu Y, et al. (2000) JMCC ,**32**:2151-62.
[4] Brynnel et al. (2018). Elife, **7**, pii: e40532
[5] Eckels EC, et al. (2018). Annu Rev Physiol.,**80**:327-51.

In vivo muscle dynamics in steady and non-steady bipedal locomotion in guinea fowl

[1,2]**Monica A. Daley,** [3]**Andrew A Biewener** [1]**Joanne C Gordon**
[1]Comparative Biomedical Sciences, Royal Veterinary College, Hatfield, Hertfordshire, UK
[2]Ecology and Evolutionary Biology, UC Irvine, Irvine, CA, USA
[3]Organismic and Evolutionary Biology, Harvard University

corresponding author: monica.a.daley@gmail.com

Birds are diverse and agile vertebrates with exceptional ecological range, capable of many combinations of aerial, terrestrial, and aquatic locomotion. Although birds are most noted for prowess in flight, birds are also adept terrestrial bipeds, with a 230-million-year evolutionary legacy from theropod dinosaurs. Consequently, guinea fowl and other ground birds serve as useful animal models to study the mechanics and neuromuscular control of bipedal locomotion [1]. Comparative animal studies can help reveal neuromuscular mechanisms using direct measurements that are infeasible in human studies and can provide insight into how biomechanical function varies with morphology and body size.

In this talk, I will review work using *in vivo* recordings of muscle dynamics to reveal the neuromuscular mechanisms used by guinea fowl to achieve stable and agile bipedal locomotion. The muscles of the limb must function to move an animal effectively over varied terrains while maintaining stability and avoiding injury. Studies of steady level and incline locomotion highlighted a division of labor within limb muscles, with large, parallel fibered muscles in the proximal limb specialized for power and large joint excursions, and short-fibered pennate muscles in the distal limb specialized to facilitate economic weight support and tendon elastic energy cycling [2,3]. Relatively little is known about how differences in muscle architecture influence neuromuscular function for non-steady locomotor tasks, such as perturbation recovery and navigating uneven terrain.

Experiments in guinea fowl running over an unexpected 'pothole' perturbation (a sudden drop in terrain height) revealed rapid intrinsic mechanical responses that facilitate disturbance rejection and stable recovery [3,4,5]. Based on *in vivo* measures of muscle-tendon dynamics during terrain perturbations, we discovered that distal muscles exhibited rapid changes in length, force and work output in response to changes in leg posture and loading, which helped to stabilize gait and minimize risk of injury [4,5]. We have compared *in vivo* force-length and activation dynamics of guinea fowl leg muscles during locomotion over: 1) steady level terrain, 2) constant incline 3) unexpected drops in terrain, and 4) periodically repeating obstacles [2, 4, 5, 6]. These studies have revealed that distal leg muscles of guinea fowl are inherently sensitive to changes in leg posture and loading, due to intrinsic mechanical effects and rapid proprioceptive feedback. The findings suggest that the pennate architecture of distal muscles facilitates rapid stabilization and suggests a trade-off in leg morphology for economy *versus* stability that might explain why most animals have relatively large distal limb muscle mass.

In on-going work, we are investigating the contributions of intrinsic muscle dynamics, proprioceptive feedback and anticipatory (feedforward) control in the neuromuscular control of locomotion. We have developed a 'self-re-innervation' procedure in guinea fowl to investigate the muscular effects of nerve injury recovery and the functional consequences of proprioceptive deficit in a bipedal animal model. The nerve branches to the lateral gastrocnemius (LG) muscle is cut and immediately repaired. The repaired nerves re-innervate the muscle, leading to full recovery of motor output within 6 weeks, with long-term proprioceptive deficit. By comparing *in vivo* muscle function and locomotor dynamics of intact and reinnervated birds, we are evaluating functional integration and trade-offs between feed-forward, feedback and intrinsic mechanical control mechanisms. This approach also provides a useful bipedal animal model to investigate neuromuscular plasticity and functional consequences of proprioceptive deficits due to disability or disease.

REFERENCES

[1] Daley, MA and Birn-Jeffery, A (2018) *J Exp Bio*, *221*: jeb152538.
[2] Daley, MA and Biewener, AA (2003) *J Exp Bio*, *206*:2941-2958.
[3] Biewener, AA and Daley, MA (2007) *J Exp Bio 210*:2949-2960.
[4] Daley, MA, Voloshina, A and Biewener, AA (2009) *J Physiol*, *587*: 2693-2707.
[5] Daley, MA and Biewener, AA (2011) *Phill Trans Roy Soc B, 366*:1580-1591.
[6] Gordon, JC, Rankin, JW and Daley, MA (2015) *J Exp Bio*, 218: 3010-3022.

Muscle-tendon-fascia system as a fibre-reinforced entity of actuators and springs: *in vivo* and *ex situ* evidence

Yasuo Kawakami[1,3], Shun Otsuka[2], Xiyao Shan[2]
[1]Faculty and [2]Graduate School of Sport Sciences, Waseda University, Saitama, Japan
[3]Human Performance Laboratory, Organization of University Research Initiative, Waseda University, Tokyo, Japan
corresponding author: Yasuo Kawakami, Email: ykawa@waseda.jp

INTRODUCTION

Skeletal muscles are comprised of muscle fibres packed in bundles (fascicles) that extend from proximal to distal tendinous tissues (tendons and aponeuroses). Each skeletal muscle therefore can be regarded as a muscle-tendon unit (MTU) where fascicles function as actuators while tendinous tissues act as linear viscoelastic springs in series with fascicles [1]. However, there is evidence that the tendinous tissues, aponeuroses in particular, show anisotropic behaviour with unequal elasticity in the longitudinal (along the muscle's line of action) and transverse directions [2].

The aponeurosis is a part of fascial structures that provide geometrical and mechanical support for muscle contraction [3]. Considering the function of the aponeurosis as a base for muscle fibre attachment as well as a spring to store and release elastic energy during exercise, other fascial structures could bear similar functions. The deep fascia for instance is thought to unite underlying MTUs as a whole, and owing to the collagen fibres that formulate layered sheaths as comprising elements, the deep fascia can be an elastic structure [4]. In my talk some evidence is introduced to discuss a possibility that MTUs and fascial structures together work as a system functioning as actuators and multi-functional springs.

SOME EVIDENCE

Shan et al. [5] found that the human triceps surae muscles' aponeuroses *ex situ* showed site-related differences in thickness and anisotropic mechanical properties. Higher values of longitudinal than transverse stiffness and Young's modulus of the aponeuroses were more pronounced than *in vivo* observations, suggesting inherent material design of the aponeurosis that could be associated with three-dimensional contractile behaviour of muscle fibres.

Otsuka et al. [6] studied in detail cadaveric fascia lata samples, and found site-specific differences in thickness (thickest on the lateral aspect), fractions of collagen fibres in different directions (more longitudinally oriented in the lateral aspect) and stiffness (stiffer antero-laterally), which were gender-specific. They suggested that such site- and gender-specificity of the morphological characteristics and elastic properties of the fascia lata reflect underlying MTUs' architecture to match their functions.

We further carried out *in vivo* measurements of human fascia lata elasticity using ultrasonography and elastography [7]. It was found that the fascia lata stiffness changed as a function of muscle activation level. This suggests the role of the fascia lata as the stabilizing base of muscle contraction. The fascia lata stiffness also demonstrated anisotropy, possibly reflecting its unique role that regulate underlying MTUs' deformation (Figure 1).
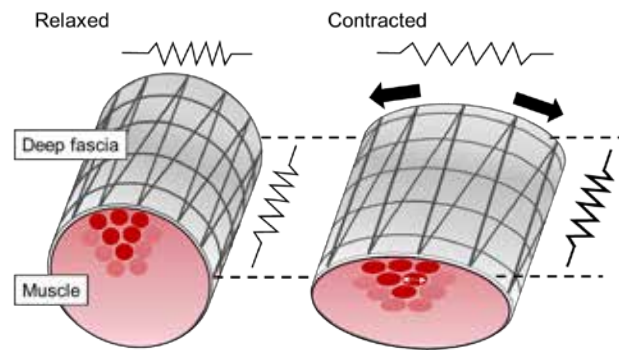

Figure 1: Schematic illustrations of the changes in fascia lata with muscle contraction. Anisotropic stiffening in the longitudinal and transverse directions is illustrated [7].

DISCUSSION

In vivo as well as *ex situ* evidence hints to the notion that the muscle-tendon units should be regarded as a functional entity connected throughout the multi-level fascial system. As a mechanical interface between muscle fibres and bony attachments, the fascial system may act as a mediator of MTU functions for optimizing motor performance.

ACKNOWLEDGEMENTS

REFERENCES

[1] Kawakami Y and Fukunaga T (2006). *Exerc Sport Sci Rev*, **34**: 16-21.
[2] Iwanuma S et al. (2011). *J. Appl. Physiol.* **110**:1615–1621.
[3] Huijing PA et al. (2007). *J Electromyogr Kinesiol*, **17**: 680-689.
[4] Stecco C et al. (2014). Surg Radiol Anat, **36**: 25-32.
[5] Shan X et al. (2019). *PLoS One*, **14**: e0211485.
[6] Otsuka S et al. (2018). *J Biomech*, **77**: 69-75.
[7] Otsuka S et al. (2019). *J Electromyogr Kinesiol*. **45**: 33-40.

Session 1:
Molecular Muscle Mechanics / Physiology

Venus Joumaa

Anthony Hessel

Kiisa Nishikawa

Matthew Millard

Seong-won Han

Kaylyn Bell

Tim Leonard

Chairperson: Rick Lieber

Residual Force Enhancement: Towards a Better Understanding of Muscle Contraction

[1]**Venus Joumaa**, [1]Timothy R. Leonard, [1]Walter Herzog
[1]Faculty of Kinesiology, University of Calgary, Calgary, Alberta, Canada
corresponding author: vjoumaa@ucalgary.ca

INTRODUCTION

When a skeletal muscle is actively stretched, the isometric force reached at steady-state following the stretch is always greater than the purely isometric contraction performed at the same final muscle length and level of activation. This history-dependent property, named residual force enhancement (RFE), has been observed in all muscle preparations, ranging from in vivo muscles to myofibrils [1].

The classic cross-bridge theory is unable to account for RFE. According to this theory, isometric muscle force depends on the amount of overlap between actin and myosin and not on the history of contraction. The mechanisms proposed to explain RFE have been (1) the development of sarcomere length non-uniformities, and (2) the engagement of a passive element upon activation and stretch.

Mechanism 1 suggests that sarcomere length instabilities on the descending limb of the force-length relationship result in individual sarcomeres stretching by different amounts during active stretch [2]. Some sarcomeres are pulled beyond overlap and are supported by passive force, while the remaining sarcomeres are stretched by a small amount. This behaviour leads to a situation in which force is greater after stretch than that produced during an isometric contraction when sarcomeres are relatively uniform.

Mechanism 2 involves the structural protein titin which has been suggested to play a role in RFE [3,4] by various means such as titin changing its stiffness by binding calcium or by decreasing its length, and thus increasing force upon active stretch.

However, there has been little direct in-depth investigation of these mechanisms. Furthermore, understanding how a muscle is able to increase its isometric force would provide great insight into the mechanism of active force regulation.

PURPOSE

The aim of our research has been to investigate the mechanism(s) of RFE and thus provide insight into active force production and regulation in skeletal muscle.

APPROACHES

In order to explore the mechanism(s) of RFE, we have been using three approaches: 1) mechanical testing on single myofibrils and skinned muscle fibres, 2) assessing muscle energetics and the energy cost of force production, and 3) exploring the structure of the sarcomere after active stretch by using small angle x-ray diffraction.

MAIN FINDINGS

We tested the main predictions of the sarcomere length non uniformity theory in single myofibrils. We found that RFE was not associated with sarcomere instability and dynamic redistribution of sarcomere lengths after stretch, but rather RFE seems an inherent sarcomeric property of contraction.

We then investigated the potential role of titin in RFE, by testing the effects of partial titin depletion on force after active stretch in myofibrils. We found that force after active stretch was greatly reduced when titin-based force was reduced, suggesting that titin is likely directly involved in the increase in force at steady-state after active stretch. Furthermore, we found that the purely isometric active force was reduced when titin was partially degraded and this reduction was correlated with the reduction in passive force. This result suggests that titin can modulate not only the increase in active force after active stretch but also adjusts purely isometric active force.

It has been suggested that titin might modulate active force by exerting a lateral force that compresses the lattice spacing and thus regulates the proportion of attached cross-bridges. To test this hypothesis, we used dextran in skinned muscle fibres to adjust the lattice spacing when titin was partially degraded. We found that the compression of lattice spacing alone was not enough to recover the contractile properties before and after active stretch in the absence of titin. Therefore, titin seems to influence active force not just by compressing the lattice spacing, but by either directly producing force that contributes to the total active force or by acting on the structure of the contractile filaments and modulating their cross-bridge based force.

The involvement of a passive element in active force production after active stretch is supported by our energetics experiments performed in skinned muscle fibres. We showed that the energy cost of force production was reduced at steady-state after active stretch compared to a purely isometric contraction.

To investigate the potential changes in the structure of the sarcomere and cross-bridges after active stretch, we used small angle x-ray diffraction in skinned muscle fibre bundles. Our results showed structural and mechanical evidence for the absence of an increase in the proportion of attached cross-bridges after active stretch and that RFE is likely accompanied by an increase in cross-bridge disorder and/or a change in the conformation of cross-bridges.

CONCLUSION

We have confirmed that RFE is an inherent property of sarcomere contraction, and that titin plays a major role in active force regulation in skeletal muscle.

A three-filament model of muscle contraction, comprised of actin, myosin and titin, is likely more accurate to predict muscle behaviour than the classic cross-bridge theory based on actin and myosin alone.

ACKNOWLEDGEMENTS

REFERENCES

[1] Herzog W. (2017). *J Neuroeng Rehabil*, **14**.
[2] Morgan DL. (1990). *Biophys J*, **57**: 209-221.
[3] Edman KAP et al. (1982). *J Gen Physiol*, **80**: 769-784.
[4] Herzog W & Leonard TR. (2002). *J Exp Biol*, **205**: 1275-1283.

X-ray diffraction analysis before and after active and passive stretch in skinned muscle fiber bundles from wild type and *mdm* mice

[1,2]**Anthony L. Hessel**; [1]Dhruv Mishra; [3]Weikang Ma; [4]Venus Joumaa; [3]Thomas C. Irving; [1]Kiisa C. Nishikawa
[1]Department of Biological Sciences, Northern Arizona University, Flagstaff, AZ, USA
[2]Movement Science Laboratory, Faculty of Sports Science, Ruhr University Bochum, Bochum, Germany
[3]Department of Biological Sciences, Illinois Institute of Technology, Chicago, Illinois, USA
[4]Human Performance Laboratory, Faculty of Kinesiology, University of Calgary, Calgary, AB, Canada
corresponding author: Anthony.hessel@rub.de

INTRODUCTION

Muscular dystrophy with myositis (*mdm*) mice carry a small deletion in titin that includes part of Ig83 in the N2A region, which leads to a decrease in isometric force as well as loss of force enhancement and depression in skeletal muscles [1,2], presumably by decreasing titin-based stiffness. The mechanisms responsible for these changes in muscle mechanics are unclear. The small deletion in Ig83 in *mdm* muscles may produce changes in sarcomere structure that could help to explain these differences. Therefore, we used X-ray diffraction to investigate sarcomere structure during and after passive and active stretch of wild type and *mdm* muscles.

METHODS

The Institutional Animal Care and Use Committee at Northern Arizona University and the Illinois Institute of Technology approved all husbandry and experimental protocols. Extensor digitorum longus (EDL) muscles were extracted from euthanized wild type and *mdm* mice. Skinned fiber bundles were prepared [3] and attached to a custom-built mechanical fiber apparatus. X-ray diffraction images were captured using small-angle diffraction on the BioCAT beamline 18 ID at the Advanced Photon Source, Argonne National Laboratory [4]. Equatorial and meridional spacings and intensities were measured using the software package MuscleX [5]. Measured spacings of the 1,0 and 1,1 equatorial reflections from the diffraction pattern were converted to inter-thick filament spacing (lattice spacing, LS). Changes in radial position of the myosin heads were estimated from the 1,1 / 1,0 intensity ratio. Using the 2D modelling equation for the equatorial intensities, the parameter σd is interpreted as a measure of the width of the distribution of lattice spacing between different myofibrils in the sample. We also measured positions and intensities of meridional reflections M3 (~14.3 nm), M6 (~7.2 nm), and A6 (~5.9 nm). M3 is dominated by the myosin head position. M6 and A6 arise from periodic features along the thick and thin filament backbones, respectively, and are used to estimate filament strain. X-ray reflections were measured before and after passive and active stretch (0.1 μm s^{-1}) from average sarcomere lengths of 2.4 to 3.2 μm for wild type (n = 10) and *mdm* (n = 10) fiber bundles.

To assess whether the *mdm* mutation affected sarcomere structure as observed using equatorial and meridional reflections, we used a full factorial ANOVA design, with fixed factors of genotype (wild type, *mdm*), activation (passive, active) and length condition (isometric at 2.4 μm, immediately following stretch to 3.2 μm, and after return to steady state after stretch to 3.2 μm). Individual muscles were nested within genotype as a random effect. For post-hoc tests, a Tukey's HSD multiple comparison procedure was implemented. For all tests, best Box-Cox transformations were used to ensure normality and homoscedasticity, and alpha values were set at 0.05.

RESULTS AND DISCUSSION

No differences in measured reflections were observed between immediately after stretch and steady state after stretch, for either activation or genotype conditions, most likely due to the slow stretch rate which likely reduced the contribution of viscous forces. LS decreased with activation and stretch, and decreased more in wild type than *mdm* fibers, suggesting an effect of *mdm* on regulation of LS. σd increased with activation and stretch in both genotypes. The intensity ratio increased with activation in both genotypes as expected [3]. However, the 1,0 intensity almost disappears after active stretch of *mdm* fibers, perhaps due to a decrease in thick filament order. M3 spacing increased with activation and stretch in both genotypes. M6 spacing increased with stretch (~0.8%) in both genotypes and was unaffected by activation. Neither M3 nor M6 intensities differed between genotypes. Neither A6 spacing nor intensity was affected by activation, length or genotype.

CONCLUSIONS AND FUTURE DIREECTIONS

These results suggest that the structure of the sarcomere and thick filaments are affected by the small deletion in Ig83 of the N2A region of titin in permeabilized *mdm* fibers. *Mdm* sarcomeres and thick filaments appear to be less organized than wild type. The inability of *mdm* titin to hold thick filaments centrally within the hexagonal array of thin filaments during contraction could account for these results from x-ray diffraction as well as for the reduction in isometric force and loss of FE and FD in *mdm* muscles. This idea was suggested previously in a study using ionizing radiation to degrade titin [6]. Future studies will be needed to further quantify destabilization of thick filaments during contraction of *mdm* muscles.

ACKNOWLEDGEMENTS

REFERENCES

[1] Tahir et al. (2019). *In revision for J Exp Biol.*
[2] Hessel A & Nishikawa K (2017). *J Exp Biol,* **220**: 4177–4185.
[3] Joumaa V & Herzog W (2014). *Am. J. Physiol,* **307**: C395–401.
[4] Ma et al. (2018). *Biophys J,* **115**: 1580–1588.
[5] Jiratrakanvong, J. (2018). BioCAT Argonne Nat. Labs.
[6] Horowits et al. (1986). *Nature*, **323**: 160–164.

Calcium-dependent Titin – Thin Filament Interactions in Muscle: Observations and Theory

Kiisa Nishikawa[1], Samrat Dutta[1], Brent Nelson[2], Matthew J. Gage[3], and Jenna A. Monroy[4]

[1]Department of Biological Sciences, Northern Arizona University, Flagstaff, AZ USA 86011-5640
2 Department of Mechanical Engineering, Northern Arizona University, Flagstaff, AZ USA 86011-15600
3Chemistry Department, University of Massachusetts at Lowell, Lowell, MA USA 01854
4W. M. Keck Science Center, Claremont Colleges, Claremont, CA 91711-5916
corresponding author: Kiisa.Nishikawa@nau.edu

Gaps in our understanding of muscle mechanics demonstrate a need for improved models of muscle function. Increasingly, it appears that a role for titin in active muscle contraction might help to fill these gaps. While such a role for titin is increasingly accepted, the underlying molecular mechanisms remain unclear. The goals of this paper are to review recent studies demonstrating Ca^{2+}-dependent interactions between N2A titin and actin *in vitro*, to explore theoretical predictions of muscle behavior based on this interaction, and to review observational data related to the predictions.

CA²⁺-DEPENDENT INTERACTIONS BETWEEN N2A TITIN AND THIN FILAMENTS

In a recent study [1], we used co-sedimentation assays, dynamic force spectroscopy, and *in vitro* motility assays to test whether the N2A region of titin - parts of which have been overlooked in previous studies - interacts with actin in the presence of Ca^{2+}. The results demonstrated that Ca^{2+} increases the association constant between N2A titin and F-actin; that Ca^{2+} increases rupture forces between N2A titin and F-actin; and that Ca^{2+} and N2A titin reduce sliding velocity of F-actin and reconstituted thin filaments. The high rupture forces (~100 pN) measured between N2A titin and F-actin at pCa = 4 suggest that, if binding occurs *in vivo*, it could potentially account for all of the energy stored in muscle during active stretch [2]. Preliminary data from current studies support a role for the Ig83 domain within the N2A region, but other Ig domains may also be involved.

N2A – ACTIN INTERACTIONS: THEORETICAL PREDICTIONS

If N2A titin binds to thin filaments upon calcium influx in muscle sarcomeres, then two mechanical consequences are predicted. First, the length of titin's freely extensible I-band must decrease upon activation [3] because the bound N2A would allow only the PEVK region to extend during active stretch. Second, because by low-force straightening of the proximal tandem Ig domains limits titin stiffness [4], binding between thin filaments and N2A titin is required for increased titin stiffness in active muscle. N2A – titin binding would permit only the relatively stiffer PEVK region to extend during active stretch.

TITIN – ACTIN INTERACTIONS: EVIDENCE FROM MECHANICAL BEHAVIOR OF MUSCLE

There is experimental support for both of these predictions in wild type skeletal muscles and both fail to be observed in skeletal muscles of *mdm* mice with a 53 amino acid deletion in Ig83 of the N2A region [5]. Monroy et al. [6] found that equilibrium length after elastic recoil was 15% shorter in active than in passive mouse soleus muscles, and there was a 2.9-fold increase in the slope of the stress - strain relationship during unloading. In contrast, soleus muscles from *mdm* mice showed no change in equilibrium length and no effect of activation on the slope or intercept of the stress - strain relationship. These results are consistent with the idea that Ca^{2+}-dependent binding of titin to actin reduces titin free length and increases titin stiffness, but not in *mdm* muscles.

Recent studies provide evidence that titin force and stiffness increase in calcium-activated myofibrils. Powers et al. [7] demonstrated that titin force and stiffness are greater in actively stretched than in passively stretched single mouse psoas myofibrils, when myofibrils were stretched beyond overlap of thick and thin filaments where cross bridges cannot contribute to force or stiffness. The *mdm* mutation prevents the increase in titin-based stiffness [8] that normally occurs upon activation of wild type myofibrils.

ACCEPTED FUNCTIONS OF TITIN IN ACTIVE MUSCLE REQUIRE HIGH STIFFNESS

Numerous observations suggest a role for titin in transmitting and distributing forces within muscle sarcomeres under a wide variety of conditions, although it is debated whether this role is direct or indirect. Because titin stiffness is limited by straightening of proximal tandem Ig domains in the I-band under low-force [4], a mechanism such as Ca^{2+}-dependent binding of N2A titin to actin is a theoretical requirement for titin to play even an indirect role in transmitting and distributing forces within active muscle sarcomeres.

CONCLUSIONS

Experimental observations demonstrate strong interactions between N2A titin and actin *in vitro*. In theory, N2A - actin interactions predict a decrease in the length of titin's freely extensible I-band must decrease upon activation and an increased titin stiffness in active muscle, but not muscles from *mdm* mice. Evidence from muscle mechanics supports both of these prediction.

ACKNOWLEDGEMENTS

REFERENCES

[1] Dutta et al. (2018). *Sci Rep,* **8**: 14575.
[2] Linari et al. (2003). *J Physiol*, **548**: 461-474.
[3] Nishikawa et al. (2012). *Proc Biol Sci,* **279**: 981-990.
[4] Linke et al. (1998). *PNAS*, **95**: 8052-8057.
[5] Garvey et al. (2002). *Genomics*, **79**: 146-149.
[6] Monroy et al. (2017). *J Exp Biol,* **220**: 828-836.
[7] Powers et al. (2014). *J Exp Biol,* **217**: 3629-3636.
[8] Powers et al. (2016). *J Exp Biol* **219**: 1311-1316.

A THREE FILAMENT MUSCLE MODEL BASED ON A TITIN-MYOSIN INTERACTION

[1]**Matthew Millard**, [2]David Franklin, and [3]Walter Herzog
[1]Optimization, Robotics and Biomechanics Group, Heidelberg University, Heidelberg BW, Germany
[2]Neuromuscular Diagnostics Group, Technical University of Munich, Munich BY, Germany
[3]Human Performance Laboratory, University of Calgary, Calgary AB, Canada
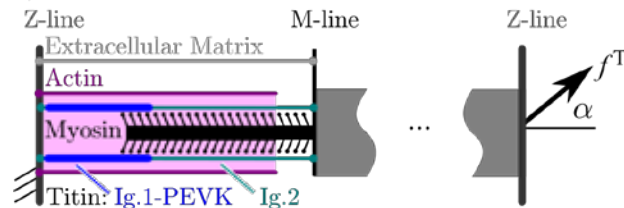corresponding author: matthew.millard@ziti.uni-heidelberg.de

INTRODUCTION

The mechanical impedance of active muscle affects the stability of musculoskeletal systems to perturbations. Active muscle exhibits positive stiffness both when stretched modestly [1] and when stretched beyond actin-myosin filament overlap [2], which neither a Hill nor a Huxley muscle model can replicate. Following the work of DuVall et al. [3], we have developed a three filament muscle model in which myosin loads titin when shortening and clutches onto titin during lengthening. A virtual active lengthening experiment indicates that this mechanism can explain the steady increase of force during muscle stretching but that the model is missing terms related to residual force enhancement.

METHODS

We model the musculotendon as a scaled half-sarcomere composed of actin, myosin, titin, and an extracellular matrix (Fig. 1a). The passive elastic component of the fibre has been partitioned into a 60% extracellular matrix component and a 40% titin component [4]. Titin's elasticity has been further decomposed into a lumped proximal Ig and PEVK section, and a distal Ig section, which maintain the relative passive strains observed by Trombitás et al. [5].

The model has two kinematic degrees of freedom: the length (ℓ^M) of the fibre, and the length (ℓ^1) of the proximal lumped section of titin. We formulated the state derivatives so that during active shortening the cross-bridges within the actin-myosin overlap (ℓ^W) pull on titin (Fig. 1b). During active lengthening, the cross-bridges continue clutching titin (Fig. 1c). We evaluated the model by simulating an active stretch [1] using both the proposed model and a Hill model [6].
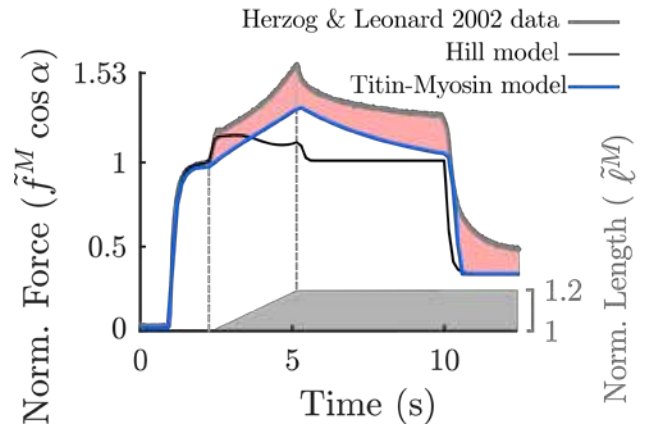

Figure 2: Simulation of an active lengthening experiment.

RESULTS AND DISCUSSION

The proposed model exhibits positive stiffness during active lengthening while the Hill model exhibits a region of negative stiffness (Fig. 2). It is interesting to note that while the Hill model's force-velocity curve allows it to follow the initial force transient of the experimental data, this transient may not be due to damping: after the ramp ends the Hill model's damping forces vanish but in the experimental data these forces persist. The consistency of the error from the proposed titin-myosin model (Fig. 2, pink region) suggests that the same phenomena might be responsible for short-range-stiffness, residual-force-enhancement, and passive force enhancement.

ACKNOWLEDGEMENTS

REFERENCES

[1] Herzog W et al. (2002). J Exp Biol, 205:1275-1283.
[2] Leonard TR et al. (2010). J Biomech, 43: 3063-3066.
[3] DuVall MM et al. (2017). J Exp Biol, 220: 4418-4425.
[4] Prado LG et al. (2005). J Gen Physiol, 126: 461-480.
[5] Trombitás K et al. (1998). J Struct Biol, 122: 188-196.
[6] Millard M et al. (2013). J Biomech Eng, 135: 021005.

Figure 1: A three-filament half-sarcomere model

Residual Force Enhancement in Cardiac Myofibrils on the Ascending Limb of the Force-Length Relationship

Seong-won Han[1], Venus Joumaa[1], Azim Jinha[1], Walter Herzog[1]

[1]Human Performance Laboratory, Faculty of Kinesiology, University of Calgary, Calgary, AB, Canada

Email: seongwon.han@ucalgary.ca

Introduction

Residual force enhancement (RFE) is defined as the increase in the steady-state, isometric force of a muscle following an active stretch compared to the corresponding (same length, same activation) force of a purely isometric contraction. RFE has been consistently observed in skeletal muscle. However, there are conflicting observations regarding the occurrence of RFE in cardiac muscle [1, 2]. The presence of RFE in cardiac muscle may not necessarily improve cardiac function but may provide insight into the possible mechanism of RFE. It has been suggested that the molecular spring, titin, plays a major role in RFE in skeletal muscle. Cardiac muscle has shorter titin isoforms than skeletal muscle, and thus might show different RFE properties. The purpose of this study was to re-examine RFE in cardiac myofibrils, thereby resolving the controversy that exists in the literature [1, 2], and gain novel insights into cardiac RFE based on the eventual findings.

Methods

RFE was measured following active stretching of rabbit cardiac myofibrils across three different sarcomere length ranges: i) 1.8-2.0 µm, ii) 2.0-2.2 µm, and iii) 2.2 – 2.4 µm. Eight myofibrils were used for the first two length ranges, and four myofibrils were tested for the third length range. Myofibrils isolated from the left ventricle of rabbits were set at an average sarcomere length (SL) of 1.8 µm, 2.0 µm, or 2.2 µm, passively stretched to an average SL of 2.0 µm, 2.2 µm or 2.4 µm, respectively, and then activated to measure the purely isometric force (control experiments). Myofibrils were then quickly shortened to the initial lengths, and actively stretched back to an average SL of 2.0 µm, 2.2 µm, or 2.4 µm to induce RFE, if present. Wilcoxon signed-rank testing was used to compare the purely isometric force and the steady-state, isometric force after active stretch.

Results and Discussion

In total, all 20 myofibrils showed RFE in this study. Specifically, RFE was observed at all length ranges tested: after active stretch from an average SL of 1.8 µm to an average SL of 2.0 µm (Fig. 1b, mean ± SD = 20.7 ± 9.1 %, p = 0.008), from an average SL of 2.0 µm to an average SL of 2.2 µm (Fig 1b, mean ± SD = 16.8 ± 3.2 %, p = 0.012), and from an average SL of 2.2 µm to an average SL of 2.4 µm (Fig 1b, mean ± SD = 13.4 ± 3.7 %). There was no statistical difference in RFE between the length range of 1.8 µm – 2.0 µm and 2.0 µm – 2.2 µm. Further data will be collected for the third length range.

RFE is thought to be caused by a stiffening of titin upon muscle activation, by either calcium binding to titin and/or

titin binding to actin [3]. Since cardiac muscle is able to produce RFE, we may suggest that cardiac titin can lead to RFE. The mechanism by which titin indeed regulate active force needs further investigation.
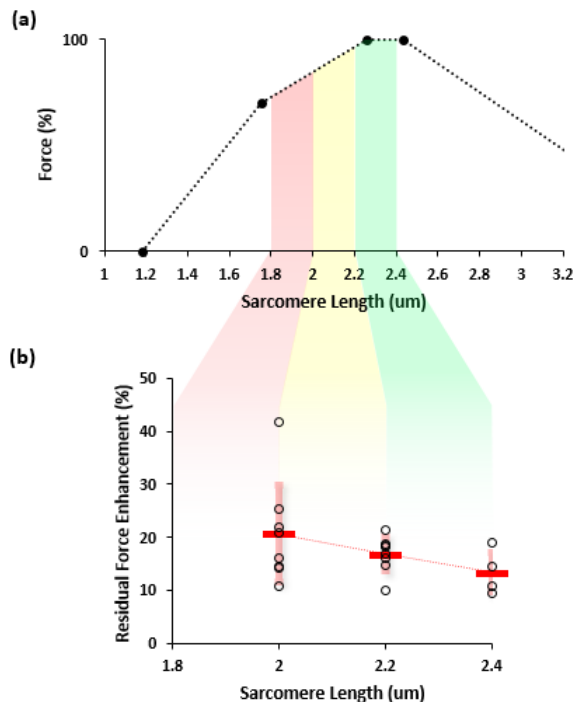

Figure 1. (a) Force-length relationship of rabbit muscle; (b) RFE (%) as a function of the length range tested. Each open circle is a single data point and the solid red bar shows the average of the given length ranges.

Conclusions

Cardiac myofibrils expressing shorter titin isoforms show RFE, suggesting that RFE is not specific to skeletal muscle and can be obtained with vastly different titin isoforms.

Acknowledgments

References

[1] Cornachinone A. S. et al. (2016). *Am J Physiol Cell Physiol*, **310**: C19-C26.
[2] Boldt K. et al. (2015). *Biophysical Society Meeting*
[3] Herzog W. et al. (2006). J Physiol, **574(Pt 3)**: 635-42.

The Muscle Mechanical Basis of Freeman-Sheldon Syndrome

Kaylyn M. Bell[1], William A. Kronert[2], Yiming Guo[2], Deepti Rao[2], Alice Huang[1], Sanford I Bernstein[2], Douglas M. Swank[1]
[1]Department of Biological Science and Biomedical Engineering, Center for Biotechnology and Interdisciplinary Studies,
Rensselaer Polytechnic Institute, Troy, NY, USA
[2]Department of Biology, San Diego State University, San Diego, CA, USA
Email: bellk2@rpi.edu

SUMMARY

We have engineered the first animal models to study Freeman-Sheldon Syndrome (FSS) by expressing transgenic myosin containing FSS-causing point mutations Y583S and T178I in *Drosophila* [1]. We studied the mutations' effects on indirect flight muscle (IFM) and jump muscle mechanical properties to elucidate possible mechanisms of disease. We found that increased muscle stiffness leads to diminished power production.

INTRODUCTION

Freeman-Sheldon syndrome is the most severe form of distal arthrogryposis and is characterized by facial and distal muscle contractures, paired with increases in muscle stiffness. These ailments lead to immobilization of patients' extremities, resulting in a negative impact on their lives.

METHODS

We performed skinned muscle mechanical analysis on *Drosophila* IFM and jump muscles dissected from heterozygous FSS mutant flies. Sinusoidal analysis and work loop experiments were used to measure maximum power generation, stiffness and overall muscle kinetics in IFMs by oscillating the muscle fibers at various frequencies and muscle length amplitudes.

To investigate mechanistic changes of a single cross-bridge cycle step, we varied [ATP] and performed IFM sinusoidal analysis to assess how ATP response varied in the FSS mutants.

Activation and relaxation experiments were performed on the jump muscles. Muscles underwent repetitive activation events using a rapid bath exchange system, while tension was continuously recorded. Data were fit with a logistic curve to calculate rates.

RESULTS AND DISCUSSION

The most striking alterations were the 70% and 77% increases in elastic moduli for the Y583S and T178I IFM fibers, respectively, which coincides with the human disease phenotype of increased stiffness (Figure 1). Increased stiffness impaired maximum power production, as it decreased by 45% and 62% due to an increased amount of work being absorbed by the muscle during lengthening. A contributing factor to both decreased power and increased stiffness was a slowing of at least one cross-bridge cycle transition. This was inferred from 17% and 31% decreases in the frequency that generated maximum power (f_{max}).
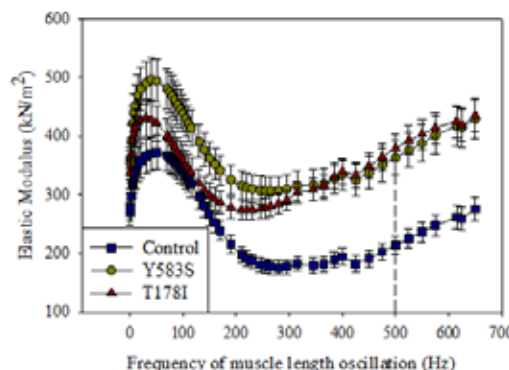

Figure 1: FSS mutations drastically increase muscle stiffness. Dashed line at 500 Hz is where percent increases were calculated.

f_{max} vs. [ATP] data were fit with a Michaelis Menten curve, which revealed that the T178I myosin has a lower affinity for ATP, as shown by a larger K_m value. Therefore, T178I myosin spends a prolonged period of time bound to actin, contributing to the increase in stiffness.

This prolonged binding also impedes T178I muscle's ability to relax as shown by a 16% decrease in relaxation rate. Additionally, Y583S and T178I activation rates slowed by 21% and 15%, respectively. We speculate that the rate of Pi release is influencing these changes in activation rates since it has been shown to influence force generating steps of the cross-bridge cycle [2]. It could be valuable to examine the rate of Pi release in the Y583S mutant since no difference in ATP affinity was observed.

CONCLUSIONS

Understanding the disease mechanisms behind FSS will help improve research for treatment options in patients currently suffering from its symptoms. Our work suggests that FSS myosin spends prolonged periods of time bound to actin due at least in part to low ATP affinity. We conclude that contractures seen in Freeman-Sheldon Syndrome likely result from elevated muscle stiffness and decreased ability to power limb movement.

ACKNOWLEDGMENTS

REFERENCES

[1] Rao D et al. (2019). *Mol. Biol. Cell*, **30**: 30-41.
[2] Hibberd MJ. (1985). *Science*, **228**: 1317-1319.

Adductor Longus Myofibrillar Passive Stiffness is Reduced in Cerebral Palsy

Timothy Leonard, Venus Joumaa, Kelly Larkin-Kaiser, Walter Herzog
Faculty of Kinesiology, University of Calgary, Calgary, Alberta, Canada
corresponding author: leonard@ucalgary.ca

INTRODUCTION
It is generally accepted that spastic cerebral palsy (CP) muscle is stiffer than normal muscle in whole muscle and single fibers, but there is little agreement on the mechanisms behind this observation. Previous research has shown that the CP sarcomere is overstretched compared to normal, and operates at long sarcomere lengths [1]. At these increased lengths, the overstretched sarcomeres would have low active force-generating capacity and high passive forces. However, it is not clear whether the sarcomeres are intrinsically stiffer in CP compared to normal muscles. The isolated myofibril is devoid of passive structural elements outside of the sarcomere, such as collagen, and so experiments at this hierarchical level may provide crucial insight into the stiffness of sarcomeres in CP.

PURPOSE
To compare passive stress generation under stretch (i.e. stiffness), titin isoforms and *in-vivo* sarcomere lengths between myofibril samples acquired from children with CP and those from typically developing children.

METHODS
Under general anesthesia, biopsies of operated adductor longus muscle (CP=9, non-CP=2) were obtained and held at the *in vivo* length for later *in-vivo* sarcomere length (SL) determination. Samples of muscle were collected and either frozen in liquid nitrogen for later titin gel electrophoresis or were placed in a special rigor solution for generation of myofibrils for mechanical testing [2]. Statistical significance was set at $p < 0.05$.

RESULTS AND DISCUSSION
At all ranges of matched SL under 4 μm, passive steady-state stress was significantly lower in CP compared to non-CP myofibrils (Figure 1). The elastic modulus for CP was 98±45kPa and was significantly smaller than for non-CP (166±22kPa; p=0.0005).
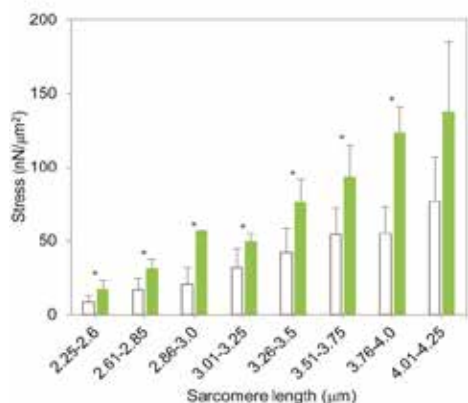

Figure 1: Passive steady-state stress (Mean±SD) versus sarcomere length for adductor longus CP (white) and non-CP (green) myofibrils. * indicates a significant difference from non-CP.

Titin molecular weight for CP and non-CP were not different (3611±41kDa and 3615±32kDa respectively, p=0.76) but the ratio of titin:nebulin content for CP was lower from non-CP (1.47±0.37 vs. 3.26±0.16, (p=0.004)), indicating a reduction in titin quantity in the CP tissue.

The mean *in vivo* SL for CP was 3.6±0.3μm, much longer than the *in vivo* SL reported for the adductor longus from typically developing children (2.6μm) [3].
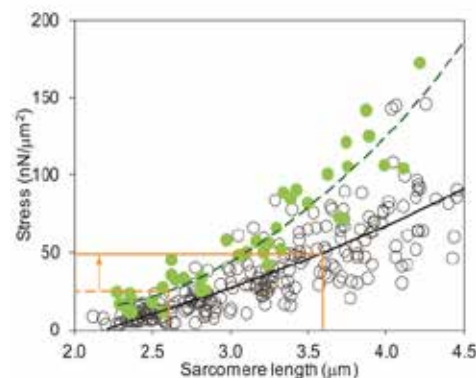

Figure 2: Best fit curves for passive stress versus sarcomere length for adductor longus CP (black line, white circles) and non-CP (dashed green line, green circles) myofibrils. CP myofibrils are under increased stress at *in vivo* sarcomere lengths (3.6 μm-orange solid line) compared to stress for typically developing children (SL 2.6 μm-orange dashed line). CP stresses *in vivo* are significantly higher (orange arrow) than for typically developing controls.

At matched SL, passive stresses and elastic moduli were lower in CP myofibrils compared to typically developing controls. This is in contrast to findings in single fibres, fascicles and muscles, and might be an adaptation to reduce an already excessive passive force in spastic muscles. Despite the lower stresses in CP compared to control myofibrils, passive stress at *in vivo* sarcomere lengths is greater in CP than in typically developing children due to the long SL in CP (Figure 2). A ~50% reduction in the titin:nebulin ratio seems to relate well to the ~50% reduction in passive stress and elastic modulus of CP sarcomeres, and might be an adaptive response to partially offset the high passive stresses at *in vivo* sarcomere lengths of CP patients.

REFERENCES
[1] Lieber & Fridén. (2002). *Muscle Nerve*, **25**, 265-270.
[2] Joumaa et al. (2008). *Proc. R. Soc. B.,* **275**, 1411-1419.
[3] Mathewson et al. (2015). *J. Orthop. Res.*, **33**, 33-39.

34

Session 2:
Cellular Muscle Mechanics / Physiology

David Corr

Douglas Swank

Marlies Corvelyn

Ridhi Sahani

Nicole Mazara

Eng Kuan Moo

Chairperson: Venus Joumaa

History-Dependent Behaviour in *Drosophila* Jump Muscle: Do Myosin Kinetics Influence Force-Depression?

[1]Ryan A. Koppes, [1,2]Douglas M. Swank, **[1]David T. Corr**
[1]Department of Biomedical Engineering, Rensselaer Polytechnic Institute, Troy, NY, USA
[2]Department of Biological Sciences, Rensselaer Polytechnic Institute, Troy, NY, USA
corresponding author: corrd@rpi.edu

INTRODUCTION

Force depression (FD), the reduction of isometric force following active shortening, is a well-accepted, yet poorly understood, characteristic of skeletal muscle. The steady-state magnitude of FD (FD_{ss}) increases with the amplitude of shortening, and decreases with the speed of shortening. Our investigations of transient aspects of FD revealed that force redevelops more slowly with increased FD_{ss}; strongly suggesting a kinetic mechanism for FD [1]. Thus, the underlying mechanism(s) for FD likely resides, at least in part, in actin-myosin cross-bridging. Unfortunately, there are limited experimental ways to probe this phenomenon.

We recently developed a *Drosophila melanogaster* (fruit fly) model to study FD. *Drosophila* is an established, and genetically mutable animal, and our group has shown the Tergal Depressor of the Trochanter (TDT), or "jump muscle", closely mimics the biomechanics of mammalian skeletal muscle [2], and exhibits both transient and steady-state FD similar to mammalian skeletal muscle (*e.g.*, FD_{ss} increases with larger amplitudes and slower rates of shortening, and force redevelops more slowly with increased FD_{ss}) [3]. Thus, when coupled with our ability to manipulate sarcomeric structure and kinetics through transgene expression in *Drosophila*, the TDT provides unprecedented insight into the underlying mechanism(s) of FD. Herein, we explore the effect of expressing slower and faster myosin isoforms in the TDT, to gain insight into the role of myosin kinetics in this history-dependent behaviour.

METHODS

Drosophila TDT muscles were dissected from a fly line expressing wild-type myosin in its jump muscle (JMI), as well as two other fly lines: one transgenically expressing a slower, embryonic myosin isoform (EMB) [2], and one transgenically expressing the faster, indirect flight myosin isoform (IFI) [3]. Briefly, TDTs were dissected form the thoraces of 2-3 day-old female *Drosophila*, chemically demembranated, T-clipped, and mounted for testing on a custom microscope-based, multi-welled single-fiber mechanics rig. A battery of active shortenings was performed, starting from a stable isometric contraction on the descending limb and shortening to optimal length (FL_{opt}) [4]. To explore the influence of shortening amplitude and rate, fibers were shortened over three amplitudes (5, 10, 20% FL_{opt}) at the slowest rate (4% FL_{opt}/s), and at three different rates (4, 20, 200% FL_{opt}/s) over the longest amplitude (20% FL_{opt}). After shortening, the muscle length was held constant for 30s to allow force to return to steady-state, and the force over the final 3s was averaged to obtain the shortened steady-state value. FD_{ss} was calculated by subtracting this value form the isometric force at the final length, then normalizing by this isometric force to obtain FD_{ss} as a percent reduction in force.

Transient force recovery immediately after shortening was analyzed by fitting the force-time data with a double exponential recovery function, $F(t) = F_{inf} - (A_1 e^{-k_1 t} + A_2 e^{-k_2 t})$, to account for the fast (phase 1) and slow (phase 2) recoveries described by Ford et al. [5]. A_1 and A_2 are the amount, and k_1 and k_2 the rates, of fast and slow force recovery, respectively [4]. A block design two-way ANOVA was used to determine significant differences ($p < 0.05$), and regression analyses explored correlations between FD_{ss} and redevelopment rates (k_1, k_2).

RESULTS AND DISCUSSION

The three myosin isoforms displayed notable differences in the TDT. Isometric force at FL_{opt} was significantly higher in slow myosin (EMB) jump muscles, and lower in fast myosin (IFI) jump muscles, as compared to wild type (JMI). However, all myosin isoforms exhibited classic force depression behaviour: FD_{ss} increased with shortening amplitude, and decreased with shortening speed. The EMB line produced significantly higher proportional amounts of FD_{ss} (*i.e.*, % FD_{ss}) than both the IFI and JMI muscle lines, which were not statistically different themselves. Transient force recovery for each line exhibited a fast (A_1, k_1) and slow (A_2, k_2) phase of recovery, which was well described by the double exponential function. Following active shortening, the fast rate of recovery (k_1) has been associated with rotation of attached cross-bridges from a weakly-bound to strongly-bound state, whereas the slower recovery rate (k_2) is indicative of cross-bridge attachment (cycling) [5].

Regression analyses revealed that FD_{ss} did not correlate with k_1 in all three lines, nor with k_2 in the fast myosin (IFI) TDTs. However, FD_{ss} showed a strong negative correlation with k_2 in the EMB and JMI lines, indicating a slower phase 2 force recovery with increasing steady-state FD. This suggests that the FD mechanism plays a dominant role in the slower phase of force recovery, and thus is likely associated with cross-bridge cycling in the EMB and JMI lines. Additionally, because FD was significantly increased with the slower embryonic myosin (EMB), and the faster IFI line exhibited contrasting k_2 results to the two slower lines, these findings indicate that there is a kinetic mechanism to FD, and that is affected by myosin isoform dynamics.

REFERENCES

[1] Corr DT & Herzog W (2005) *J Appl Physiol*, **99**: 252-260.
[2] Eldred CC et al. (2010) *Biophys J,* **98**: 1218-1226.
[3] Zhao C & Swank DS (2017) *Am J Physiol Cell Physiol,* **312**: C111-C118.
[4] Koppes RA et al. (2014) *J Appl Physiol*, **116**: 1543-50.
[5] Ford LE et al. (1977) *J Physiol*, **269**: 441-515.

A myosin based mechanism for stretch activation and its possible purpose revealed by varying phosphate concentration in mammalian skeletal muscle fibers

[1]Chad R. Straight, [2]Kaylyn M. Bell, [2]Jared N. Slosberg, [1]Mark S. Miller, **[2]Douglas M. Swank**
[1]Department of Kinesiology, University of Massachusetts, Amherst, MA, USA
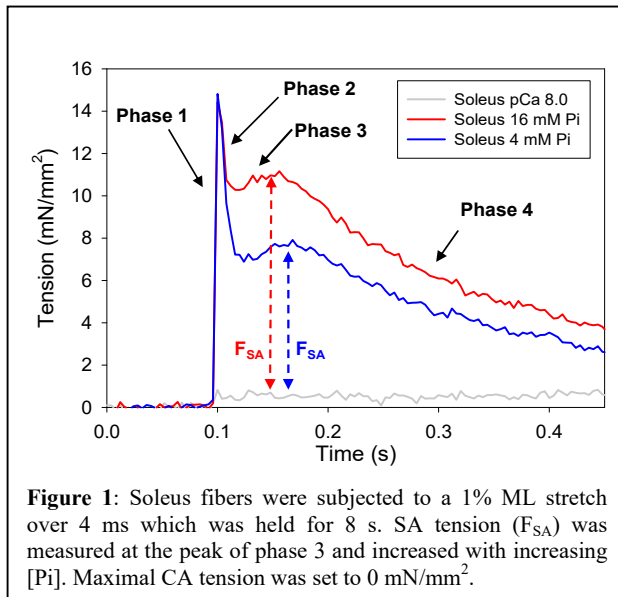[2]Departments of Biological Sciences & Biomedical Engineering
Rensselaer Polytechnic Institute, Troy, NY, USA
Corresponding Author: swankd@rpi.edu

INTRODUCTION

Stretch activation (SA) is a delayed increase in force following a rapid muscle length increase (phase 3 peak in Figure 1). SA is best known from asynchronous insect flight muscle where its very high magnitude enables it to replace calcium's typical role of modulating muscle force levels during a contraction cycle. SA also occurs in mammalian skeletal muscle, but has previously been thought to be too low in magnitude, relative to calcium-activated (CA) force, to be a significant contributor to force generation during locomotion.

Our recent myosin isoform exchange experiments in *Drosophila* jump muscle suggest that a myosin isoform based mechanism is responsible for setting SA force levels in muscles that display either minimal or moderate SA magnitudes. Elevated phosphate was critical for increasing jump muscle SA force, up to 4-fold higher, which suggests that SA force in mammalian skeletal muscle might also be higher when [Pi] is elevated, such as during extended use, and that skeletal muscle might use the same myosin isoform based mechanism.

Figure 1: Soleus fibers were subjected to a 1% ML stretch over 4 ms which was held for 8 s. SA tension (F_{SA}) was measured at the peak of phase 3 and increased with increasing [Pi]. Maximal CA tension was set to 0 mN/mm^2.

METHODS

To test these suppositions, we compared SA and CA tension at different Pi concentrations (0-16 mM) in skinned mouse soleus (slow-twitch) and extensor digitorum longus (EDL, fast-twitch) muscle fibers.
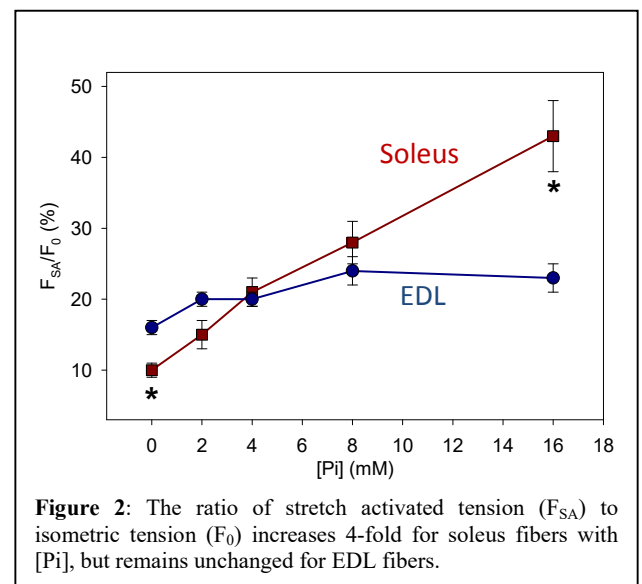
RESULTS AND DISCUSSION

CA isometric force decreased similarly in both muscles with increasing Pi, as expected. SA force decreased by 40% with

Pi in EDL, leaving the SA to CA force ratio relatively constant (17-25%) across Pi concentrations (Figure 2). In contrast, SA force increased in soleus, 42% (Figure 1), causing a quadrupling of the SA to CA force ratio, from 11% at 0 mM Pi to 43% at 16 mM Pi (Figure 2). This demonstrates that SA is a significant force modulator in slow-twitch mammalian fiber types.

This modulation would be most prominent during prolonged muscle use, which increases Pi concentration and impairs calcium cycling. To test if the timing of our *in vitro* SA kinetics matches the sarcomere length change rates used by mice while running, we overlaid a soleus muscle length change pattern with a 16 mM Pi SA trace from a soleus fiber. Synchronizing the start of the lengthening portions revealed that the phase 3 peak (SA peak) occurs when the soleus muscle powering running is shortening. This looks highly promising for skeletal F_{SA} to be physiologically relevant because augmenting force during the shortening portion of the soleus muscle's contraction cycle would increase work and power output.

Based upon our previous *Drosophila* myosin studies and this work, we propose two mechanisms to explain the different SA responses of EDL and soleus. A rapid stretch of a slow-twitch fiber, in the presence of Pi, reverses myosin's power stroke enabling quick rebinding to actin and enhanced force production, while in fast-twitch fibers stretch and Pi cause myosin to detach from actin without reversing the power stroke.

Figure 2: The ratio of stretch activated tension (F_{SA}) to isometric tension (F_0) increases 4-fold for soleus fibers with [Pi], but remains unchanged for EDL fibers.

ACKNOWLEDGEMENTS

37

Skeletal muscle stem cell properties from young children with Cerebral Palsy.

[1]**Marlies Corvelyn**, [2]Karen Maes, [2]Ghislain Gayan-Ramirez, [3]Anja Van Campenhout, [3]Sandra Prinsen, [1]Maurilio Sampaolesi, [4]Kaat Desloovere, [1]Domiziana Costamagna

[1]Stem Cell Biology and Embryology, Department of Development and Regeneration, KU Leuven, Leuven, Belgium
[2]Pneumology, Department of Chronic Diseases, Metabolisms and Ageing, KU Leuven, Leuven, Belgium
[3]Pediatric Orthopedics, Department of Development and Regeneration, KU Leuven, Leuven, Belgium
[4]Neurorehabilitation group, Department of Rehabilitation Sciences, KU Leuven, Leuven, Belgium
corresponding author: domiziana.costamagna@kuleuven.be

INTRODUCTION

Cerebral palsy (CP) is the single largest condition leading to childhood physical disability. This neurodevelopmental disorder is characterized primarily by neural deficits caused by a non-progressive lesion in the immature brain, and secondly by musculoskeletal problems that progress with age. The muscles of these patients develop differently than normal and alterations have been observed on macroscopic (e.g. reduced muscle volume, shorter muscle belly, longer tendons) as well as microscopic (e.g. hypertrophic extra-cellular matrix and fibrotic tissue accumulation) levels [1]. Unfortunately, the onset and the development of these muscle alterations are not well understood, since data on young CP patients are still lacking.

The skeletal muscle is a highly dynamic tissue, able to repair injuries by activating resident adult muscle stem cells, namely satellite cells (SCs) that after proliferation, start myogenesis. Other stem cell populations have been discovered to directly form new fibres such as mesoangioblasts (MABs) [2], or indirectly support the myogenesis through secretion of cytokines such as fibro/adipogenic progenitor cells (FAPs) [3, 4]. In CP children of different ages only a reduced number of SCs [5] with a lower myogenic potential have been reported [6].

The aim of this study is to analyze the proliferation and differentiation abilities of muscle stem cells together with their interactions in young children with CP.

METHODS

The current pilot study on children with CP and healthy volunteers (HV) has been set-up, as a starting point for an extended research project on macroscopic and microscopic muscle properties of CP growing children and age-matched typically developing children. A minimally invasive microbiopsy needle (14G) was used to obtain biopsies from the *Medial Gastrocnemius.* No pain or discomfort was reported due to this technique. Biopsies were collected from seven CP children, from 3 to 9 years old, with Gross Motor Function Classification System (GMFCS) level I-III and from three HVs between 20 and 30 years old. The muscle microbiopsies were cultured through explant technique for *in vitro* examination. SCs, MABs and FAPs were obtained using Fluorescence-activated cell sorting based on the expression of CD56, Alkaline Phosphatase and PDGFRa, respectively, as specific markers. We applied a 6-day myogenic differentiation on SCs and MABs and a 10-day adipogenic differentiation protocol on MABs and FAPs. Immunofluorescent analysis, based on Myosin Heavy Chain (MyHC) was used to assess the myogenic features of these cells.

RESULTS AND DISCUSSION

The results confirmed the feasibility of the muscle microbiopsy technique to obtain the three most frequent skeletal muscle stem cell populations and to perform differentiation experiments. Myogenic differentiation of SCs *in vitro* seemed to be impaired in CP patients based on MyHC$^+$ myotube morphology (Fig. 1). Moreover, the nuclear migration was found to be disturbed, since the nuclei rather co-localize instead of spreading along the myotube (white arrows, Fig. 1). As for SCs, also MABs fusion index will be analysed. FAP-like cell adipogenic potential, ELISA and qRT-PCR are expected to better elucidate gene activation and secreted cytokines able to guide muscle differentiation.

In conclusion, muscle stem cell differentiation abilities seem to be impaired in young children with CP. In the next phase, higher number of patients and age-matched typically developing children will be included.
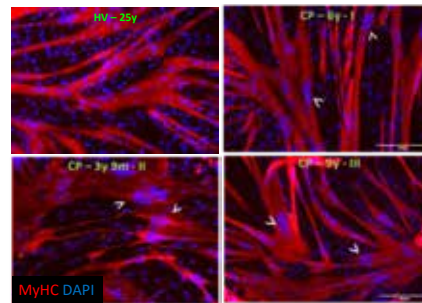

Figure 1: **myogenic differentiation of SCs from healthy volunteer and CP patients.** Immunofluorescent staining for 1 HV and 3 CP patients (Myosin Heavy Chain: red, Dapi: blue). White arrows indicate nuclear accumulation within the myotubes. Age and GMFCS levels are also indicated at the top of every image. Scale bar: 200μm.

ACKNOWLEDGEMENTS

REFERENCES

[1] Mathewson MA & Lieber RL. (2015). *Phys Med Rehabil Clin N Am,* **26**: 57-67.
[2] Sampaolesi M et al. (2003). *Science*, **301**:487-92.
[3] Joe AW *et al.* (2010) *Nat. Cell Biol*, **12**: 153–163.
[4] Uezumi A *et al.* (2010) *Nat. Cell Biol*, **12**: 143-152.
[5] Dayanidhi S *et al.* (2015). *J. Orthop. Res*, **33**: 1039–1045.
[6] Domenighetti AA *et al.* (2018). *Am J Physiol Cell Physiol*, **315**: 247–257.

Collagen Preferred Direction Relative to Muscle Fiber Direction in Three and Six-Month-Old Mdx Mice

[1]**Ridhi Sahani**, [1]Silvia S. Blemker

[1]Department of Biomedical Engineering, University of Virginia, Charlottesville, VA, USA

corresponding author: rs8te@virginia.edu

INTRODUCTION

Duchenne Muscular Dystrophy (DMD) is a fatal genetic disease with no effective cure or treatment to date. Progressive muscular degeneration results from a total lack of dystrophin, triggering an inflammatory cascade and excessive accumulation of extracellular matrix components such as collagen. As healthy muscle is replaced with fibrotic tissue, muscle stiffness increases and leads to dysfunction. While it is often assumed that an increase in collagen directly correlates with fibrosis, experimental and agent-based models of *mdx* mice revealed that an increase in area fraction of collagen correlates with decreased passive stiffness of *mdx* muscle [1]. Therefore, an increase in amount of collagen is not an effective predictor of increased muscle stiffness. Instead, changes to collagen's unique organizational structure may explain differences in mechanical properties of dystrophic muscle. The goal of this study is to capture collagen remodelling in DMD. In order to visualize collagen organization, we collected scanning electron microscopy (SEM) images of the epimysial layer at multiple scales. This allowed us to quantify collagen preferred direction relative to muscle fiber direction at collagen fiber and fibril levels and compare results between three and six-month-old *mdx* mice. We hypothesized greater disorganization in the six-month-old group, as DMD is a devastating muscle wasting disease that progresses with age.

METHODS

Four diaphragm samples were collected per age group and cut relative to muscle fiber direction. Decellularization protocol was followed to isolate collagen structure with digestion in 10% sodium hydroxide solution [2]. Samples were prepared and mounted for SEM and imaged at magnification ranging from 40 X to 200 KX. An image processing algorithm was developed to compare distribution of collagen orientation across magnification scales (Matlab). Each image was discretised into 32, 48x64 pixel windows and canny edge detection was used to determine fiber boundaries. The radon transform was computed at fiber boundaries, with rotation angle at the maximum peak used as a measure of dominant orientation and therefore collagen preferred direction. Images at 1 KX and 50 KX were selected for comparison of fiber and fibril orientation. At 1 KX, images revealed organization of collagen fiber (~10um) and muscle fiber direction was measured (ImageJ). At 50 KX, images revealed organization of individual collagen fibrils (~100nm). For both magnifications, collagen preferred direction relative to muscle fiber direction was reported with variance. An ANOVA was performed between the three and six-month-old groups at 1 KX and 50 KX. Independent two sample t tests assuming unequal variance were performed between the groups at each magnification and paired sample t tests were performed for each individual group between the magnifications.

RESULTS AND DISCUSSION

Images at 1 KX show a preferred direction of collagen fibers relative to muscle fiber direction. In the six-month-old group, fibers appear wavier as compared to the relatively straight fibers in the three-month-old group. Images at 50 KX show greater disorganization at the fibril level in both groups (Figure 1A). Variance in relative direction reveals greater anisotropy in the six-month-old group at the fiber level and greater anisotropy in fibrils for both groups (Figure 1B). At 1 KX, collagen preferred direction relative to muscle fiber direction was significantly different between groups. Additionally, collagen maintained its preferred direction relative to muscle fiber direction at the fiber and fibril level only in the three-month-old group (Figure 1C).
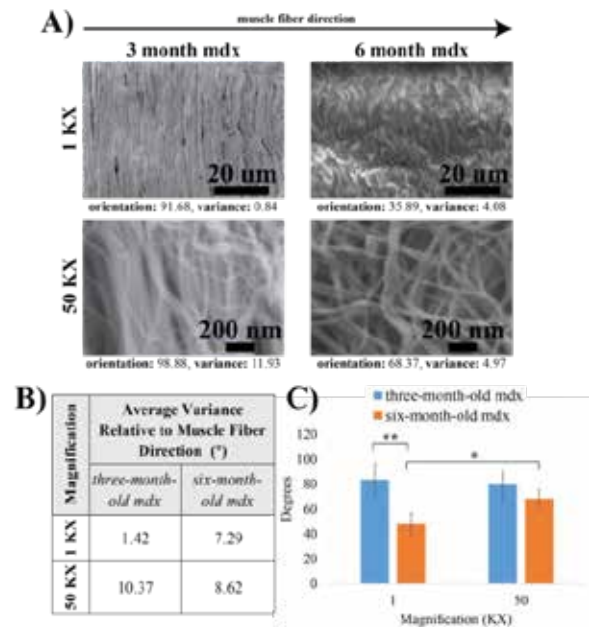

Figure 1: (A) SEM images of collagen relative to muscle fiber direction. (B) Average variance in measurements. (C) Average collagen preferred direction relative to muscle fiber direction with significance of $p<0.05$ (*) and $p<0.01$ (**).

Our findings suggest that collagen has a preferred direction relative to muscle fiber direction that is altered as DMD progresses with age in *mdx* mice. An increase in variance at low magnification also suggests that collagen remodelling is more apparent in individual fibrils. It is possible that disorganization begins in the collagen fibrils and extends to collagen fibers as DMD progresses. This approach to characterizing collagen remodelling allows us to better understand the physiology of dystrophic muscle. The relationship between collagen preferred direction and muscle fiber direction may explain force production of dystrophic muscle and will be further investigated.

ACKNOWLEDGEMENTS

REFERENCES

[1] Virgilio, K. et al. (2018) *In prep for J. Physiology.*

[2] Sleboda, D. et al. (2018) *Society for Integrative and Comparative Biology Annual Meeting.*

The Effect of Ca^{2+} on Rate of Force Redevelopment of Single Muscle Fibres in Young and Older Adults

[1]Nicole Mazara, [2]Derek P. Zwambag, [1]Alex M. Noonan, [1]Erin Weersink, [1]Stephen H.M. Brown, [1]Geoffrey A. Power
[1]Department of Human Health and Nutritional Science, University of Guelph, Guelph, ON, Canada
[2]Department of Kinesiology and Physical Education, Wilfrid Laurier University, Waterloo, ON, Canada
Nicole Mazara: mazaraln@uoguelph.ca

INTRODUCTION

Natural adult aging is associated with declines in skeletal muscle performance, and the underlying cellular mechanisms are still unclear. Cross-bridge mechanics are one area of potential influence on age-related muscle declines. Rate of force redevelopment (k_{tr}) is one measure used to explore the rate of cross-bridge attachment independent of regulatory proteins. In animal models, k_{tr} is [Ca^{2+}]-dependent [1], however it is unknown if this is also the case in human skeletal muscle or across age.

Recently, it has been shown that single muscle fibres of older adults have impaired Ca^{2+}-sensitivity compared to young adults [3,4]. It is likely that k_{tr} is also [Ca^{2+}]-dependent in humans, and if so, there could be an altered k_{tr}-Ca^{2+} relationship in older adult single fibres with impaired Ca^{2+}-sensitivity.

The purpose of this study was to investigate the k_{tr}-Ca^{2+} relationship of single muscle fibres from young and older adults, and to explore the effect of age-related alterations in Ca^{2+}-sensitivity on k_{tr}. We expected the k_{tr}-Ca^{2+} relationship to be similar to that of animal models, and that the impaired Ca^{2+}-sensitivity of older adult single fibres would be related to an age-related difference in k_{tr}.

METHODS

Participants included 8 young (22-35yrs) and 8 older (60-81yrs) males who were living independently and performing all activities of daily living. All procedures and protocols were approved by the local Research Ethics Board.

A percutaneous muscle biopsy of the *vastus lateralis* of each participant was performed. The muscle sample was put into storage solution (relaxing-glycerol 50:50 with protease inhibitors) for 24 hours and then placed in fresh storage solution at -20°C for at least 1 week and up to 4 weeks. Mechanical tests included maximal Ca^{2+}-activated force (P$_o$), force-pCa curves, and k_{tr}. All tests were performed at 16°C and ~2.8μm sarcomere length.

Fibre typing (type I [TI]; type II [TII]) was completed using SDS-PAGE. A pCa$_{50}$ value was calculated to determine differences in Ca^{2+}-sensitivity. A mono-exponential equation was used to fit the raw data trace from the slacken-restretch manoeuvre and calculate the rate constant k_{tr}. Analysis of mechanical tests were performed using custom programming in Matlab R2014b. Statistical analysis was completed in SPSS (IBM SPSS Statistics Version 25) and significance was set at alpha = 0.05.

RESULTS AND DISCUSSION

Of 182 single fibres tested, 67 (young) and 55 (old) were successful and used in analysis. 27 TI and 40 TII fibres in young, and 42 TI and 13 TII fibres in old were identified.

P$_o$ of the young fibres was 33% and 43% greater than old TI and TII fibres, respectively. Old TI fibres had a lower pCa$_{50}$, derived from force-pCa curves, compared to young TI that was trending toward significance (5.91 vs. 6.01; p=0.095), but old TII fibres had a significantly lower pCa$_{50}$ than young TII (6.06 vs. 5.91; p<0.05).

TII fibres had 48% and 40% higher k_{tr} than TI in young and old, respectively (p<0.05), however within fibre type, there was no age-related difference in k_{tr} (TI p=0.505; TII p =0.909). There was a main effect of pCa on k_{tr} for all groups (p<0.05).

There was no relationship between pCa$_{50}$ and k_{tr} for young TI (r^2=0.05, p=0.29) and TII fibres (r^2=0.08, p=0.08). However, there were significant k_{tr}-pCa$_{50}$ relationships for old TI (r^2=0.30, p<0.05) and TII fibres (r^2=0.44, p<0.05).
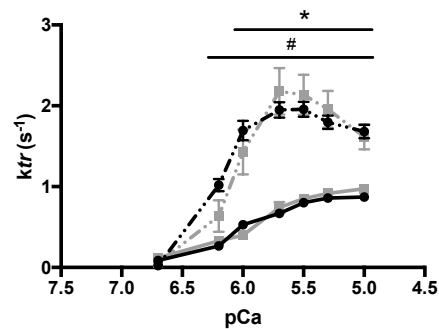

Figure 1: Average rate of force redevelopment (k_{tr}; s^{-1}) at each pCa level (5, 5.3, 5.5, 5.7, 6.0, 6.2 & 6.7) for each group: young (black circles), old (grey squares), type I (solid line), type II (dashed line). *significantly different from young and old type I, p<0.05. #significant effect of pCa on k_{tr} for all groups, p<0.05. Data mean ± S.E.M.

We showed a decrease in pCa$_{50}$ in old TII fibres compared to young, corroborating previous research [3,4]. Similar to animal models, k_{tr} behaves in a Ca^{2+}-dependent manner such that with increasing [Ca^{2+}], k_{tr} increases, to a plateau. Interestingly, k_{tr} was not different between young and old muscle fibres, despite a previous study indicating otherwise [4]. Furthermore, we found an association between pCa$_{50}$ and k_{tr} in both old TI and TII fibres. This Ca^{2+} association, combined with research indicating impairments in older adults Ca^{2+}-handling [3,4] suggests a potential Ca^{2+}-dependent mechanism for decline in skeletal muscle performance. Future research is needed to explore the role Ca^{2+} could be playing in age-related whole muscle declines.

ACKNOWLEDGEMENTS

REFERENCES

[1] Brenner B (1988). *PNAS*, **9**: 3265–3269.
[2] Lamboley CR et al. (2015). *J Physiol,* **11**: 2499–2514.
[3] Straight CR et al. (2018). *Exp Gerontol,* **102**: 84–92.
[4] Power GA et al. (2016). *Am J Physiol,* **4**: C318–C327.

The Influence of Muscle Architecture on Sarcomere Force-length Relationship in Intact Muscle

[1]**Eng Kuan Moo**, [1]Timothy R. Leonard, [1]Walter Herzog
[2]Faculty of Kinesiology, The University of Calgary, Calgary, AB, Canada
Corresponding author: ekmoo@ucalgary.ca

INTRODUCTION

Based on the 'sliding filament' theory [1], the maximal isometric force of a muscle at steady state depends on the sarcomere length (SL) and can be predicted from the thick and thin filament lengths. The sarcomere force-length (FL) relationship (also known as theoretical FL curve) has been validated experimentally for cylindrical-shaped single fibres [1] and myofibrils [2], but not for whole muscles. In the whole muscle, there exist great sarcomere length non-uniformities, complex geometries, and mechanical interactions between muscle cells and the surrounding structural network. It has been shown that the muscle architecture, such as muscle fibre length and pennation angle, can affect the functional properties of muscle [3]. Therefore, it is likely that sarcomeres residing in their natural environment behave differently from sarcomeres in isolated fibres/myofibrils, thus raising doubts on applying the sarcomere FL curve directly to a whole muscle. Due to the difficulty of visualizing single sarcomeres in activated muscles, the average SLs in resting muscles have been used to infer the maximal isometric force capacity of a muscle. Here, we developed a novel technique to examine if *in situ* SLs and forces measured in intact whole muscles reflect the theoretical FL curve.

METHODS

10 – 12 week-old mice (n=6) were anaesthetized, and the skin overlying the left tibialis anterior (TA) was removed. The distal tendon of the TA was removed from the foot and attached to an instrumented micro-manipulator that allowed for automated control of TA length and TA force measurement. After identifying a consistent reference length (L_r), the TA was stretched to five different muscle-tendon unit (MTU) lengths (L1: L_r+0.5mm; L2: L_r+1.5mm; L3: L_r+2.0mm; L4: L_r+3.0mm; L5: L_r+4.0mm). The TA was then supra-maximally stimulated. Muscle forces were measured and sarcomeres were imaged using second harmonic generation (SHG) microscopy for active and passive conditions at the five defined muscle lengths (L1–5). The resulting passive force–SL data were best-fitted to an exponential curve. The active force was derived by subtracting the passive force from the total force while taking into account the activation-induced shortening of the parallel elastic components [4]. SLs were measured from the mid-TA over an area of $160 \times 3 \mu m^2$. The theoretical FL curve was constructed based on thick (1.6 μm) and thin filament lengths (0.95 – 1.2 μm) found in the literature [5, 6].

RESULTS AND DISCUSSION

Muscle activation produced a distinct sarcomere shortening. Sarcomere lengths were not uniform at the five tested muscle lengths, as reflected by the horizontal error bars (± 1 standard deviation, SD) associated with each data point (Fig. 1). The experimental active sarcomere FL relationship exhibited the inverted U-shape of the theoretical FL curve with an ascending and a descending limb (Fig. 1A). The

passive sarcomere FL curve increased exponentially with increasing SL (Fig. 1B).
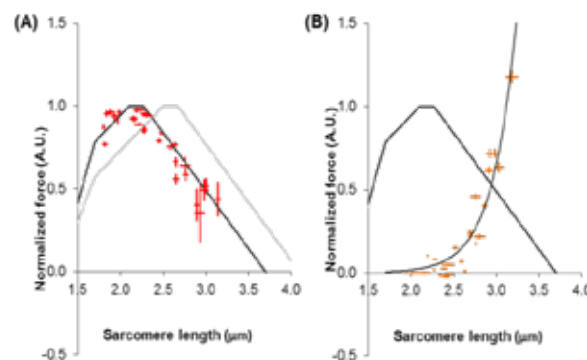

Fig. 1. Scatter plot of active sarcomere force-length data (A) and the passive sarcomere force-length data (B). There are thirty data points in each graph representing the average (mid-point) ± standard deviation (horizontal and vertical error bars) of sarcomere lengths and active forces measured in six muscles held at five MTU lengths. The black and grey inverted U-shaped curves represent the theoretical FL curve constructed using thin filament lengths of 0.95 μm [5] and 1.2 μm [6], respectively

The experimentally-measured FL curve fitted the theoretical FL curve constructed using thin filament length of 0.95 μm well, but was shifted to the left of the theoretical FL curve built using a thin filament length of 1.2 μm.

The 25% difference in thin filament lengths found in the literature [5, 6] was likely due to the age of the animals. Actin filament lengths in the mouse have been found to be longer in the first few weeks after birth than when the animals are skeletally mature [6]. The actin filament lengths of 1.2 μm and 0.95 μm were obtained from animals of 10-days old [5] and 11 – 12 week-old [6], respectively. [5]. Therefore, it appears to be important to construct the theoretical FL curve using thin filament length of the same species and age for accurate prediction of muscle force.

In conclusion, despite sarcomere length non-uniformity and the complex muscle architecture, the mean value of sarcomere lengths measured from a minute volume of the muscle predicts maximal isometric force as a function of length accurately. However, the theoretical FL curve needs to be constructed based on the length of the thin filaments that matches the species and age of the muscles used in the experiment. Our results validate the use of the sarcomere FL relationship in whole muscle, and should encourage extensive use of the sarcomere FL relationship in predicting human muscle properties in healthy and diseased states.

REFERENCES

[1] Gordon et al. (1966). *J Physiol*, **184**: 170-192
[2] Bartoo et al. (1993). *J Muscle Res Cell Motil*, **14**: 498-510
[3] Burkholder et al. (1994). *J Morphol*, 221: 177-190
[4] Rode et al. (2009). *J Mech Med Biol*, **9**: 105-122
[5] Witt et al. (2006). *EMBO J*, **25**: 3843-3855
[6] Gokhin et al. (2014). *Front Physiol*, **5**: 375

rMMs

Session 3:
In vivo Animal Muscle Function

Sabrina Lee

Marie Janneke Schwaner

Emily Abbott

Benjamin Binder-Markey

Tobias Siebert

David Lin

Heiliane de Brito Fontana

Chairperson: Monica Daley

rMMs

Musculoskeletal changes and adaptions – from aging to pathology in humans

[1]**Sabrina S.M. Lee**

[1]Department of Physical Therapy and Human Movement Science, Northwestern University, Chicago, IL, USA
corresponding author: s-lee@northwestern.edu

INTRODUCTION

Classic research in comparative morphology suggests that musculoskeletal structure are determinants of locomotor speed and other specialized functions. From fast running animals that have high gear ratios of the plantarflexors (Hildebrand, 1960) to specific moment arms of frogs (Lutz and Rome, 1994; Lieber and Boakes, 1988), to specialized muscle architecture such as longer fascicle length and greater pennation angle of racing dogs (Alexander, 1974) and frogs (Burkholder et al., 1994), it appears that the relationship between structure and function is tightly tuned in these animals that have specific functional demands. What about humans? One can contest that humans are not specialized in any particular task; rather, humans are capable of specializing, to a degree, in addition to daily tasks, a variety of demanding tasks such as sprinting, long distance running, and jumping. Furthermore, our functional demands and physiological changes across our lifespan due to age and pathology, require our musculoskeletal system to adapt to these changes. Here, using ultrasonograpy (B-mode and shear wave elastography) we will explore and discuss these changes and possible adaptations of musculoskeletal properties of the plantarflexor muscles (moment arm, architectural parameters, and mechanical properties) across several populations and the influence of these changes on force generation and performance.

REFERENCES

[1] Alexander RM (1974). *J Zool.*, **194**: 539-552.
[2] Burkholder TJ et al. (1994). *J Morphol.*, **221**: 177-190.
[3] Lieber RL and Boakes JL. (1988). *Am J Physiol.,* **254**:C769-C772.
[4] Lutz GJ and Rome LC. (1994). *Science*, **263**, 370-372.

Muscle Dynamics of the Vastus Lateralis in Jumping Kangaroo Rats (*D. deserti*)

Schwaner, M J [1], Lin, D C [2] and McGowan, C P [1, 3]

[1]Comparative Neuromuscular Biomechanics Lab, Department of Biological Sciences, University of Idaho, Moscow, ID USA
[2] School of Chemical Engineering and Bioengineering, Washington State University, Pullman, WA USA
[3]WWAMI Medical Education Program, Moscow, ID USA
e-mail: janneke.schwaner@gmail.com, web: http://www.webpages.uidaho.edu/McGowanLab/Research.htm

INTRODUCTION

Kangaroo rats, bipedal hopping rodents (family: Heteromyidae), use erratic vertical leaps to out-jump attacking snakes [1]. During these leaps the ankle joint is the main contributor to leg joint work [2]. In addition, up to 30% of the net joint work, measured at the ankle joint by inverse dynamics analysis, is being transferred from proximal muscles via bi-articular ankle extensors.

Therefore, the vastus lateralis (VL), a major knee extensor muscle, likely plays an important role in propelling the animal up in the air during take-off. Here, we examined the in-vivo performance of the VL muscle during vertical leaps over a range of jump heights. We hypothesized that that knee extension, muscle activity, and shortening strain all increase when jump height increases.

METHODS

Sonomicrometry (SONO) crystals and electromyography (EMG) electrodes were surgically implanted in the VL muscle of wild-caught desert kangaroo rats (*D. deserti*). Animals were stimulated to jump over an obstacle which was changed in height every trial (0.1 – 0.5 m), while taking-off from a force plate.

SONO and EMG data were collected at 2000Hz and simultaneously video data (200Hz) were collected using a high-speed camera (Xcitex Inc, Woburn, MA, USA), which was positioned perpendicular to the experimental set-up.

Data were analysed using a custom analysis script for Matlab (2015a, MathWorks, Natick, MA, USA). Jump height was calculated using ballistic equations and force data.

RESULTS AND DISCUSSION

Our data suggests that our hypothesis is supported. When jump height increases, net knee extension, muscle activity, and net muscle contraction (i.e. shortening strain) increase. These results suggest that, despite relatively small contributions by the knee to net joint work with increasing jump height [2], the VL likely increases the mechanical work it develops as jump heights get higher. Some portion of the energy generated by the VL may be transferred to the ankle joint via the biarticular ankle extensors. These results highlight the need to use caution when interpreting muscle function from inverse dynamics alone.
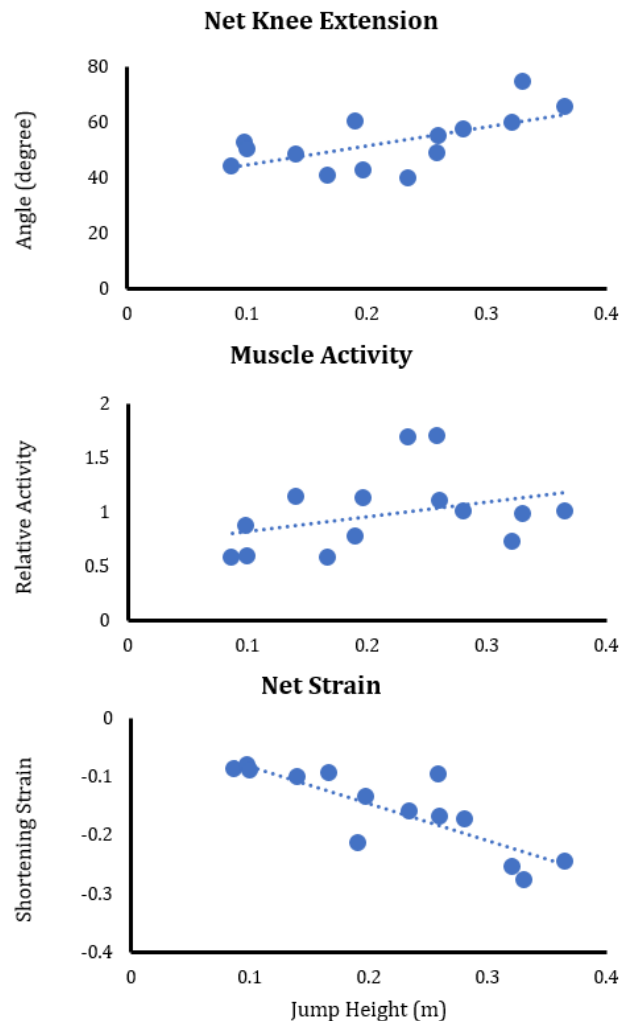

Figure 1: Knee extension, muscle activity and muscle shortening strain of the vastus lateralis (VL) muscle over jump height. Muscle shortening shows no change with increasing jump height. Net knee extension, muscle activity and, relative EMG activity (normalized against a maximal jump) does show a linear relationship with jump height.

ACKNOWLEDGEMENTS

REFERENCES

[1] Webster D & Webster M. (1980). *Am. Zool.*, **20**: 247-254.
[2] Schwaner MJ et al. (2018). *J Exp. Biol.,* **221** (22).

45

rMMs

Examining In Situ Changes to Proprioceptive Signals with Increased Muscle-Tendon Compliance

Emily M. Abbott[,1,2], Paul Nardelli[1], Timothy Cope[,1], Gregory S. Sawicki[1,2]
[1]School of Biological Sciences, Georgia Institute of Technology, Atlanta, GA, USA
[2]The George W. Woodruff School of Mechanical Engineering, Georgia Institute of Technology, Atlanta, GA, USA
Email: emily.abbott@me.gatech.edu

Summary

A major challenge in neuromechanics, particularly relevant to human health, is linking muscle-tendon (MT) morphology to proprioception. In anesthetized rats, we recorded intra-axonal sensory signals from active MT contractions. To modify the functional morphology, we physically added in-series springs. We demonstrated that as compliance increases, the gain of a muscle spindle declines. Therefore, conditions that alter MT compliance, like exercise, pregnancy, disease or aging, may modulate movements informed by sensory feedback.

Introduction

Muscle-tendon (MT) compliance can be altered by pregnancy, exercise, aging or disease, but, we know little about how series compliance affects sensory signals. This is because the field of sensory physiology has focused on conditions where MT length and fascicle length are coupled (passive stretches) and has often ignored the influence of elastic tissues (tendons, aponeuroses) on muscle dynamics. During a contraction, the presence of series elastic elements allows active muscle fascicles to shorten against net MT length that is isometric or stretched [1].

Generally, we characterize sensory sensitivity as a function of firing rate (FR) plotted against muscle length where the slope is called gain ($\Delta FR/\Delta L_{MT}$). With added compliance, we expect that the gain of length-related sensors (classically muscle spindles) will decrease and the threshold ($L_{MT}{}^*$) will increase in response to active MT stretching. Here, we only examine the gain component of sensitivity.

Methods

To create a mechanistic understanding of how MT morphology affects the sensory system, we combined in situ MT preparations with simultaneous intra-axonal recordings (female Wistar rats, IACUC #: A18042).
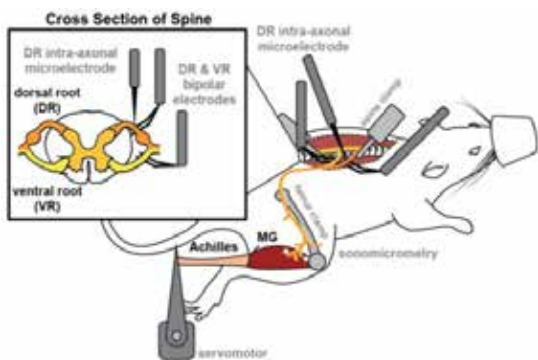

Figure 1: Medial gastrocnemius (MG) activated by stimulation of ventral root and instrumented with sonomicrometry crystals to measure muscle fascicle length. Firing rate of proprioceptors measured with intra-axonal microelectrode in the dorsal root and physiologically characterized as a muscle spindle or golgi tendon organ [2].

We changed fixed end compliance (FEC, muscle fascicle strain in response to isometric MT contraction) by suturing surgical tubing to the MT.

Results and Discussion

In this repeated measures study, we found that acute changes in MT compliance decrease the muscle spindle gain. These data suggest changes in morphology can affect sensory feedback.
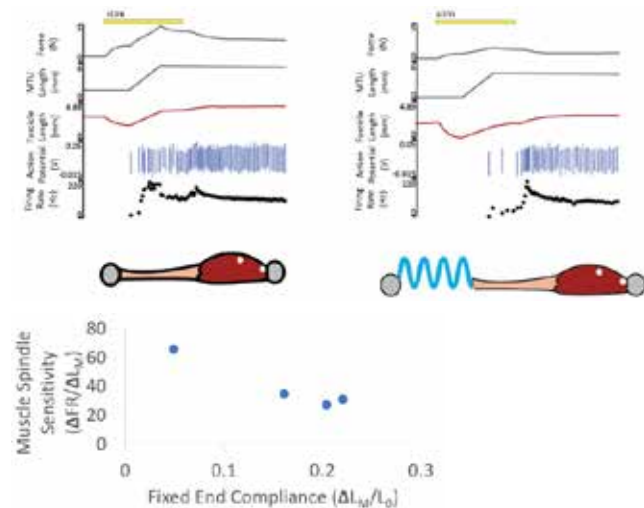

Figure 2A: We added compliance to change functional morphology of the MT. From top panel to bottom: MT Force (N), MT Length (mm), Muscle Fascicle Length (mm), Muscle Spindle Action Potential (V), Instantaneous Firing Rate (Hz). **2B:** During active stretch, muscle spindle gain decreased with added compliance.

Conclusions

Despite the importance of musculoskeletal morphology, we know little about how it relates to sensory physiology. We demonstrated that as MT compliance increases, the sensitivity of this muscle spindle feedback declines. This indicates that, without compensatory changes in motor coordination, conditions where MT compliance tends to increase (ex. aging, pregnancy), attenuated spindle feedback may impair response to locomotor perturbations. We expect to apply this paradigm to directly compare young and old MTs and gather insight into how assistive technologies could modify morphology to mitigate sensory deficits due to increased compliance [3].

References

[1] Sawicki et al. (2015). *J. Exp. Biol.,* **218**: 3150-3159.
[2] Vincent et al. (2017). *J. Neurophysiol.,* **118**: 2687–2701
[3] Robertson & Sawicki (2015). *Proc. Natl. Acad. Sci.,* **112**, E5891–E5898.

Intramuscular Anatomy Drives Muscle Collagen Content Variation, Likely Impacting Passive Muscle Stiffness

Benjamin I Binder-Markey[1,2], Nicole Broda[2], Richard L Lieber[2,1]
[1]Department of Physical Medicine and Rehabilitation, Northwestern University, Chicago, IL, USA
[2]Shirley Ryan AbilityLab, Chicago, IL, USA
Email: bbindermar@sralab.org

INTRODUCTION

Collagen is thought to be the main load bearing structure within muscle tissue [1]. However, previous studies have demonstrated a weak or non-existent correlation between collagen content and passive stiffness for both human and rodent muscles [2,3]. This may result from variability in the intramuscular anatomy and distribution of stiff (internal tendons and fascial sheets) and compliant (muscle fibers) tissues within the muscle such that a single collagen content value does not adequately represent the connective tissue load bearing capacity of a muscle. The purpose of this study was to quantify the relationship between collagen content and muscle anatomical variability.

METHODS

Four muscles, with varying actions and anatomy were dissected from 12-week old C57Bl6 mice hindlimbs (4 male, 4 female). Muscles included rectus femoris (RF), semimembranosus (SM), tibialis anterior (TA), and lateral gastrocnemius (LG). External tendons were removed and ~10 mg samples were blocked from proximal, middle, and distal regions of each muscle. In addition, samples of pure muscle, visible internal tendons or fascia removed, were taken from the midbelly of each muscle to estimate "pure" muscle collagen content. Collagen content was measured biochemically using a colorimetric hydroxyproline assay.
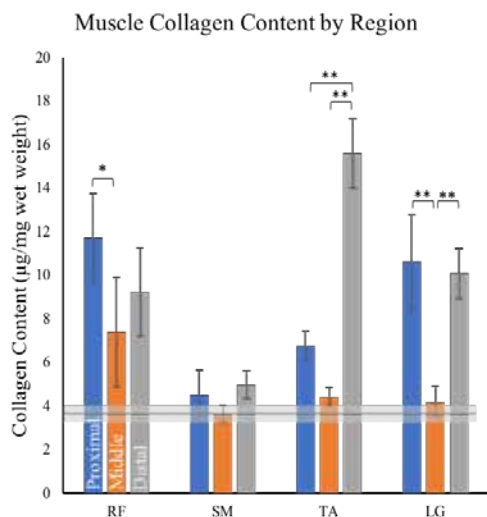

Figure 1: Mean±standard error of muscle collagen content by region (n=6/bar). Shaded grey line mean±standard error of pure muscle collagen content (n=16). (* <0.05, ** p<0.001)

To estimate the distribution of stiff and compliant tissues throughout the muscles, volume fraction of internal tendon and fascial sheets (V_t) and muscle (V_m) were calculated from the average collagen content (Col_{tot}), "pure" muscle collagen content (Col_m=3.6µg/mg), literature values of tendon content (Col_t=250µg/mg), and tissue density (ρ_m=1.06mg/mm^3, ρ_t=1.12mg/mm^3).

$$Col_{tot} = \frac{Col_t V_t \rho_t + Col_m V_m \rho_m}{V_t \rho_t + V_m \rho_m}$$

To verify volume fraction estimates, histological sections throughout the muscle lengths were stained with picosirius red to quantify the area fraction of internal tendons and fascial sheets. Area fraction was summed over 4-6 sections to match sample volume used in hydroxyproline assay.
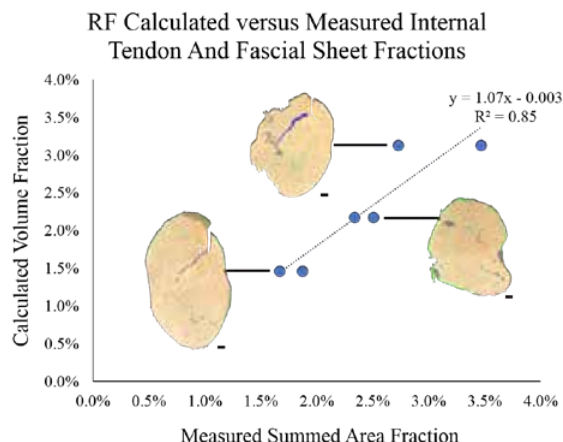

Figure 2: Correlation between histologically measured area fraction (n=2) and biochemically calculated volume fraction of internal tendon (blue) and facial sheet structures (green) within the RF. With representative sections (Scale bars=250µm)

RESULTS AND DISCUSSION

Collagen content varied widely from less than 4 µg/mg wet weight to over 14 µg/mg depending on muscle and region (Figure 1). Two-way ANOVA revealed a highly significant effect of muscle (p <0.001), region (p <0.001), and muscle x region interaction (p <0.001). In contrast to high variability across muscles, a one-way ANOVA did not reveal a significant difference in collagen content of pure muscle across muscles (p =0.098, power =0.497) (Figure 1).

The volume faction of internal tendon and fascial sheets likely drives the high variations in collagen content for the greatest variability occurred in pennate muscles with internal tendons, such as the RF, LG and TA. Within the RF we were able to estimate the volume fraction of internal tendon and fascial sheets using the total collagen content and verified these measurements using histologically measured area fraction (Figure 2). Quantification with increased sample size and remaining muscles is underway.

CONCLUSION

Collagen content variations associated with internal tendons and fascial sheets indicate that a single collagen value cannot adequately represent the muscle's connective tissue load bearing capacity. Future studies will investigate how collagen content and intramuscular anatomy can be used to predict the passive stiffness of whole muscles.

ACKNOWLEDGEMENTS

REFERENCES

[1] Purslow, P, (1989). *J Biomech*, **22**(1): 21-31.
[2] Chapman, M, et al. (2015). *J Biomech*, **48**(2): 375-8.
[3] Smith, L, et al. (2011). *J Physiol*, **589**(Pt 10): 2625-39.

47

Uniaxial transverse loading decreases muscle force

[1]**Tobias Siebert,** [2]Christian Rode, [1]Norman Stutzig
[1]Motion and Exercise Science, University of Stuttgart, Stuttgart, Germany
[2]Institut für Spezielle Zoologie und Evolutionsbiologie, Friedrich-Schiller-University, Jena, Germany
corresponding author: tobias.siebert@inspo.uni-stuttgart.de

INTRODUCTION

Muscles are embedded within other muscles, connective tissue, and bones. These neighbouring tissues may introduce longitudinal [1] and transverse forces (e.g. when sitting on the *M. gluteus maximus*) to the muscle that potentially modify e.g. the muscle architecture [2]. Recent studies restricting transverse muscle deformation by elastic bandages [3], rigid tubes [4], and plungers in transversal direction [5] showed changes in muscle architecture and performance, e.g. in muscle force, shortening, and work in the direction of the muscle's line of action. In this study, the influence of uniaxial transverse muscle compression via constant transverse loads on muscle force and geometric muscle deformation was examined and modelled.

METHODS

Isometric experiments were performed on isolated rat *M. gastrocnemius medialis* (n=9). Transverse loads of 0.64 to 2.60 N (6 - 23% maximum isometric muscle force, F_{im}) were applied. Loaded and unloaded contractions with supramaximal stimulation were compared. Muscle force was measured at the distal tendon and vertical movement of the plunger was determined using a high-speed camera. To simulate the interaction of a muscle with a uniaxial transverse load we used a Hill-type muscle model [6] with a geometric lever mechanism accounting for the influence of transverse load on longitudinal force (cf. Fig. 1A). The gearing (G) describes inversely proportional length changes and forces

$$G = \Delta h/\Delta l_{CC} = \Delta F_{im}/F_G,$$

with ΔF_{im} the decrease in F_{im}, F_G the gravitational load, Δh lifting height of the load, and Δl_{CC} shortening of the contractile component (Fig. 1A). During activation, the contractile component (CC) shortens by Δl_{CC} thereby stretching the series elastic component (SEC) by the same amount. At the same time, the load is lifted by Δh in transverse direction. Constancy of the muscle belly area (Fig. 1B, pink-colored) represents volume constancy in real muscle (neglecting change in muscle width), and represents the gearing G. We tested if this model can reproduce experimental changes in ΔF_{im} and Δh for increasing transverse loads. Three different gearing ratios were tested: (I) constant G_c, representing the idea of a muscle specific gearing parameter (e.g. predefined by the muscle geometry), (II) G_{exp} determined in experiments with varying transverse loads, and (III) G_f that reproduced experimental ΔF_{im} for each transverse load.

RESULTS AND DISCUSSION

Experimental muscle force decreased almost linearly from 4.9±1.4% to 12.8±2.0% with increasing transversal loads (0.64N to 2.60N) compared to the unloaded reference

contractions. Simulations using G_c overestimated ΔF_{im} (up to 59 %) and Δh (up to 136%) for increasing loads. For the lower loads (0.64, 1.13, 1.62 N), the model assumption (equal G for forces and length changes) held using G_{exp} and G_f. However, simulations resulted in underestimation of ΔF_{im} by 38% and overestimation of Δh by 58% for the largest load, respectively. To simultaneously reproduce experimental ΔF_{im} and Δh for the largest loads (2.11 and 2.60 N), it was necessary to reduce F_{im} by 1.9 % and 4.6 %, respectively. Moving towards three-dimensional computational neuromechanical animal models, the influence of transversal loads on muscle force should not be neglected. Recent studies [7,8] reported a reduction of 8-20% in muscle package force compared to the sum of forces generated by the isolated muscles.
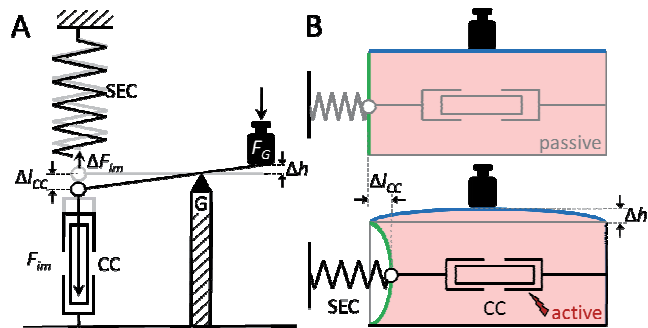

Figure 1: The simple model applied to account for a muscle deformation effect. (A) The lever model [6] for interaction of the muscle with transverse loads (Δh, Δl_{CC}, ΔF_{im}, F_{im} and F_G are magnitudes of vector quantities). (B) Schematic representation of muscle deformation. Constancy of the muscle belly area (pink-colored) represents volume constancy in real muscle (neglecting change in muscle width), and represents the gearing G. Colored green and blue lines represent elastic membranes allowing muscle deformation in longitudinal and transverse direction, respectively.

Our study shows that a constant, identical gearing between the considered forces and length changes does not exist. However, using a linear, load-dependent function for G, the model holds for transverse loads up to about 15 % F_{im} and may be applicable as a simple expansion of Hill-type muscle models to account for muscle deformation effects.

REFERENCES

[1] Huijing, P.A. (2009) *J Biomech* **42**, 9-21.
[2] Wick C et al. (2017) *JMBBM*, **83**: 20-27.
[3] Wakeling JM et al. (2013) *J Appl Biomech* **29**, 360-364
[4] Azizi E et al. (2017) *BMMB*, **16**: 1633-1643.
[5] Siebert T et al. (2014) *J Biomech,* **47**: 1822-1828.
[6] Siebert T et al. (2018) *J Biomech,* **66**: 57-62.
[7] de Brito Fontana et al. (2018). *J Biomech*, **79**: 15-20.
[8] Han et al. (2019). *J Exp Biol,* **222**.

How do the Contractile Properties of Individual Muscles within a Synergistic Group Combine?

[1,2]**David C. Lin**, [1]Mehrdad Javidi, [3]Craig P. McGowan
[1]Voiland School of Chemical Engineering and Bioengineering, Washington State University, Pullman, WA, USA
[2]Department of Integrative Physiology and Neuroscience, Washington State University, Pullman, WA, USA
[3]Department of Biological Sciences, University of Idaho, Moscow, ID, USA
corresponding author: davidlin@wsu.edu

INTRODUCTION

Multiple muscles often synergistically generate forces and moments across a common joint. Therefore, the contractile properties of the individual muscles within the synergistic group combine to form the mechanical properties of the joint. It could be that the combined properties are simply a weighted sum (based upon cross-sectional area) of the individual muscle properties, or how they combine may depend upon the joint angle, velocity, and/or moment.

The aim of this work is to determine how the force-length (F-L) and force-velocity (F-V) properties of individual plantarflexors of the kangaroo rat (k-rat) combine to determine the plantarflexor group properties. By recording the group properties under static and isotonic conditions while simultaneously measuring length changes in the individual muscles, we were able to separate the individual muscles contributions to the group F-L and F-V curves.

METHODS

All procedures were approved by the Institutional Animal Care and Use Committee at WSU and performed with 6 adult k-rats (*Dipodomys deserti*). Plantarflexors except for the soleus (2% of plantarflexor mass) were isolated *in situ*. Sonometric (SONO) crystals were placed on the medial and lateral gastrocnemii and plantaris (MG, LG, and PL respectively). Group musculotendon (MT) length or force was controlled by a servo motor attached to the combined tendons of the MG, LG, and PL.

For the F-L measurements, maximum isometric force from the group was elicited at 7 different MT lengths. The data collection was repeated after removing the PL and its tendon so that we could measure the F-L curve of just the LG and MG together (GAS), which have an integrated tendon in the k-rat. With the two F-L data sets and the SONO measurements, we were able to estimate the F-L curves for each muscle (GAS and PL) individually as well as in relation to a length scale relative to the group MT length.

For the F-V measurements, 9 isotonic trials were performed, ranging from 0.1 to 1.0 F_{max} (F_{max}=group isometric force). We then used two models to estimate the contributions from individual muscles. The first model assumed that the percent contributions did not change with isotonic load. The second model assumed that the F-V relationship of fibers within each muscle were identical (corresponding to fast fibers in k-rats) and included architectural differences amongst the muscles. Model predictions were statistically compared to calculations based upon SONO data, from which each muscle's force was estimated from its tendon stretch.

RESULTS AND DISCUSSION

The F-L curves showed that the optimal length of individual muscles did not align relative the group properties (Figure 1). The misalignment was equal to 1.8 mm, which was an amount that produced a maximal force within 5% of the greatest maximal force (when the optimal lengths are aligned). This suggests that the F-L curves of the two muscles combine to generate the greatest force possible, rather than extend the length range of force generation (when the optimal lengths are more misaligned).
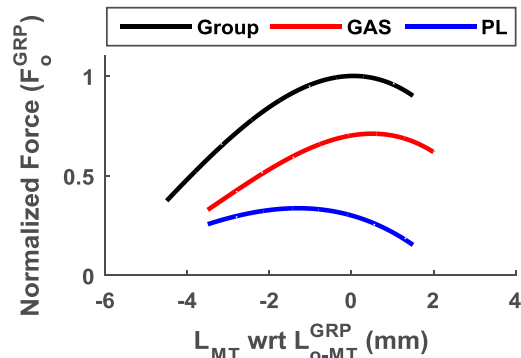

Figure 1: The group and individual F-L curves with force normalized to group isometric force (F_o^{GRP}) and length relative to the optimal length of the group F-L curve of the MT (L_{o-MT}^{GRP}).

For the F-V data, the first model predictions were significantly different than the SONO based calculations (P=0.0007), whereas the second model predictions were not (P=0.4690). The second model predicted that force contributions changed with the load (Figure 2), in agreement with SONO based calculations. Thus, the changes in the contributions were mainly due to differences in muscle architecture, namely fiber length and pennation angle, which determined fiber velocity for a given group muscle velocity.
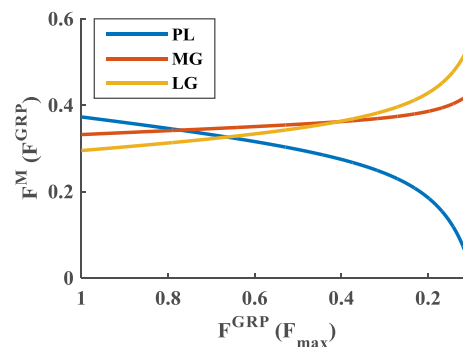

Figure 2: Contribution of individual muscles F^M (expressed as a fraction of the muscle group force (F^{GRP})) as a function of isotonic load of the muscle group (normalized to F_{max}).

ACKNOWLEDGEMENTS

Loss in agonistic muscle torque during simultaneous (submaximal) activation

[1]**Heiliane de Brito Fontana**, [2]Andrew Sawatsky, [2]Seong-won Han, [1]Daiani de Campos, [2]Walter Herzog
[1] Biological Sciences Center, Federal University of Santa Catarina, Florianópolis, SC, Brazil
[2]Faculty of Kinesiology, University of Calgary, Calgary, AB, Canada
Corresponding author: heiliane.fontana@ufsc.br

INTRODUCTION

Recently, it was shown that the maximal torque generating potential of individual muscles of the rabbit quadriceps group decreases, on average, by 20% when the muscles contract simultaneously [1].

We investigated three potential causes for the observed losses in torque generating potential during simultaneous activation compared to isolated activation: i) changes in moment arm, ii) interconnections between muscles and/or iii) intermuscular pressure. We hypothesized that (i) a similar amount of loss in muscle torque and force would be observed, (ii) removing intermuscular connections would not affect force or torque loss, and (iii) that decreasing inter-muscular pressures associated with decreasing activation/force levels would result in a decreasing loss in force generating potential of skeletal muscles during simultaneous activation [2].

METHODS

Five female New Zealand White rabbits were used in this study (average mass = 4.0 kg). All procedures were approved by the University's Animal Ethics Committee.

The branches of the femoral nerve responsible for the innervation of VL, VM, and RF muscles were dissected, and a nerve cuff type electrode was placed on each branch [3].

VL, VM and RF muscles were stimulated through electrical stimulation of the corresponding nerves in four experimental conditions: VL activation alone, VM activation alone, RF activation alone, and activation of all three muscles together.

Two animals underwent a submaximal activation testing protocol (knee 90° and frequency of stimulation from 20 to 100 Hz). For the other three animals, stimulation conditions were applied with the muscles intact initially, and then with muscles separated through blunt dissection (knee angle ranged from 40 to 120°, 100Hz).

Torque and force were simultaneously measured during contractions through a joint servomotor and a force transducer implanted in the patellar tendon. Torque and force output were compared between a) the value obtained by adding the output produced by VL, VM and RF when stimulated in isolation (SUM) and b) the output obtained from all three muscles activated simultaneously (SIM).

RESULTS AND DISCUSSION

The sum of the maximum torque capacity for the isolated stimulation (SUM) exceeded the maximum torque capacity for simultaneous stimulation (SIM) by 10-50% across all levels of activation (Figure 1). Regardless of joint angle and intermuscular connections between VL, VM, and RF, the differences in torque between SIM and SUM were also observed for the directly measured force values (Table 1).
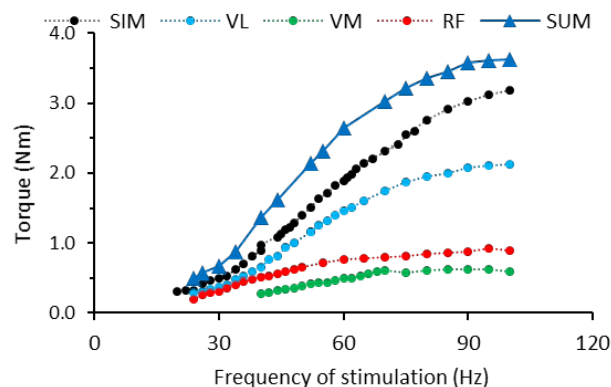

Figure 1: Torque produced by VL, VM and RF when stimulated in isolation and the resulting sum (SUM) and the torque produced by all muscles (VL, VM, RF) activated simultaneously (SIM).

Table 1: Loss in torque and force during simultaneous activation in muscles intact and separated through blunt dissection

		DIFFERENCE SIM -SUM (%)*	
		intact	separated
TORQUE	Rabbit1	$17 \pm 6\%$	$18 \pm 6\%$
	Rabbit2	$25 \pm 5\%$	$19 \pm 5\%$
FORCE	Rabbit1	$14 \pm 4\%$	$17 \pm 4\%$
	Rabbit2	$21 \pm 2\%$	$20 \pm 8\%$

* Values are normalized to torque/force at maximum force production under simultaneous activation of intact muscles.

There was a significant negative correlation ($r= - 0.738$, $p <0.001$) between the percent difference in torque generating potential between SIM and SUM and knee extensor torque/force (Figure 2),
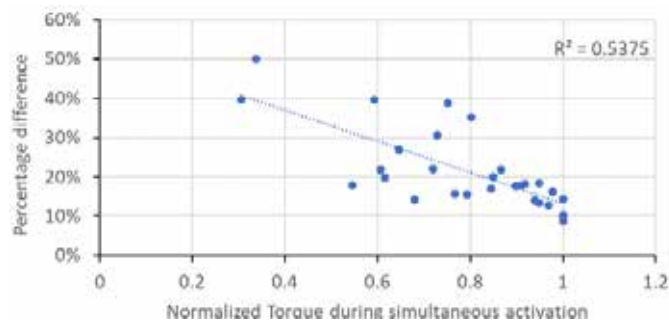

Figure 2: Torque loss during simultaneous activation ((SUM-SIM)/SIM*100 at each angle) as a function of torque level.

Neither intermuscular pressure, changes in moment arm, or intermuscular force transmission seem to be the cause for the force deficit observed in the SIM compared to the SUM conditions. Our findings imply that everyday movements performed at low levels of activation are affected by this force loss.

REFERENCES

[1] de Brito Fontana H et al. (2018). *J Biomech*, **79**: 15-20.
[2] Siebert T et al (2016). *J Biomech,* **49**: 1156–61.
[3] Han SW et al. (2019). J Exp Biol **in press**

Session 4:
In vivo Human Muscle Function

Daniel Hahn

Amy Adkins

Pavlos Evangelidis

Katherine Knaus

Ian Smith

Kaat Desloovere

Chairperson: Yasuo Kawakami

rMMs

History dependence of in vivo muscle force production: the role of muscle-tendon unit compliance

[1,2]**Daniel Hahn**, [1]Brent J. Raiteri
[1]Faculty of Sport Science, Ruhr University Bochum, Bochum, NRW, Germany
[2]School of Human Movement and Nutrition Sciences, The University of Queensland, Brisbane, QLD, Australia
Corresponding author: daniel.hahn@rub.de

INTRODUCTION

Active muscle shortening and active muscle lengthening respectively reduces and enhances the subsequent active force capacity of skeletal muscle. These phenomena describe the history dependence of muscle action [1,2] and have mainly been examined *in vivo* during dynamic contractions. However, even at a fixed muscle-tendon unit (MTU) length, history-dependent effects can occur. This is because of in-series compliance within intact MTUs, which permits muscle fascicles to shorten and lengthen during fixed-end contractions of increasing and decreasing force.

The purposes of this study were two-fold. First, we wanted to examine whether residual force depression (rFD) was present during voluntary fixed-end contractions of a moderately compliant MTU, the human tibialis anterior (TA). Second, during fixed-end contractions, we aimed to determine whether a reduction in muscle activity from a high to moderate level could abolish the initial rFD level.

METHODS

Ten participants performed fixed-end dorsiflexion ramp contractions to a low, moderate or high level while dorsiflexion force, electromyography (EMG) and ultrasound images of TA were recorded. Contractions were force- or EMG-matched and after the low or high contraction level was attained, participants respectively increased or decreased their force/EMG to a moderate level. Participants also performed moderate level contractions while the TA MTU was lengthened during the force/EMG rise to the reference MTU length.

Contractions were performed on an isokinetic dynamometer (IsoMed2000, D&R Ferstl, GmbH, Germany) with a custom-made force plate, which utilised four micro load cells (CZL635, Phidgets, Calgary, Alberta, Canada), attached to the dynamometer arm. The force signal was sampled at 1 kHz and amplified with a custom-built amplifier. EMG of the TA muscle was recorded using two electrodes (8 mm recording diameter, Ag/AgCl, Covidien, Mansfield, MA, USA) placed in a bipolar configuration at the distal portion of TA. A ground electrode was placed on the right ankle over the lateral malleolus. EMG signals were amplified 1000 times (AnEMG12, OT Bioelettronica, Torino, Italy) and band-pass analog filtered between 10 and 500 Hz, prior to being sampled at 2 kHz using a 16-bit Power-3 1401 and Spike2 data collection system (Cambridge Electronics Design, Cambridge, UK). TA muscle fascicle lengths and pennation angles with respect to the central aponeurosis were imaged using a linear, 128-lement transducer (LV7.5/60/128Z-2, Telemed) Ultrasound images were captured at a frequency of 6 MHz with a field of view of 60 × 50 mm (width × depth) and a frame rate of ~60 Hz using Echowave II software (Telemed). For further details, see [3].

RESULTS AND DISCUSSION

Dorsiflexion force in the force-matched session and TA EMG in the EMG-matched session matched the default forces and activity levels with ≤6% MVC difference between the default force/EMG and measured force/EMG.

Equivalent fascicle shortening over moderate and low to moderate level contractions did not alter EMG (P = 0.45) or dorsiflexion force (P = 0.47) at the moderate level. Greater initial fascicle shortening magnitudes (1.7 mm; P ≤ 0.01) to the high contraction level did not alter EMG (P = 0.45) or dorsiflexion force (P = 0.30) at the subsequent moderate level compared with moderate level contractions. TA MTU lengthening during the initial force/EMG rise reduced TA fascicle shortening (−2.5 mm; P ≤ 0.01), which respectively reduced EMG (−3.9% MVC; P < 0.01) and increased dorsiflexion force (3.7% MVC; P < 0.01) at the moderate level compared with fixed-end moderate level contractions.

The decrease in EMG and increase in dorsiflexion force induced by small reductions in fascicle shortening (20%-30%) during the force/EMG ramps provide indirect evidence of rFD in the TA during fixed-end contractions. A further key finding from the fixed-end contractions performed in this study was that initially greater fascicle shortening magnitudes during ramp contractions to a high level did not increase the steady-state EMG or reduce the dorsiflexion force at the subsequent moderate level compared with the purely moderate condition (where muscle fascicles shortened less overall). We speculate that the initially greater fascicle shortening to achieve the high contraction level induced more rFD and that greater rFD was not observed because of mechanisms related to residual force enhancement (rFE) that are triggered during active fascicle stretch as muscle activation declines and there is partial recoil of the in-series elastic tissues.

Our results indicate that the true in vivo force capacity of compliant MTUs is likely unknown. This is important for the scaling of force-length curves in Hill-type muscle models used in simulations of human movement. Further, we hypothesise that muscle history dependence is an important neuromuscular feature for human locomotion [3].

REFERENCES

[1] Chen, J., Hahn, D., Power, G.A. (2019). Shortening-induced residual force depression in humans. *J Appl Physiol* **126**, 1066-1073.
[2] Seiberl, W., Power, G.A., Hahn D. (2015). Residual force enhancement in humans: Current evidence and unresolved issues. *J Electromyogr Kinesiol*, **25**, 571-580.
[3] Raiteri, B.J., Hahn, D. (2019). A reduction in compliance or activation level reduces residual force depression in human tibialis anterior. *Acta Phys* **e13198**.

Quantifying in vivo variability in sarcomere length along the length of the long head of the biceps brachii

[1][4][5]**Amy N. Adkins**, [1][2][3]Julius P.A. Dewald, [1][2][3][4][5]Wendy M. Murray
Departments of [1]BME, [2]PM&R, and [3]PTHMS, Northwestern University, Chicago, IL, USA
[4]Shirley Ryan AbilityLab, Chicago, IL, USA
[5]Edward Hines, Jr. VA Hospital, Hines, IL, USA
corresponding author: **adkins@u.northwestern.edu**

INTRODUCTION

Whole muscle is made up of hundreds of thousands of sarcomeres arranged in series and in parallel. The lengths of a muscle's sarcomeres are a primary determinant of its ability to contract and produce force. In addition, when quantifying muscle architecture, sarcomere length is a critical parameter that is required to make meaningful comparisons of both the force-generating and excursion capacities of different muscles. With the advent of second harmonic generation (SHG) microendoscopy for measuring sarcomere length minimally invasively, there are exciting and novel opportunities to measure sarcomere length in vivo. Importantly, this method provides a small field-of-view (82µm x 82µm, ~20-35 sarcomeres in series). Animal muscle studies [e.g. 1] and a single in vivo study on the tibialis anterior [2] illustrate that sarcomere length can vary considerably throughout a muscle. Given these data, it is necessary to evaluate intramuscular variability in sarcomere length in vivo, in order to develop robust experimental protocols that ensure the data provide accurate representations of a muscle's sarcomere lengths.

In this pilot study, we evaluated the variability of sarcomere lengths along the length of the long head of the biceps brachii in vivo by repeating measurements at multiple locations along its proximal-distal axis.

METHODS

Sarcomere lengths in the biceps brachii were measured in four locations under passive conditions in a single individual (1 female, 28 yrs) with the shoulder abducted 85° and the elbow extended 25° (Figure 1). The participant provided informed consent; Northwestern University's Institutional Review Board approved this study's procedures.

To image sarcomeres *in vivo*, a microendoscopic needle was inserted into the long head of the biceps brachii with its optical lenses aligned parallel to the fascicle direction. Insertion of the probe was guided through palpation techniques and ultrasound imaging. A microscope (Zebra Medical Technologies, Palo Alto, CA) which uses second-harmonic generation to capture the intrinsic striation pattern (A-bands) of sarcomeres was attached to the needle for imaging. Four insertions were made; insertions near the distal and proximal ends of the muscle belly (position 1 and 4), and two insertions in the center of the muscle belly approximately 1cm apart (positions 2 and 3). Images were collected at 1.9Hz for about 2-5 minutes (~250-600 images). Offline, the fast Fourier transform (FFT) of each image was taken and noise in the spatial frequency was smoothed and filtered. Mean sarcomere length per image was calculated by determination of the fundamental spatial frequency of the striation pattern along the muscle fiber direction [3].

RESULTS AND DISCUSSION

Median sarcomere lengths among all images collected at each insertion site were 3.86µm for positions 1-3 and 3.59µm for position 4 (Figure 1). Assuming a biceps fascicle length measurement of 14 cm in the same limb posture, the differences between median sarcomere lengths measured along the proximal-distal axis would yield differences in optimal fascicle length calculations of less than 1 cm (average: 0.35cm, range: 0-0.7cm). For positions 1-3, the full range of sarcomere lengths measured at each insertion site was as large as the maximum difference in median lengths (0.27 µm) among sites. Assuming these results are consistent among additional participants, they support the approach of obtaining data from a single, central insertion site in the muscle belly as opposed to subjecting an individual subject to multiple needle insertions for this fusiform muscle.

REFERENCES

[1]   Moo et al. (2016). *Front Physiol,* **7**: 187.
[2]   Lichtwark et al. (2018). *J App Physiol,* **6:** 1812-20.
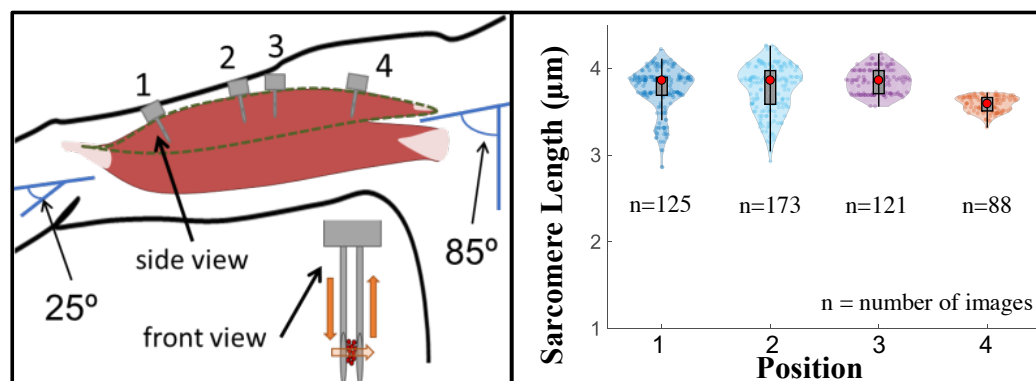[3]   Sanchez et al. (2015). *Neuron*, **88**:1109-1120.

Figure 1 – (left) Schematic of arm position and location of probe insertion in the long head of the biceps brachii. Illustration of probe showing the direction of laser light (orange). (right) Violin plot showing median of data (open circle), interquartile range (box plot), all the data per position (filled in circles), and probability density of data at each sarcomere length value (filled in shape).

Fatigue-induced Changes in Hamstrings Shear Modulus and Load Distribution Depend on Contraction Type.

[1,2]**Pavlos Evangelidis**, [1]Xiyao Shan, [1]Shun Otsuka, [1]Chi Yang, [1]Takaki Yamagishi, [1]Yasuo Kawakami
[1]Faculty of Sport Sciences, Waseda University, Tokyo, Japan
[2]Japan Society for the Promotion of Science, Tokyo, Japan
corresponding author: pavlos.evangelidis@gmail.com

INTRODUCTION

Following exercise, hamstrings exhibit inter-muscular differences in neural [1] and metabolic activity [2] suggesting selective recruitment and fatigue. It is expected that the most fatigued muscle would have reduced capacity to actively exert contractile forces and/or resist excessive mechanical strains, with the latter possibly related to susceptibility to strain injury. However, the influence of fatigue and contraction type on load distribution and stiffness of individual hamstring muscles remains unclear. Muscle shear modulus during contraction, measured with shear wave elastography (SWE), is closely related to muscle activation and force response and has been used as an index of load distribution among agonist muscles [3]. We used SWE to examine the effect of neuromuscular fatigue on shear modulus and load distribution among the individual hamstring muscles during an isometric (ISO), concentric (CON) and eccentric (ECC) submaximal task.

METHODS

Nine young active males with no history of hamstring injuries completed a fatiguing task (99 knee flexions at 50% MVC, 5-s contraction-5-s rest) on a Con-Trex isokinetic dynamometer (prone position, 30° hip angle, 0° full extension) in three separate randomized conditions: ISO, CON and ECC. The dynamic contractions were performed at $8°$ s^{-1} (ROM: 0-40°) and the isometric at 30° knee flexion. In the dynamic conditions, the leg was passively returned to starting position after every contraction. SWE (Aixplorer, SuperSonic Imagine) was used to measure shear modulus during contraction in biceps femoris long head (BFlh), semitendinosus (ST) and semimembranosus (SM) muscles in an alternating fashion so that each muscle was measured 33 times in total. MVC was assessed before and after the task while T2-weighted MR images were taken before, immediately after and 48 h post-exercise. All measurements were performed at 50% thigh length. The shear ratio (individual muscle shear modulus/ sum shear modulus of all hamstrings) was calculated as an index of load distribution. Changes in torque, shear modulus and shear ratio for each muscle were calculated as: (average final 10 contractions-average first 10 contractions) / (average first 10 contractions)*100. One-sample t-tests were used to examine changes in torque, shear modulus and shear ratio and paired t-tests for changes in MVC and T2 values. Bivariate correlations were examined with Pearson's r. The level of significance was set at $p < 0.05$.

RESULTS AND DISCUSSION

Knee flexor MVC decreased after all conditions (-18.4% to -33.6%, $p < 0.01$). During the exercise, the largest decline in torque was exhibited in CON (-15.3±13.8%, $p= 0.010$) followed by ECC (-4.5±4.3%, $p= 0.014$) and ISO (-2.1±4.9%, N.S). On a group level, BFlh shear modulus decreased significantly in ECC ($p= 0.042$) and SM shear modulus in CON ($p= 0.001$) (Figure 1). In contrast, ST shear modulus changes were not significant in any condition. BFlh shear ratio increased significantly only in ISO ($p= 0.002$) while there were no significant changes in SM or ST in any conditions. Notably, individual responses in shear modulus were highly variable, both in magnitude and direction, across all conditions and muscles (CV; BFlh= 26.2-30.0%, ST= 35.8-38.3%, SM= 28.6-32.9%). Shear modulus and torque during exercise were significantly related for BFlh in CON (r= 0.48) and ECC (r= 0.62), ST in CON (r= 0.79) and SM in all conditions (r= 0.49-0.64). Despite similar torque decline in ISO and ECC, BFlh shear modulus changed in opposite directions suggesting increased load borne in ISO but reduced in ECC. The larger explained variance in BFlh shear modulus by torque changes in ECC (39%) compared to ISO (5%), suggest that the reduction in BFlh shear modulus in the former condition was due to fatigue. This implies a compromised capacity of the BFlh to absorb energy during lengthening muscle actions, rendering this muscle more susceptible to strain injury. Nevertheless, on an individual level, shear modulus and load distribution changes were mixed and highly variable. In conclusion, these findings suggest that fatigue-induced changes in hamstrings muscle stiffness and load distribution are contraction type-specific and may explain the higher risk of strain injuries in BFlh.
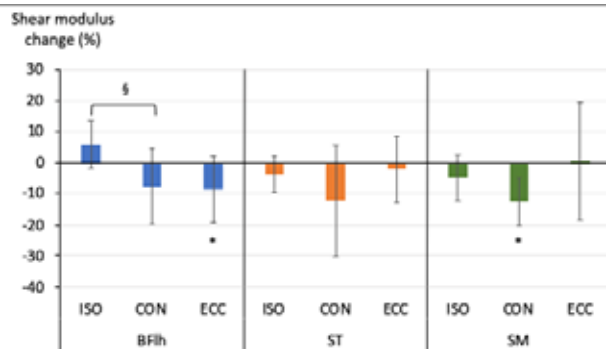

Figure 1: BFlh, ST and SM shear modulus changes (mean±sd) during the ISO, CON and ECC conditions. * denotes different from 0, § denotes different from CON, $p < 0.05$.

REFERENCES

[1] Timmins RG et al. (2014). *Scand J Med Sci Sports*, **24**: e299-e305.
[2] Schuermans J et al. (2014). *Br J Sports Med*, **48**: 1599-1606.
[3] Bouillard K et al. (2012). *J Biomech*, **45**: 1424-1429.

3D Representation of Complex Soleus Aponeurosis Geometry and Muscle Fiber Architecture Based on Magnetic Resonance Imaging and Laplacian Flow Simulation

[1]Katherine R. Knaus, [1]Silvia S. Blemker

[1]Department of Biomedical Engineering, University of Virginia, Charlottesville, VA, USA
corresponding author: ker4e@virginia.edu

INTRODUCTION

The soleus muscle is important in locomotion. Biomechanical modelling is often employed to understand its healthy and pathologic function. Soleus function is inherently linked to its structure, with short fibers and large PCSA at the extremes for skeletal muscle. Complex 3D soleus architecture, with multiple compartments of dissimilarly arranged fibers, has been observed in cadavers and *in vivo* using DTI [1,2].

Laplacian flow simulation can provide *in silico* determination of complex muscle fiber arrangement but relies on accurate representation of aponeurosis geometry [3]. In the soleus, it's quite complex, comprising a posterior aponeurosis that is continuous with the Achilles tendon and serves as the insertion of posterior soleus fibers, from which protrudes the median septum on which anterior fibers insert. An anterior aponeurosis interdigitates with these and serves as origin for both anterior and posterior fibers [4]. In additiona to providing a framework for fiber architecture, aponeuroses play a mechanical role in transmitting muscle forces.

Accurate 3D representations of both muscle and aponeurosis are needed to investigate soleus biomechanics while avoiding errors of more simplified models. The goal of this work is to develop a 3D model of the soleus that utilizes magnetic resonance imaging to define external muscle configuration and internal aponeurosis geometry, and Laplacian flow simulations to determine complex fiber arrangement *in silico*.

METHODS

Using high resolution IDEAL-SPGR MRI of the right leg of a healthy male (height 191cm, mass 88.4 kg, age 22 years), we manually outlined the soleus muscle and aponeuroses in axial images using in-house MatLab segmentation software. In Autodesk Inventor, a 3D muscle surface was lofted from closed spline loops and 3D structures of anterior and posterior aponeurosis and median septum were lofted from open splines. Aponeurosis volume was subtracted from muscle.

Muscle models were exported to Autodesk CFD, where Laplacian simulations were performed as reported previously [3] with incompressible, highly viscous, laminar flow parameters. Pressure boundary conditions of 1 and 0 Pa were prescribed to the fiber origins and insertions, respectively, defined as the surfaces created from aponeurosis subtraction. Simulation vector results were used to track streamlines representing muscle fiber paths from origin to insertion. These streamlines were used to compute fascicle lengths for comparison to DTI data reported in the literature [2].

RESULTS AND DISCUSSION

Removal of aponeuroses split the soleus into compartments. Laplacian flow simulations resulted in a radially uni-pennate posterior portion and bi-pennate anterior portion. Simulated soleus fiber tract lengths were slightly shorter than lengths determined with DTI in both compartments [2]; however, model results included fibers in the distal and proximal ends of the muscle which were not captured with DTI and tended to be shorter. The model also had slightly larger pennation angles which would correspond with shorter fibers.

This model can be used for finite element simulation of soleus contraction to investigate the biomechanical relationships of complex aponeurosis geometry and fiber architecture and their role in locomotor function.

REFERENCES

[1] Agur, A et al. (2003). *Clinical Anatomy* **16**:285-293
[2] Bolsterlee, B et al. (2018). *Peer J*, **6**:e4610.
[3] Handsfield, G et al. (2017). *BMM*, **16**(6):1845-1855
[4] Hodgson, J et al. (2006). *J Morphology* **267**:584-60
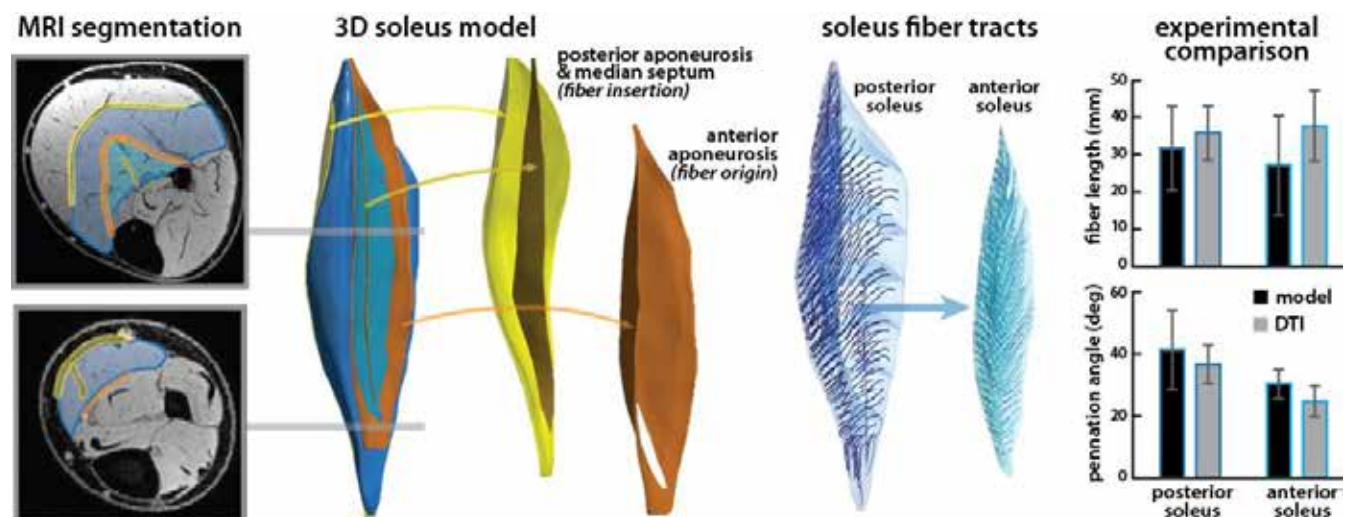
Figure 1: 3D muscle and aponeurosis geometry were defined from MRI and used with Laplacian flow simulations to determine fiber tracts.

Summation Properties are Improved by a Preceding Contraction and Intervening Rest Period

[1]**Ian C. Smith**, [1]Franziska Onasch, [1]Walter Herzog
[1]Faculty of Kinesiology, The University of Calgary, Calgary, AB, Canada
Corresponding Author: icsmith@ucalgary.ca

INTRODUCTION

Post-activation performance enhancement (PAPE) refers to improved voluntary performance following an intense but brief warm-up activity [1]. PAPE is typically seen 3-10 minutes after the warm-up and is most apparent for well-practiced movements [2]. The mechanisms resulting in PAPE are not well understood, but likely involve neural, intramuscular, and psychological factors. PAPE by any mechanism seems attributable to an increased rate of torque development [3]. While PAPE does not temporally coincide with contraction-induced increases in twitch torque (i.e. twitch potentiation) [4], it is possible that the warm-up activity can enhance twitch summation properties to beneficially affect performance. This hypothesis has not been previously tested. The aim of this study was to determine if twitch summation properties are enhanced by a preceding contraction, thereby providing preliminary evidence of an intramuscular contribution to PAPE in human skeletal muscle.

METHODS

Healthy adults were recruited based on sex (male n=26 vs female n=10) and their self-identified status as an established strength or power-trained athlete (strength trained n=23 vs non-strength trained n=13). People casually participating in resistance training were not recruited.

Subjects were secured in an upright seated position in a dynamometer (Biodex System 3, Biodex Medical Systems Inc., Shirley, NY, USA) with the knee bent at 90º. Quadriceps muscles of the right leg were activated by percutaneous stimulation of the femoral nerve. Stimulation parameters were controlled using a Grass Model S8800 Stimulator and a Grass Model SIU8T Stimulus Isolation Unit (Grass Instruments Co., W. Warwick, RI, USA).

We performed 2 experiments.

Experiment 1 was designed to compare twitch kinetics before, and at 1-minute intervals for 10 minutes after an electrically-evoked conditioning protocol. The conditioning protocol consisted of 3 20-pulse unfused tetani delivered at 5-second intervals with individualized stimulation rates (inter-pulse intervals set to 1.25× time to peak torque; mean ± SD = 6.5 ± 0.5 Hz).

Experiment 2 was designed to assess contraction-induced changes to summation properties. We evoked 3 unfused tetani (Set 1 Contractions 1-3; S1C1-3) with simulation parameters identical to the conditioning protocol of experiment 1. Our participants rested for 5 minutes, and then 3 more unfused tetani with the same stimulation parameters were evoked (Set 2 Contractions 1-3; S2C1-3).

Twitch time-course data were analyzed using repeated measures ANOVA followed by Fisher-LSD post hoc test when significant differences were indicated. Summation parameters were compared using paired Student's t-tests. Differences were considered significance at α=0.05.

RESULTS AND DISCUSSION

Neither sex nor training status affected measures of summation properties. All data were therefore pooled.

Experiment 1 (Not depicted): Following the conditioning protocol we found potentiation of twitch torque which decayed to a steady state after 6 minutes of rest. We also observed a transient increase in the time to 50% relaxation after 4- and 5-minutes of rest.

Experiment 2 (see Fig. 1): Relative to S1C1, S2C1 had a) a higher ratio of pulse 2 torque to pulse 1 torque, b) a higher ratio of maximum torque to pulse 1 torque, c) less relaxation following pulse 1, and d) larger declines in force after the initial rise (i.e. sag). These measures were not different in comparisons of S1C2 to S2C2, and S1C3 to S2C3.

We interpret the slowed relaxation and associated improvements in summation properties as a slowing of cross-bridge turnover rates. This effect could enhance torque at the onset of motor unit activation and contribute to PAPE.
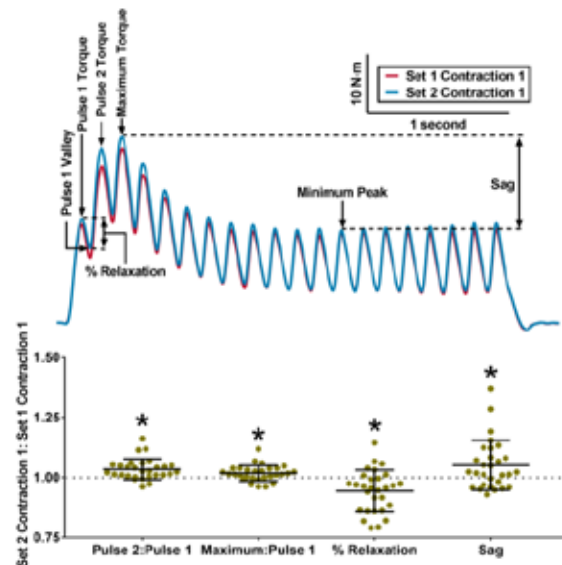

Figure 1: Summation was initially improved by the conditioning protocol. * - Set 2 Contraction 1 ≠ Set 1 Contraction 1; *P*<0.05)

ACKNOWLEDGEMENTS

REFERENCES

[1] Cuenca-Fernández et al. (2017). *Appl. Physiol. Nutr. Metab.,* **42**:1122-1125
[2] Wilson et al. (2013). *J. Strength Cond. Res.*, **27**: 854–859
[3] Baudry & Duchateau. (2007). *J. Appl. Physiol.*, **102**: 1394–1401.
[4] MacIntosh et al. (2012). *Appl. Physiol. Nutr. Metab.*, **37**:546–550.

Macroscopic morphological muscle properties to feature spasticity phenotypes in children with cerebral palsy

[1]Kaat Desloovere, [1]Britta Hanssen, [1]Nicky Peeters, [1]Nathalie De Beukelaer, [2]Anja Van Campenhout, [1,3]Lynn Bar-On
[1]Department of Rehabilitation Sciences, KU Leuven, Leuven, Belgium
[2]Department of Development and Regeneration, KU Leuven, Leuven, Belgium
[3]Department of Rehabilitation Medicine, Amsterdam University Medical Centers, Amsterdam, The Netherlands
corresponding author: kaat.desloovere@kuleuven.be

INTRODUCTION

Classical definitions state that spasticity is velocity-dependent (VD). Yet, instrumented spasticity assessments (ISA), based on electrophysiological and biomechanical signals, revealed also length-dependent (LD) spasticity patterns in children with cerebral palsy (CP), suggesting the presence of different spasticity phenotypes [1]. Yet, the underlying pathophysiology of these phenotypes is not clear. Since previous discussions in literature suggest that spasticity patterns may be related to muscle structure [2,3], we hypothesized that muscle imaging will help to delineate these phenotypes. Hence, the aim was to compare muscle morphology between VD and LD spasticity phenotypes.

METHODS

We recruited 33 children with spastic CP (8±3yrs, GMFCS-I/II/III=18/10/5) who were planned for lower limb botulinum toxin (BoNT) treatment. The number of previous BoNT sessions were extracted from the clinical files. All children received ISA and muscle imaging by means of 3D-freehand ultrasound (3DfUS), before and after treatment. The current study focused primarily on the analysis of the pre-treatment data related to the gastrocnemius. To define the alterations from normal, data were compared to established control data-sets of age-matched typically developing (TD) children.

ISA quantified spasticity [4]. Sagittal ankle movements were performed to stretch the relaxed gastrocnemius at slow and fast velocities. Muscle activity, joint motion and net ankle torque were simultaneously recorded by means of electromyography (EMG), inertia sensors and a force sensor, respectively. Length-dependent hyperactive stretch-reflexes were defined as the average change in RMS-EMG collected between the start and end of the slow stretch. The change in RMS-EMG between slow and fast stretch represented velocity-dependent activation. Muscles that showed >5% normalized length-dependent RMS-EMG, were categorized as having a LD phenotype. 3DfUS was used to estimate the morphology of the medial gastrocnemius [5]. Conventional 2D US was combined with motion analysis, to capture the position and orientation of the probe and subsequently create 3D muscle reconstructions. Muscle volume normalized to body mass (nMV), as well as muscle and tendon length, normalized to muscle-tendon-unit length (nML, nTL), were estimated at resting ankle angle and at maximum dorsiflexion angle.

Muscle morphology of CP children was compared to TD control data and between CP children with LD and VD spasticity phenotypes using Mann-Whitney-U tests (p<0.05).

RESULTS AND DISCUSSION

The study sample included 8 children who were BoNT-naïve, while 15 and 7 children received 1-3 and >3 previous BoNT treatment sessions, respectively. The muscle volume and lengths were not found to be influenced by previous BoNT treatments. In agreement with previous studies, children with CP presented with reduced muscle volume, shorter muscle lengths and longer tendon lengths compared to their TD-peers. Compared to the children with a VD phenotype (N=17: GMFCS I/II/III:14/3/0), the children with a LD phenotype (N=16:GMFCS I/II/III:4/7/5) showed reduced (21.4%) normalized muscle volume and shorter (12.5%) normalized muscle belly lengths combined with longer (14.5%) normalized tendon lengths (Figure 1).
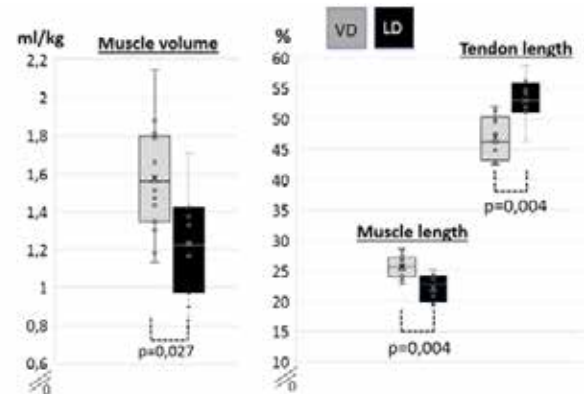

Figure 1: Normalized muscle volume (per kg), and muscle and tendon length (% of muscle-tendon unit length) between velocity-dependent (VD: grey) and length-dependent (LD: back) phenotypes.

CONCLUSIONS

Altered muscle morphology in CP is more pronounced in children who present with an LD spasticity phenotype. This LD-group included more children with GMFCS-level II and III, compared to the LD-group, explaining the greater muscle alterations. Since muscle contracture is considered a crucial cause of an excessive response to stretch [3], the shorter muscle belly length in this group is expected to result in a reduced spastic velocity threshold, explaining the observed muscle activity while stretching slowly.

ACKNOWLEDGEMENTS

REFERENCES

[1] Bar-on L et al. (2014). *PLoS One*, **9**.
[2] Bar-on L et al. (2018). *Front. Pediatr*, **5**.
[3] Gracies (2005). *Muscle & Nerve*, **31**: 552-571.
[4] Bar-on L et al. (2013). *Gait & Posture*, **38**: 141-147.
[5] Cenni F et al. (2016). *Comput Methods Programs Biomed*, **1**: 179-187.

Poster Session 1:

Matthew Millard

Ashley Oldshue

Amy Adkins

Amy Loya

Kevin Boldt

Kaat Desloovere

Atuski Fukutani

Giovanni Martino

Nathalie De Beukelaer

Brian Horslen

Anouk Agten

Dominiziana Costamagna

IS TITIN ACTIVELY PRELOADED?

[1]Matthew Millard, [2]Timothy Leonard, and [2]Walter Herzog
[1]Optimization, Robotics and Biomechanics Group, Heidelberg University, Heidelberg BW, Germany
[2]Human Performance Laboratory, University of Calgary, Calgary AB, Canada
corresponding author: matthew.millard@ziti.uni-heidelberg.de

INTRODUCTION

The active lengthening experiments of Leonard et al. [1] make it clear that titin is involved in the production of tension both within the actin-myosin overlap zone and beyond. While titin is thought to be solely responsible for bearing 'active' force beyond the actin-myosin overlap, the state of titin prior to active lengthening is unknown. Here we determine indirectly if titin is actively preloaded comparing the slope of force development within the overlap (K_A) to that beyond the overlap zone (K_B). Since the active lengthening experiments of Leonard et al. [1] start at an average sarcomere length of $2.7\pm0.6\mu m$, where titin generates little force, any significant preload in titin at this length would require active work. If titin is not preloaded prior to lengthening the slope of force development within region A should be less than region B since the force contribution from cross-bridges will decrease as the actin-myosin overlap is lost (Fig 1A). Conversely, if titin is preloaded the slope within the two regions would be similar (Fig 1B).
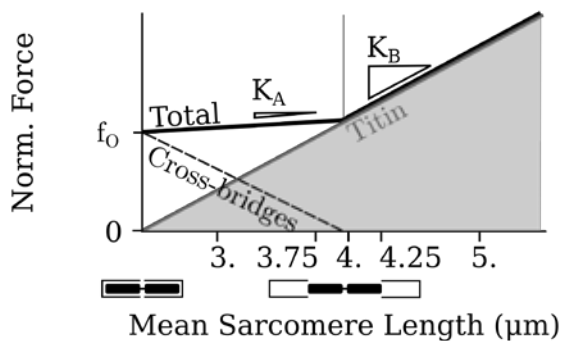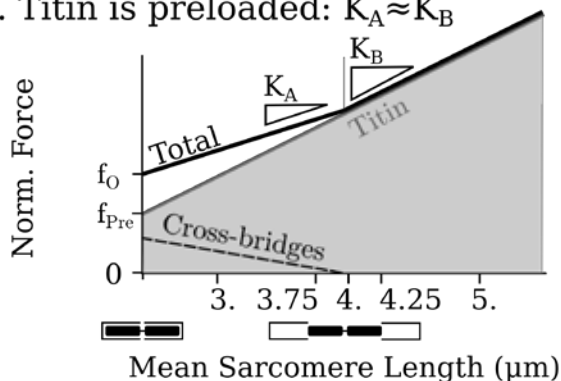

Figure 1: During active lengthening, the slope within the actin-myosin overlap will differ from the slope beyond the overlap if titin is not preloaded (A). This difference will be less pronounced if titin is preloaded (B).

METHODS

The active lengthening recordings of Leonard et al. [1] are partitioned into data within the actin-myosin overlap (3-3.75μm) and beyond (4.25-5μm). The gap between the two regions has been introduced so that the effects of sarcomere non-uniformity between these two regions are reduced. Ten trials that included measurements for both regions A and B were included for analysis. Since each fibril differs in cross-sectional area and strength we normalized the force by the tension developed at an average sarcomere length of 4μm and report the normalized slope in units of $(\mu m)^{-1}$. Lines of best fit were computed for region A and B separately by minimizing the sum of squared errors. Finally, we used a T-test to determine if the slope in regions A and B differ.

RESULTS AND DISCUSSION

There was no statistically significant difference between the slopes within the actin-myosin overlap region and the region beyond myofilament overlap (p=0.197). The slope within and beyond the actin-myosin overlap regions was 0.53 ± 0.17 and 0.71 ± 0.33 respectively. The line of best fit matched the data closely with an RMSE of 0.019 ± 0.03 and 0.008 ± 0.019 in regions A and B.

However, there was a pattern between the length of failure and the slope in regions A and B: fibrils that failed at shorter lengths (5.0 μm) have $K_B \approx K_A$. When the 3 fibrils which failed at 5.0 μm were removed the remaining 7 fibrils have a statistically significant difference (p=0.014) between K_A and K_B. The slope within and beyond the overlap for this reduced set was 0.46 ± 0.11 and 0.82 ± 0.34 respectively. To see if the change in slope can be attributed to changes in titin we repeated the analysis on the passively stretched fibrils and those fibrils that were stretched in a BDM and high calcium concentration and found no statistically significant differences in either case (p=0.11 and p=0.71 respectively). These results also hold when the regions of analysis are expanded to 3-4μm and 4.5-5.5μm.

Assuming that the 3 fibrils that failed at 5.0 μm are outliers, the data suggest that titin is not actively preloaded. These results support several models in the literature [2,3] that have been published. However, the possibility that titin is actively preloaded, as suggested by [4, 5], cannot be rejected when all of the data is included.

ACKNOWLEDGEMENTS

REFERENCES

[1] Leonard et al. (2010) *J Biomech*,**43**:3063-3066
[2] Rode et al. (2009) *J Theo Biol*, **259**: 350-360
[3] Schappacher-Tilp et al. (2015) *PLoS One,***10**:1-16
[4] Nishikawa et al. (2012) *Proc R Soc B*, **279**:981-990
[5] DuVall et al. (2017) *J Exp Biol*, **220**:4418-4425

Modeling muscle cross-bridge dynamics for movement simulations

[1]**Ashley H. Oldshue**, [2]Laksh K. Punith, [3]Kyle P. Blum, [2]Gregory S. Sawicki, [1,2]Lena H. Ting
[1]Emory University, Atlanta, GA, USA
[2]Georgia Institute of Technology, Atlanta, GA, USA
[3]Northwestern University, Evanston, IL, USA
Email: aoldshu@emory.edu

INTRODUCTION

Hill-type muscle models have historically been poor at modeling the forces generated in-vivo during locomotion as they do not simulate transient and history dependent properties of muscle [1]. Transient forces that emerge from acto-myosin interactions could significantly influence energy storage and transfer within muscle-tendon units, particularly when locomoting over complex and uneven terrains.

Our objective was to generate a half-sarcomere model of cross-bridge kinematics appropriate for musculoskeletal simulations for movement. We performed *in silico* simulations of the half-sarcomere to replicate classic constant length and constant velocity experiments. We characterized the force-length and force-velocity properties emergent from the model.

METHODS

Our contractile element model consists of a single half-sarcomere with 6.9×10^{16} cycling cross-bridges. The simulation takes as inputs the fraction of activated actin binding sites and the length change of the half-sarcomere. The active force is calculated by summing the forces of all the attached myosin heads at each point in time. The total force is the sum of the active and passive components [2].

Simulations to generate the force-length relationship were conducted by fixing the muscle model at lengths between 500 and 2000 nm and applying an activation level of 100% to the actin binding sites. The active force was taken at the end of each 10-second simulation after the simulation reached steady state. Simulations to generate the force-velocity relationship were conducted by contracting and stretching the muscle at constant velocities from -0.02 μm/s to 0.04 μm/s for a 4-second duration. Initial lengths were specified such that all simulations reached optimal fiber length at the midpoint of the stretch period, where the active force was evaluated.
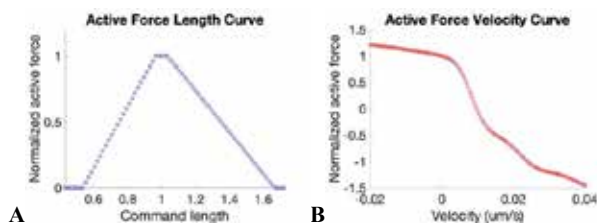
RESULTS AND DISCUSSION

Figure 1: (A) Normalized cross-bridge forces plotted against muscle length as a fraction of the optimal length; (B) Normalized cross-bridge plotted against stretch velocity.

Our simulations produced characteristic force-length and force-velocity curves (Figure 1). Maximum isometric force occurs at the half-sarcomere's optimal length (Figure 1a). Due to the 80nm bare zone on the thick filament, where there are no myosin heads, optimal length occurs when actin-myosin overlap reaches 100% between 1120 nm and 1200 nm. The ascending limb of the active force-length curve is 47% steeper than the descending limb. Maximum muscle force during imposed velocities occurred during lengthening and active force exhibited a characteristic sharp decline as the shortening velocity increased (Figure 1b). The cross-bridges produce negative forces at high shortening velocities [3].

CONCLUSIONS

We validated that characteristic force-length and force-velocity relationships in muscle were emergent from the cross-bridge kinetics in our half-sarcomere model. The model can be used in existing simulations of movement in order to compare the performance afforded by Hill-type versus acto-myosin based muscle models. Our goal is to simulate hopping on uneven terrain to understand the effects of transient and history dependent muscle properties on stability of unsteady locomotion [4].

ACKNOWLEDGEMENTS

REFERENCES

[1] Dick TJ et al. (2017). *J Exp Biol*, **220(9)**: 1643-1653.
[2] Blum KP et al. (2018). *SfN Abstract*, 771.05.
[3] Edman KA. (2014). *Acta Physiol*, **211(4)**: 609-616.
[4] Punith LK et al. (2017). *ASB Abstract*.

61

The paretic biceps brachii contains fewer sarcomeres in series than the contralateral biceps brachii following stroke

[1][4][5]**Amy N. Adkins**, [1][3]Lindsay Garmirian, [1][3]Christa M. Nelson, [1][2][3]Julius P.A. Dewald, [1][2][3][4][5]Wendy M. Murray

Departments of [1]BME, [2]PM&R, and [3]PTHMS, Northwestern University, Chicago, IL, USA
[4]Shirley Ryan AbilityLab, Chicago, IL, USA
[5]Edward Hines, Jr. VA Hospital, Hines, IL, USA
corresponding author: **adkins@u.northwestern.edu**

INTRODUCTION

A muscle's architecture is indicative of its ability to contract and produce force. Anatomical studies in cadavers, which involve dissection and measurement across multiple scales (whole muscles, fascicles, and sarcomeres), demonstrate that a major distinction among different skeletal muscles in the human body is the number of sarcomeres in series. Serial sarcomere number (SSN) is a particularly important architectural parameter, as it describes the range of lengths over which a muscle can actively generate force. In anatomical studies, SSN is most commonly characterized by a muscle's optimal fascicle length (OFL). OFL is calculated as the average ratio between fascicle lengths measured in a muscle and sarcomere lengths in the same, dissected fascicles, multiplied by optimal sarcomere length.

Little is known about how SSN adapts in an individual human muscle after altered stimulus, use, injury, or disease. Such effects can't be studied in cadavers and in vivo measurement of sarcomere lengths have been, until recently, limited to the operating room. Here, we combine novel, minimally invasive imaging techniques to quantify muscle fascicle and sarcomere lengths, in vivo, in the paretic and non-paretic biceps brachii of individuals who have chronic hemiparetic stroke. We hypothesize that the paretic biceps will have fewer sarcomeres in series than the contralateral muscle because, following stroke, the paretic limb is used less than the contralateral limb and presents with a more flexed elbow posture, essentially "immobilizing" (e.g., [1]) the paretic biceps at a chronically shorter length.

METHODS

Optimal Fascicle length (OFL) was calculated from in vivo measures of sarcomere and fascicle lengths in biceps brachii in both arms of twelve subjects. All data were collected in the same limb posture, under passive conditions. We studied eight subjects with chronic hemiparetic stroke (3 female/5 male, 60 ± 9 yrs, Fugl-Meyer 26 ± 9, 13 ± 10 yrs post-stroke) and four age-range matched control participants who have never had a stroke (2 female/2 male, 62 ± 6 yrs).

To image sarcomeres *in vivo*, a microendoscopic needle was inserted into the long head of the biceps brachii with its optical lenses aligned parallel to the fascicle direction. A microscope (Zebra Medical Technologies, Palo Alto, CA) which uses second-harmonic generation to capture the intrinsic striation pattern of sarcomeres was attached to the needle for imaging; images were collected at 1.9Hz for about 2-5 minutes (~250-600 images). Mean sarcomere length per image was calculated offline as the fundamental spatial frequency of the striation pattern along the fiber direction [2]. In a separate session, extended field-of-view ultrasound images of the long head of the biceps brachii were obtained. Three images were obtained per arm; 4 fascicles were measured per image [3]. Both sarcomere and fascicle length measures were completed while the participants were seated, secured to a chair, with their arms supported in a controlled posture. Surface EMG was obtained during both sessions to exclude any data collected while the biceps was active.

Generalized linear mixed-effects models were implemented (SAS 9.4 software) for each group (stoke, no stroke) as a fixed effect and each muscle parameter (sarcomere length, fascicle length, optimal fascicle length) as an outcome variable. Within-subject correlation and the correlation between arms were modelled as random effects.

RESULTS AND DISCUSSION

For each individual with chronic hemiparetic stroke, the paretic muscle had a shorter OFL (p = 0.012). Fascicles were shorter (p < 0.0001) but sarcomere lengths were not significantly different in the limb posture tested (p = 0.219) (Figure 1). There were no significant interlimb differences for any of the architectural parameters observed in the age-range matched participants without stroke. Our results are consistent with a chronic loss of serial sarcomeres in the paretic biceps brachii following hemiparetic stroke.

REFERENCES

[1] Williams and Goldpink. (1978). *J Anat,* **116**: 45-55.
[2] Sanchez et al. (2015). *Neuron*, **88**: 1109-1120.
[3] Nelson et al. (2016). *J Biomech*, **49**: 1948-1952.

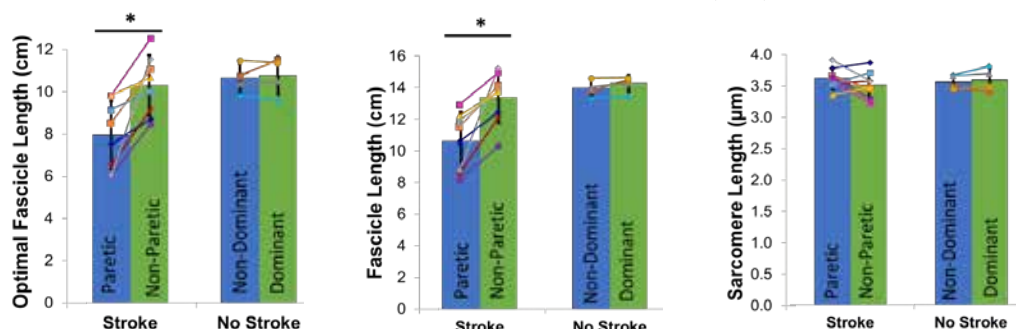**Figure 1:** Average OFL, fascicle, and sarcomere length for each arm of individuals with and without stroke. Error bars represent ± one standard deviation from the group mean. Data from individual participants are indicated with a specific shape and color and connected by a line to visualize individual interlimb differences. The * indicates a statistically significant difference from the mixed effects models.

CHARACTERIZING SHORTENING DEACTIVATION IN *DROSOPHILA* AND *LETHOCERUS* MUSCLE TYPES

[1]**Amy K. Loya**, [2]Bernadette M. Glasheen, [1,2]Douglas M. Swank
[1]Department of Biomedical Engineering, Rensselaer Polytechnic Institute, Troy, NY, USA
[2]Department of Biological Sciences, Rensselaer Polytechnic Institute, Troy, NY, USA
Corresponding Author: swankd@rpi.edu

INTRODUCTION

Shortening deactivation (SD) is a delayed decrease in force following rapid muscle shortening, while stretch activation (SA) is a delayed rise in force following muscle lengthening. The pairing of SA and SD enables higher work and power production at constant intracellular calcium (Ca^{2+}) concentrations. This relationship is most prominent in insects such as *Drosophila* and *Lethocerus* indirect flight muscles (IFM) because it is essential to sustaining flight. Similarly, in vertebrate hearts, SA increases systolic force and SD enhances ventricular relaxation for diastolic filling, which assists Ca^{2+} in modulating force levels to meet metabolic demands. Defects in SA and SD have been linked to cardiomyopathies. However, the molecular mechanisms behind SA and SD remain unknown. Specifically, the SD mechanism has not been investigated, likely because muscle physiologists have presumed that it is the same as SA. However, no experiments have been conducted to test this presumption. Therefore, we performed fiber mechanics on highly SA *Drosophila* and *Lethocerus* IFM, and minimally SA *Drosophila* jump muscle (TDT), to define SD characteristics and compare them to SA (Figure 1A).

METHODS

IFM and TDT muscles were isolated from the thoraces of 3-day-old *Drosophila* (Oregon-R) or *Lethocerus* imported from Thailand, as previously described [1]. Fibers were de-membranated then mounted between a force gauge and length actuator in relaxing solution (pCa 8.0). Each muscle was stretched by 1% of its initial length over 0.5 ms, held at this longer length for 500 ms, and shortened to the starting length over 0.5 ms. The resultant SA force after stretching and SD force after shortening were measured in solutions of increasing Ca^{2+} (decreasing pCa).

RESULTS AND DISCUSSION

All fiber types exhibited some level of SD (Figure 1B). *Lethocerus* presented the greatest tension decrease of 20 mN/mm^2 due to SD. This was ~1.5-fold greater than that of *Drosophila* TDT, and ~10-fold greater than *Drosophila* IFM. However, isometric tension in *Drosophila* TDT (34 mN/mm^2) was higher than *Lethocerus* (18 mN/mm^2) and Drosophila IFM (2 mN/mm^2). Thus, when normalized to isometric tension, *Drosophila* IFM exhibited a 120% SD tension decrease, while *Lethocerus* and *Drosophila* TDT decreased by 97% and 37%, respectively. A similar order was found when comparing normalized SA tension: 233% for *Drosophila* IFM, 76% for *Lethocerus* IFM, and 11% for *Drosophila* TDT. Surprisingly, SD tension was ~1.3-fold greater than SA tension in *Lethocerus* IFM. But in *Drosophila* IFM, SA was almost 2-fold higher than SD. The largest difference in magnitudes between SA and SD was found in *Drosophila* TDT, with SD tension being ~3.5-fold higher than SA tension.

CONCLUSIONS

To our knowledge, this is the first study to characterize SD amplitude in multiple muscle types. *Lethocerus* exhibited the greatest changes in tension due to SA and SD, but *Drosophila* IFM showed the greatest relative (compared to the maximum isometric tension) changes due to SA and SD.
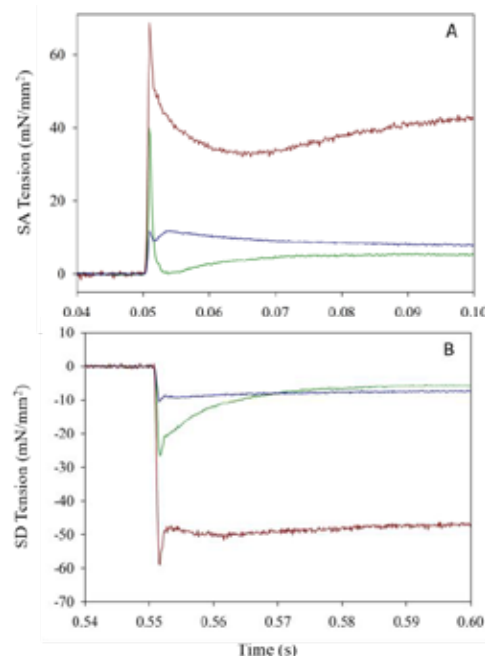

Figure 1: Representative tension traces. A) SA response for *Drosophila* IFM (blue), *Drosophila* TDT (green), and *Lethocerus* IFM (red). B) SD response. Tension is baselined prior to stretching or shortening.

The larger relative changes for both IFM muscle types compared to the TDT is likely what enables them to produce positive power for cyclical contractions at constant Ca^{2+} levels. In contrast, *Drosophila* TDT cannot produce positive power when undergoing cyclic contractions. The difference in SA and SD magnitudes within a muscle type suggests that SA and SD might be employing different mechanisms to alter tension levels. Since SD was higher than SA in TDT, SD may be more important for TDT function. With an understanding of the SD characteristics of each fiber type, we can perform experiments, such as protein isoform exchanges between *Drosophila* muscle types, to elucidate the mechanism behind SD.

ACKNOWLEDGEMENTS

REFERENCES

[1] Glasheen BM et al. (2017) *Am J Physiol Cell Physiol*, **313**: C621–C631.

63

Residual and Passive Force Enhancement in Skinned Cardiac Fibre Bundles

[1]**Kevin R. Boldt**, [1]Seong-Won Han, [1]Venus Joumaa, [1]Walter Herzog
[1]Faculty of Kinesiology, University of Calgary, Calgary, AB, Canada
Corresponding author: krboldt@ucalgary.ca

INTRODUCTION

Residual force enhancement (RFE) is a mechanical property of skeletal muscle, whereby a muscle produces a greater steady-state force following an active stretch than it does purely isometrically at the same length and level of activation [1]. Similarly, when a muscle is deactivated, the passive force is greater following an active stretch compared to the passive force following a purely isometric contraction at the same length. This is known as passive force enhancement (PFE) [2]. Despite an abundance of studies on RFE and PFE in skeletal muscle, there is little research on RFE and PFE in cardiac muscle, and the few studies that exist have reported conflicting results [3-5]. It has been proposed that titin may play a crucial role in RFE and PFE [2]. Cardiac muscle has a shorter titin isoform than skeletal muscle, and thus may provide new insight into the role of titin in RFE and PFE. Therefore, the purpose of this work was to investigate RFE and PFE in cardiac fibre bundles.

METHODS

Tissue Preparation: Rabbit cardiac trabeculae muscle was dissected and cellular membranes were chemically permeabilized. On the day of experiments, fibre bundle preparations (n=10) were isolated and suspended between a force transducer and a length controller at 15°C. Sarcomeres were set at an average length of 2.2 μm using laser diffraction, and the width and length of the fibre bundles were measured (mean length and width: 1494 and 213 μm).

Reference Force Condition (Figure 1; blue line): The fibre bundle was initially passively stretched by 15% of its initial length, held for 20 seconds to allow for stress relaxation, and then activated maximally to determine the reference isometric force. The sample was then deactivated, and the post-reference passive force was measured 20 seconds following deactivation.

Active Stretch Condition (Figure 1; red line): After a three minute rest, the sample was activated maximally at an average sarcomere length of 2.2 μm, actively stretched by 15% of its length, and held for 20 seconds. The sample was then deactivated and the post-active stretch passive force determined after 20 seconds.
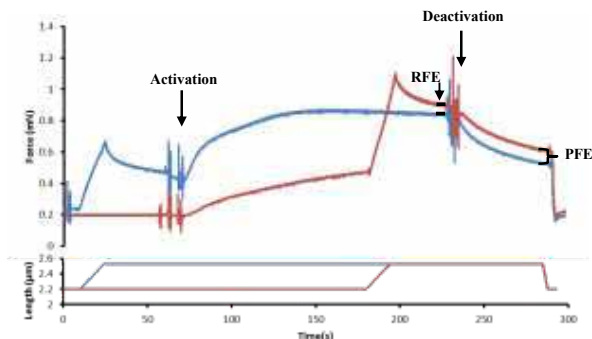

Figure 1: Sample reference (blue) and active stretch contractions (red). RFE and PFE are indicated on the trace.

Stiffness was obtained using a quick stretch release cycle (0.2% of the bundle length in 2 ms) performed during the purely isometric contraction, at steady state after active stretch, and after deactivation. Differences in stiffness were compared statistically with Wilcoxon Tests.

RESULTS AND DISCUSSION

RFE was observed in all ten fibre bundles and ranged from 2.3 to 9.4% (mean±SD: 5.5±2.5%) (Figure 2). PFE was observed in nine of the ten fibre bundles and ranged from 2.1 to 18.7% (mean±SD: 11.1±6.5%) (Figure 2). These results suggest that RFE and PFE are universal properties of striated muscle and not specific to skeletal muscle.
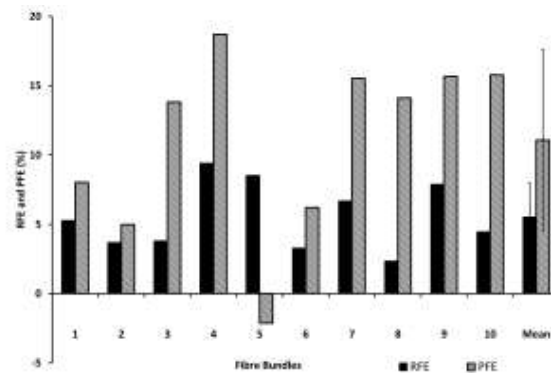

Figure 2: RFE (black) and PFE (grey) for each fibre bundle and the means±SD.

Stiffness did not differ between the isometric reference and the active stretch contractions (6.7±2.3 vs. 6.7±2.1 mN/mm), suggesting that the increase in force following the active stretch was not associated with an increase in the proportion of attached cross bridges. Furthermore, passive stiffness measured after relaxation was significantly (p=0.009) increased in the active stretch condition (4.1±0.9 mN/mm) compared to following the purely isometric contraction (3.4±1.4 mN/mm). This suggests that a passive element (possibly titin) has become stiffer in the active stretch condition compared to the purely isometric condition, and that, similar to skeletal muscle cardiac passive elements are likely playing a major role in the increase in force observed following an active stretch.

ACKNOWLEDGEMENTS

REFERENCES

[1]   Abbot et al. (1952). *J. Physiol*, **117**: 77-86.
[2]   Joumaa et al. (2008) *A. J. Phys Cell*, **294**: 74-78.
[3]   Boldt et al. (2015). *Biophys. J.*, **108**: 591.
[4]   Cornachione et al. (2016). *A. J. Phys Cell*, **25**: 374-386.
[5]   Han et al. (2019). *Biophys. J.*, **116**: 402.

Are pre-treatment assessments of muscle morphology related to the effects of treatment with Botulinum NeuroToxin-A and lower leg casting in children with cerebral palsy?

[1,2]Lynn Bar-On, [2]Nicky Peeters, [2]A. Van Campenhout, [2]F. Cenni, [2]Britta Hanssen, [2]Eirini Papageorgiou, [2]**Kaat Desloovere**.
[1]Department of Rehabilitation Medicine, Amsterdam University Medical Centers, Amsterdam, The Netherlands
[2]Department of Rehabilitation Sciences, KU Leuven, Leuven, Belgium
corresponding author email: kaat.desloovere@kuleuven.be

INTRODUCTION

Ankle joint hyper-resistance in children with spastic cerebral palsy (CP) is thought to have neural (hyperactive stretch-reflexes) and non-neural (adaptations to the muscles passive properties) origins [1]. A common treatment for ankle joint hyper-resistance, is Botulinum NeuroToxin-A (BoNT-A) combined with casting of the lower leg. However, treatment success is highly variable and may be related to the heterogeneity in initial symptoms. The aim of this study was to investigate whether pre-treatment assessments of stretch-reflexes and muscle morphology could help predict response to the combined treatment of BoNT-A and casting.

METHODS

Twenty-nine children with spastic CP indicated for plantarflexor BoNT-A injections and lower-leg (14 days) casting were enrolled. Pre- and 4-6 weeks post-treatment, children underwent 3D gait analysis, from which knee and ankle sagittal movement analysis profiles (MAP) were calculated [2]. Response to slow and fast passive plantarflexion stretches was assessed by simultaneously recording ankle joint kinematics, kinetics and surface electromyography (EMG) from the medial and lateral gastrocnemii and soleus [3]. Velocity-dependent hyperactive stretch-reflexes were defined as the average change in the summed root mean square (RMS) EMG collected between slow and fast stretches ($EMG_{FAST-SLOW}$). Length-dependent stretch-reflexes were defined as the average change in summed RMS-EMG collected between the start and end of the slow stretch (EMG_{SLOW}). Similarly, the change in the net joint ankle torque between slow and fast stretches was calculated to quantify the velocity-dependent component of ankle hyper-resistance ($Torque_{FAST-SLOW}$), while torque at slow stretch defined the length-dependent component ($Torque_{SLOW}$) [3]. 3D freehand ultrasound pre-treatment defined medial gastrocnemius morphology (muscle volume and muscle/tendon lengths) at resting and maximum dorsiflexion ankle angles [4]. Treatment effects on MAP, stretch reflexes, and torques were tested using paired Wilcoxon Signed rank tests. Individuals were categorized as responders when the average changes in passive stretch parameters and in MAP exceeded previously reported minimal detectable change values (MDC) [2,5]. Baseline measurements, as well as patient and treatment characteristics, were compared between responders and non-responders using Man Whitney U (continuous variables), Fisher-exact (dichotomized parameters), and Freeman-Halton (categorical parameters) tests. Significant variables were entered into a logistic regression and the Areas under the Receiver Operating Characteristic curve (ROC) was calculated. Significance was set to $p<0.05$.

RESULTS AND DISCUSSION

There was an average improvement of 23% in the ankles' MAP (pre-treatment 10.5±4.7° vs post-treatment 7.9±3.2°, $p=0.016$). Compared to pre-treatment, velocity-dependent stretch reflexes decreased on average by 54% (26.5±16.3µV vs 12.3±10.0µV, $p<0.001$), length-dependent by 59% (10.1±10.9µV vs 4.0±5.7µV, $p=0.001$), $Torque_{SLOW}$ by 41% ($p=0.008$), and $Torque_{FAST-SLOW}$ by 51% ($p=0.002$). There were several significant differences in pre-treatment parameters between responders and non-responders (Table 1), but in a multivariate logistic regression, only smaller normalized muscle volume was predictive of a good response (ROC curve of 0.88, $p=0.003$). Despite the study-focus being on response prediction, it is interesting to note that muscle volume did not significantly change after BoNT-A (Botox® dosage gastrocnemius: 3.6±1.7 units/Kg). The median +/- IQR of muscle volume was 34.8+/-20.1ml pre and 32.5+/-22.2ml post BoNT-A ($p=0.14$).

Table 1: Medians (IQR) of pre-treatment parameters that differed between responders (n=19) and non-responders (n=10)

	Responders	Non responders	p-value
MAPS sagittal plane ankle (deg)	11.40 (4.79)	6.27 (1.29)	0.027
Muscle volume (ml/kg)	1.26 (0.27)	1.57 (0.32)	0.002
Muscle length at rest (% leg length)	23.55 (2.31)	26.66 (3.77)	0.033
Muscle length at max. dorsiflexion (% leg length)	24.82 (2.84)	28.18 (2.66)	0.022
Length-dependent stretch-reflex activity (µV)	10.48 (7.85)	1.98 (2.07)	0.012
Length-dependent increase in ankle torque (Nm)	1.83 (2.37)	0.64 (1.14)	0.019

CONCLUSION

Estimating the volume of the medial gastrocnemius before treatment may assist in understanding response to treatment with BoNT-A combined with casting. Good response in smaller muscles is probably a reflection of disease severity, but also suggests that small volumes are not a contraindication for such treatment. Future analyses with larger sample size should confirm the baseline characteristics that predict response to BoNT-A injections.

ACKNOWLEDGEMENTS

REFERENCES

[1] Noort JC et al. (2017). *Eur. J. Neurol*. **24:** 981-e38.
[2] Baker R et al. (2012) *Gait Posture*. **35**: 612–5.
[3] Bar-On L et al. (2013) *Gait Posture*. **38:** 141–7.
[4] Cenni F et al. (2018) *Comput. Methods Programs Biomed*. **156**: 97–103.
[5] Bar-On L et al. (2014) *Arch. Phys. Med. Rehabil*. **95** 515–23.

Effect of Stretch-Shortening Cycle is Prominent in the Reduced Force Condition

[1]**Atsuki. Fukutani**, [2]Walter. Herzog
[1] Faculty of Sport and Health Science, Ritsumeikan University, Kusatsu, Shiga, Japan
[2]Faculty of Kinesiology, The University of Calgary, Calgary, AB, Canada
Atsuki Fukutani: atsukifukutani@gmail.com

INTRODUCTION

Muscle force generated during active shortening is increased by a preceding active stretch. This phenomenon has been called the stretch-shortening cycle (SSC) effect [1]. Recently, it has been suggested that residual force enhancement (RFE) contributes, at least in part, to the SSC effect [2]. Based on recent findings that RFE was preserved for reduced force conditions [3], it seems feasible to speculate that the SSC effect may also be preserved, at least in part, for reduced force conditions, and consequently, the relative influence of the SSC effect may be even more important in reduced compared to maximal force conditions. To test this hypothesis, the purpose of this study was to compare the magnitude of the SSC effect between normal and force reduced conditions.

METHODS

All Experiments were performed using skinned fibres from the rabbit soleus muscle (N = 18). The reduced force condition was achieved by adding 2,3-Butanedione monoxime (BDM), which is known to inhibit cross-bridge cycling in a dose-dependent manner, to the activating solution.

The SSC test and the pure shortening test were included for all conditions. In the SSC test, fibres were activated at an average sarcomere length of 2.4 μm, and then stretched to 3.0 μm. Immediately after the end of stretch, fibres were shortened to 2.4 μm. In the pure shortening test, fibres were activated at an average sarcomere length of 3.0 μm and then shortened to 2.4 μm. Typical force responses are shown in Figure 1.

The relative increases in mechanical work during shortening between the SSC and the pure shortening tests was taken as an index of the SSC effect, and the magnitude of the SSC effect was compared between the normal and the reduced force conditions.
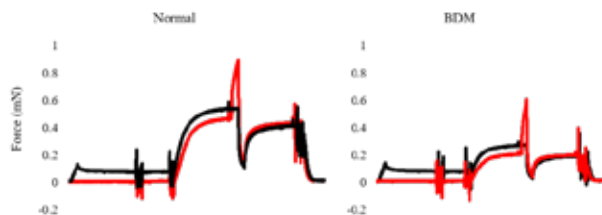

Figure 1: Typical example of changes in muscle force as a function of time. The left panel shows the force responses in the normal condition, and the right panel shows the force responses in the reduced force (BDM) condition. The red line indicates the SSC test, and the black line indicates the control (pure shortening) test.

RESULTS AND DISCUSSION

The isometric force at an average sarcomere length of 2.4 μm was smaller by 50% in the reduced force condition (0.23 ± 0.07 mN) compared to the normal force condition (0.45 ± 0.07 mN), indicating that muscle force was successfully reduced in the BDM condition.

The relative magnitude of the SSC effect was significantly greater for the reduced force (205 ± 14%) compared to the normal force (169 ± 6%) conditions (p < 0.001) (Figure 2). This result supports our hypothesis that the magnitude of the SSC effect may be more important for reduced force compared to normal force conditions. Since cross bridge cycling was partly inhibited in the reduced force condition, one would expect the SSC effect derived from cross-bridge components to be attenuated too. However, the SSC effect derived from structures other than cross-bridges may be preserved in the reduced force condition. A possible candidate for this alternate SSC effect is the structural protein titin, which would be expected to be unaffected by the reduced force achieved with BDM. The effect of titin-induced RFE may explain the greater relative SSC effect in the reduced force condition.
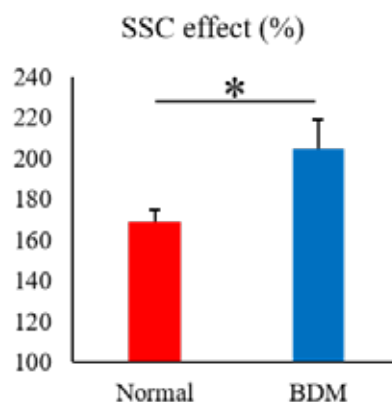
Figure 2: SSC effect for the Normal and reduced force (BDM) conditions. The SSC effect was defined as the relative increase in mechanical work during shortening for the SSC tests compared to the pure shortening tests. The SSC effect was significantly greater for the reduced force (BDM) compared to the normal force condition (p < 0.05).

ACKNOWLEDGEMENTS

REFERENCES

[1] Bosco C et al. (1982). *Acta Physiol Scand*, **114**: 543-550.
[2] Fukutani A & Herzog W (2018). *Med Sci Sports Exerc*, **50**: 2007-2014.
[3] Fukutani A & Herzog W (2018). *Med Sci Sports Exerc*, **50**: 1186-1191.

66

Simulating the pendulum test to understand mechanisms of Parkinsonian rigidity

Giovanni Martino[1], Sistania M. Bong[1], J. Lucas McKay[1], Friedl De Groote[2], Lena H. Ting[1, 3]

[1]W.H. Coulter Dept. Biomedical Engineering, Emory University and Georgia Institute of Technology, Atlanta, GA, USA

[2]Department of Movement Sciences, KU Leuven, Leuven, Belgium

[3]Department of Rehabilitation Medicine, Emory University, Atlanta, GA, USA

Email: giovanni.martino@emory.edu

SUMMARY

The pendulum test has been used to objectively quantify spasticity, but its utility in Parkinsonian rigidity has been studied much less. Our recent simulations suggest that key features of abnormal pendulum test kinematics can be attributed to elevated muscle tone and reflex gain in spastic cerebral palsy [1]. We hypothesized that muscle tone is also increased in Parkinsonian rigidity. We tested individuals with varying degrees of rigidity using the pendulum test, and simulated the resulting kinematics. Our experimental and simulation results suggest a major role of elevated muscle tone in Parkinsonian rigidity. Our work suggests that the pendulum test could be an effective tool for evaluating the mechanisms of rigidity in Parkinson's disease (PD).

INTRODUCTION

Despite extensive research, the pathophysiology of rigidity in PD remains unclear. Rigidity is evaluated by physical manipulation of the limbs in the relaxed state and in contrast to spasticity is described as being insensitive to the velocity of stretch [2]. While some research shows the involvement of velocity dependent spinal stretch reflexes [3, 4] in rigidity, there is some evidence suggesting a primary role of muscle tone [5]. The pendulum test is a diagnostic method that consists in evaluating the pattern of lower leg movement after release from the horizontal. Our recent simulation work suggests that three key features of the pendulum test related to spasticity severity can be explained by elevated tonic muscle activity and its interaction with stretch reflexes [1].

Our objective is to quantify the relationship between pendulum test outcomes and rigidity in PD. We collected pendulum test data from persons with PD who exhibit rigidity and simulated them by using a biomechanical model. Further, we investigated pendulum test outcomes when rigidity was exacerbated using two activation maneuvers (AMs) intended to elicit rigidity during clinical examination: bilateral fist clenching and unilateral finger tapping.

METHODS

Three individuals with PD (2 males/1 female, 57±9 years) off medication and 1 control (1 female, 39 years) were enrolled. Lower extremity rigidity was assessed using the Movement Disorders Society Unified Parkinson's Disease Rating Scale (MDS-UPDRS), item 3.3. The pendulum test was performed with the subject sitting on a treatment table with the trunk inclined approximately 40° from the horizontal. The examiner held the patient's foot for 30s with the knee extended before releasing it. First swing excursion (θ_1), the number (n) and duration (d) of oscillations and the resting angle (θ_r) (Fig. 1A) were assessed using kinematic data from motion capture (Vicon) in the baseline condition as well as during each of the AMs. Finally, to assess the contribution of muscle tone (T_b) and reflex gain (k_T), we simulated the pendulum test in the baseline condition based on a torque-driven biomechanical model of the lower leg [5].

RESULTS AND DISCUSSION

First swing excursion, the number and duration of the oscillations, and the resting angle all decreased progressively with increasing rigidity (Fig. 1). The AMs had an effect only in the PD participant with severe rigidity, where they reduced the resting angle (Fig. 1D). The model emulated baseline pendulum test kinematics in all participants, with T_b increasing with rigidity to account for the reduced resting angle). We were unable to capture the effects of the AMs in the severe case.
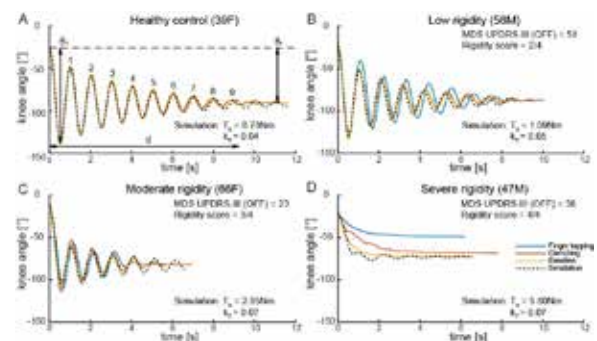
Figure 1: Knee angle responses during the pendulum test.

CONCLUSIONS

Parkinsonian rigidity altered pendulum test outcomes. Our simulations suggested an important role of increased muscle tone in Parkinsonian rigidity. However, additional damping and stiffness in a more realistic muscle model may be necessary for improved fits. Combined information from experimental data and simulations could clarify the pathophysiology of rigidity that may be important for proper diagnosis and treatment.

REFERENCES

[1] De Groote F et al. (2018). *PLoS One*, **13**: e0205763.
[2] Fung V and Thompson P (2002) *Rigidity and Spasticity* Lippincott Williams & Wilkins.
[3] Xia et al. (2009). *Clin Neurophysiol,* **120**: 1400-7.
[4] Lee HM et al. (2002). *J Neurol Neuros Psych*, **72**: 621-9.
[5] Solopova IA et al. (2014). *Hum Physiol*, **40**: 125-131.

Relationship between spasticity phenotypes and muscle morphology is different in children with spastic cerebral palsy and children with hereditary spastic paraplegia.

[1]Nathalie De Beukelaer, [1,2]Lynn Bar-On, [3]Anja Van Campenhout, [1]**Kaat Desloovere**,
[1]Department of Rehabilitation Sciences, KU Leuven, Leuven, Belgium
[2]Department of Rehabilitation Medicine, Amsterdam University Medical Centers, Amsterdam, Netherlands
[3]Department of Development and Regeneration, KU Leuven, Leuven, Belgium
corresponding author: kaat.desloovere@kuleuven.be

INTRODUCTION

Children with bilateral spastic cerebral palsy (SCP) present with lower limb muscle spasticity along with macroscopic muscle morphology alterations. Children with hereditary spastic paraplegia (HSP) are similar to SCP in clinical presentation [1]. Instrumented assessments that quantify spasticity based on electrophysiological and biomechanical signals [2], have established the existence of velocity and/or length-dependent muscle activation patterns in SCP resulting in spasticity phenotypes [3]. Preliminary evidence suggests that phenotypes may be related to underlying muscle structure [4]. However, muscle spasticity and morphology remain unstudied in HSP. Therefore, we aimed to investigate spasticity phenotypes and their relationship to muscle morphology in children with HSP and SCP.

METHODS

Thirty children (n=15 HSP, n=15 SCP), matched for age (5-17years) and Gross Motor Function Classification System (I=7, II=5, III=3), were compared to typically developing (TD) children (n=27). Medial gastrocnemius (MG) surface electromyography (sEMG) was recorded during passive ankle joint rotations at low (LV) and high velocity (HV) [2]. Length-dependent spasticity was defined as the average root-mean-square (RMS) EMG collected at LV. Velocity-dependent spasticity was defined as the average change in RMS-EMG between HV and LV (HV-LV) [3]. A validated three-dimensional freehand ultrasound technique, combining US images with motion analysis, was used to create 3D reconstructions the MG [5]. Resting MG muscle length normalized to muscle-tendon-unit length (nM-L), muscle volume normalized to body mass (nMV), and echo-intensity (EI) were estimated [6]. Kruskall-Wallis test (post-hoc Bonferroni) verified differences between the cohorts and Spearman's Rho assessed associations between spasticity-phenotypes and muscle morphology [7].

	HSP (n=15)	SCP (n=15)	TD (n=12)	TD (n=15)	HSP vs TD	SCP vs TD	HSP vs SCP
	Median (IQR)				p	p	p
RMS-EMG LV, μV	1.0 (1.3)	1.2 (4.8)	0.3 (0.3)		0.018	0.002	-
RMS-EMG HV, μV	11.5 (12.3)	9.6 (20.2)	0.6 (0.8)		≤0.001	≤0.001	-
RMS-EMG HV-LV, μV	10.5 (11.7)	8.0 (13.7)	0.2 (1.0)		≤0.001	0.003	-
nML, %	48.1 (3.0)	49.1 (7.6)		52.6 (4.1)	0.021	0.006	-
nMV, %	1.1 (0.7)	1.18 (0.6)		2.3 (0.5)	≤0.001	≤0.001	-
EI, 0-255 bit	95.0 (11.0)	98.75 (29.6)		93.5 (13.0)			-

HSP, hereditary spastic paraplegia; SCP, spastic cerebral palsy; TD, typical developing; y; IQR, interquartile ranges; y, years; GMFCS, gross motor function classification system; n, number; RMS-EMG, root mean square electromyography; LV, low velocity; HV, high velocity; nML, normalized muscle tendon unit length; nMV, normalized muscle volume; EI, echo-intensity.

Table 1: Differences in muscle spasticity and morphology between children with HSP, children with SCP and TD children.

RESULTS AND DISCUSSION

Compared to TD, both HSP and SCP had significantly higher RMS-EMG at LV, HV, HV-LV, as well as shorter nML and smaller nMV (Table 1). HSP children tended to show more velocity-dependent, and SCP more length-dependent activation, (not statistically significant). Similarly, there were trends for greater morphological alterations in HSP (except for EI). In SCP, higher RMS-EMG at HV was moderately associated with shorter nML (r_s=-0.55, p=0.041), while high RMS-EMG at LV associated with smaller nMV (r_s=-0.54, p=0.047) and higher EI (r_s=0.60, p=0.022). No correlations were found between sEMG HV-LV and nMV in SCP. In HSP, spasticity did not correlate with nML. However, higher RMS-EMG at HV was moderately associated with smaller nMV (r_s=-0.55, p=0.031) and both RMS-EMG at HV and HV-LV associated strongly with high EI values (r_s=0.68, p=0.006 and r_s=0.66, p=0.004, respectively). The presence of velocity-dependent spasticity, expressed as RMS-EMG at HV-LV, was associated with smaller muscle size and decreased muscle integrity (i.e. higher EI) in children with HSP. In contrast, in SCP, there correlations are reported for length-dependent spasticity.

CONCLUSIONS

This study revealed that MG muscle characteristics are similarly impaired in children with HSP and SCP, compared to TD children. Preliminary results suggest different spasticity-phenotypes between children with HSP and SCP. Since HSP is a genetic disorder and the age of symptom-onset could differ compared to SCP, these differences may help to better understand the pathogenesis of altered muscle characteristics in these disorders. To properly understand causational relationships and development of clinical symptoms, future studies should include follow-up measurements and investigate the interaction to treatment.

REFERENCES

[1] Salinas S et al. (2008). *Lancet Neurol*, **7**: 1127-1138
[2] Bar-on L et al. (2013). *Gait & Posture*, **38**: 141-147
[3] Bar-on L et al. (2014). *PLoS One*, **9**
[4] Bar-on L et al. (2018). *Front. Pediatr*, **5**
[5] Cenni F et al. (2016). *Comput Methods Programs Biomed*, **1**: 179-187
[6] Schless SH et al. (2018). *Dev Med Child Neurol*,
[7] Altman DG (1999). *Practical Statistics* Chapman & Hall, Londen

Acto-myosin cross-bridge stretch mechanics underlie history-dependent changes in muscle spindle sensory feedback: a multi-scale experimental and simulation study

Brian C. Horslen[1], Kenneth S. Campbell[2], Paul Nardelli[3], Kyle P. Blum[4], Timothy C. Cope[3,1], Lena H. Ting[1,5]

[1]W.H. Coulter Dept. Biomedical Engineering, Emory University and Georgia Institute of Technology, Atlanta, GA, USA
[2]Department of Physiology, University of Kentucky, Lexington, KY, USA
[3]Department of Biological Sciences, Georgia Institute of Technology, Atlanta, GA, USA
[4]Department of Physiology, Northwestern University, Evanston, IL, USA
[5]Department of Rehabilitation Medicine, Emory University, Atlanta, GA, USA
Email: lting@emory.edu

INTRODUCTION

Our goal was to determine whether small, behaviourally relevant stretch amplitudes affect muscle fiber stiffness and muscle spindle firing rate. People are constantly swaying while standing upright, this sway causes subtle stretching of the ankle musculature (<1% L_0). Muscle stiffness in both extrafusal skeletal muscle and specialized intrafusal muscle fibers within muscle spindle sensory organs is crucial for resisting and correcting perturbations to standing balance. Short-range stiffness in ankle muscles provides immediate resistance to perturbations, buying time for reflex activation [1]. We have recently shown that short-range stiffness, as predicted with an acto-myosin crossbridge model, dictates muscle spindle proprioceptive responses to stretch [2], which are crucial for triggering and shaping reactive balance responses to perturbations [3]. Both muscle spindle firing rate and muscle fiber short-range stiffness are depressed with recent muscle stretch, a process we call history-dependence. It is unclear whether muscle spindle firing rate and fiber stiffness are sufficiently high to resist perturbation during free standing because history-dependent effects have only been characterized a large stretch amplitudes (>3% L_0).

Here we combine *in vitro*, *in vivo*, and *in silico* studies to determine movement amplitude thresholds affecting history-dependence in muscle spindle firing rate and muscle stiffness. Our objectives were to determine: A) if stretching muscles in the range of human postural sway amplitudes depressed muscle short-range stiffness and muscle spindle firing rate; and B), whether acto-myosin cross-bridge kinetics is sufficient to explain history-dependent changes to muscle spindle firing rate. We find high muscle short-range stiffness and muscle spindle stretch sensitivity is preserved in the range of typical postural sway but increases in sway to a range associated with fall risk decreases both muscle stiffness and muscle spindle firing responses to stretch.

METHODS

Muscle fiber stretch mechanics *in vitro* were studied using single permeabilized rat soleus muscle fibers mounted between a muscle puller and load cell. Muscle spindle Ia afferent firing *in vivo* was recorded from exposed dorsal spinal roots in anesthetized rats during triceps surae stretch. *In silico* muscle spindle firing rate predictions were based on simulated stretch of parallel half sarcomeres whose force and yank (dF/dt) determined afferent driving potentials input to a leaky integrate-and-fire neuron model. Pre-stretch conditioning patterns were scaled to muscle/muscle fiber resting length (L_0) for each experiment (Figure 1A). Ramp-and-hold test stretches were conditioned with ramp-release conditioning stretches (variable amplitude and inter-stretch interval). We evaluated the initial burst at stretch onset and dynamic response during lengthening in the muscle spindle and short-range stiffness and impulse in muscle fibers.
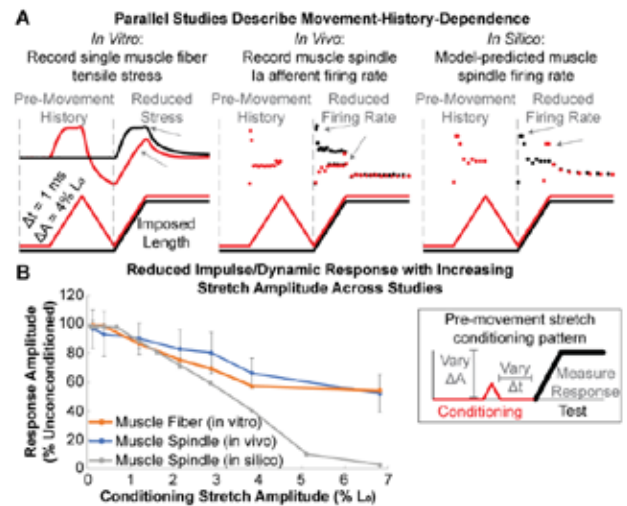
Figure 1: Variable amplitude and time interval pre-stretch movement patterns were used to condition muscle fiber stiffness and muscle spindle firing rate (A). Large conditioning stretches significantly reduced firing rate and stiffness in each study (B).

RESULTS AND DISCUSSION

Recorded and simulated muscle fiber stiffness and muscle spindle firing rate each decrease with pre-stretch amplitudes greater than healthy postural sway (>1% L_0; Figure 1B). Our mechanistic cross-bridge model predicted experimentally observed changes to muscle spindle firing rate. We interpret the similar magnitudes and patterns of change observed in the muscle fiber and simulated and recorded spindle data as evidence of a common underlying cross-bridge mechanism.

CONCLUSIONS

Muscle short-range stiffness and muscle spindle feedback is likely high during "healthy" postural sway (<1% L_0). However, larger sway amplitudes (>2%L_0) may impair both instantaneous and reflexive contributions to balance control

ACKNOWLEDGMENTS

REFERENCES

[1] De Groote F et al. (2017) *J. Biomech*, **55**:71-77
[2] Blum KP et al. (2018) *SfN Abstract*, 771.05
[3] Lockhart BD & Ting LH (2007) *Nat Neurosci*, **10**:1329-1336.

4th Rocky Mountain Muscle Symposium - Canmore Nordic Centre - July 27-29, 2019

rMMs

Muscle fibre type characteristics of the lumbar multifidus and erector spinae in persons with non-specific chronic low back pain and healthy controls.

[1]**A. Agten**, [1]S. Stevens, [1]J.Verbrugge, [1]A. Timmermans, [1]F. Vandenabeele
[1]Rehabilitation Research Centre, Faculty of Rehabilitation Sciences and Physiotherapy, Hasselt University, Diepenbeek, Belgium
corresponding author: anouk.agten@uhasselt.be

INTRODUCTION

Low back pain (LBP) is the most common musculoskeletal cause of disability and has a major socio-economic impact on today's western society [1]. In 39.5% of all persons with LBP, pain persists longer than 12 weeks and is referred to as chronic LBP. In the majority of cases, chronic LBP is due to a non-assignable cause, classified as non-specific chronic low back pain (NSCLBP) [2]. Both chronicity and lack of etiology impede the effective treatment of NSCLBP. On a macroscopic level, there is accumulating evidence that NSCLBP is associated with dysfunction of the lumbar multifidus (MF) and the erector spinae (ES) [3]. However, knowledge on a microscopic level, more particular on muscle fibre type, is very limited. The aim of this study is to investigate the structural muscle fibre type characteristics of the MF and ES, in order to further elucidate their functional capacity and their involvement in LBP.

METHODS

A cross-sectional study was performed in the Rehabilitation Research Centre, Hasselt University, Diepenbeek, Belgium. Muscle fibre type characteristics of 20 persons with NSCLBP and 18 healthy controls were investigated. Biopsy samples of the MF and the ES were taken at the level of vertebra L4 with a percutaneous fine needle biopsy technique [4]. These muscle samples were analyzed with an immunofluorescence staining of the myosin heavy chain (MHC) isoforms. In each sample, the percentage and cross-sectional area (CSA) of type I, IIa, IIax and IIx were quantified. From these data, the relative cross-sectional area (RCSA) was calculated. These outcomes were analyzed using JMP® Pro 14.1.0 software (SAS Institute Inc, Cary, NC, 1989-2007). A repeated measure analysis of variance (ANOVA) was performed.

RESULTS

Both, in the MF as well as in the ES, type I muscle fibres are predominantly present (Figure 1). In healthy controls, the RCSA of type I muscle fibres is 63.54% for the ES and 68.8% for the MF. Type I muscle fibres were significantly larger (p=0.0053) in the MF (7439.31.11µm²) compared to the ES (6279.48µm²). The mean muscle fibre type percentages were not significantly different between the lumbar ES and MF for all muscle fibre types.
A comparison between the muscle fibre type characteristics of persons with NSCLBP with healthy subjects, showed no significant between group differences for CSA in the ES. However, persons with NSCLBP displayed a higher (p= 0.0978) number of type I muscle fibres, and a significant lower (p= 0.0019) number of type IIx muscle fibres in the ES. This resulted in a higher (p= 0.0596) RCSA for type I fibres, and a significant lower RCSA for type IIx fibres (p= 0.0411). There were no significant between group differences in the MF.

.
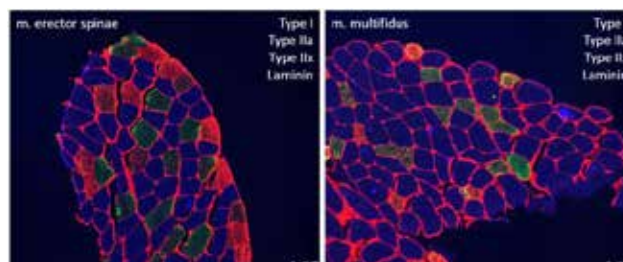
Figure 1: **Representative immunofluorescence image of the lumbar ES and MF muscle.** Muscle cross-sections were incubated with primary antibody against laminin (red), MHCI (blue), MHCIIa (green) and MHCIIx (red).

DISCUSSION

The significant larger type I muscle fibres in the lumbar MF compared to the ES, could possibly indicate that the MF seems to display muscle fibre type characteristics that are slightly more appropriate to maintain stability of the spine. However, because we did not demonstrate significant differences in RCSA between ES and MF, we cannot firmly state that there are functional differences between these two muscles only based on structural characteristics.

In contrast to current knowledge on muscle fibre typing in LBP [3], we found that the paraspinal muscles of persons with NSCLBP display a larger oxidative potential based on an increase of the number type I fibres at the expense of type IIx. However, this was the first study comparing muscle fibre type characteristics between persons with NSCLBP and healthy controls, for both the ES and MF. The larger oxidative capacity, and the decline in glycolytic capacity of the ES in persons with NSCLBP found in this study could have implications for physical rehabilitation.

REFERENCES

[1] Balague F. et al. (2012). Lancet, 379: 482-91.
[2] Airaksinen O. et al. (2006). Eur. Spine J. 15: S192-300.
[3] Cagnie B. et al. (2015). J Manipulative Physiol Ther. 38: 653-63.
[4] Agten A. et al (2018). J. Anat, 233: 542-551.

IL4 counteracts cancer-induced skeletal muscle atrophy: one cytokine for multiple effects.

[1]**Domiziana Costamagna**, [1]Robin Duelen, [2]Fabio Penna, [2]Paola Costelli, [1, 3] Maurilio Sampaolesi
[1]Translational Cardiomyology, Stem Cell Biology and Embryology, Department of Development and Regeneration, University Hospital Gasthuisberg, Leuven, Belgium; [2]Experimental Medicine and Clinical Pathology Unit, Department of Clinical and Biological Sciences, University of Turin, Italy; [3]Division of Human Anatomy, Department of Public Health, Experimental and Forensic Medicine, University of Pavia, Italy.
Corresponding author: maurilio.sampaolesi@kuleuven.be

INTRODUCTION

Cancer patients frequently present with cancer cachexia, a syndrome characterized by both fat and skeletal muscle weight loss that markedly interfere with patient tolerance to antineoplastic therapies. Cancer-induced muscle wasting results from hyperactivation of the main proteolytic systems, but also from an increase of Satellite Cell (SC) proliferation. Indeed, an increase in the amount of activated SCs in cachectic muscle, likely unable to complete the regeneration *in vivo*, has already been reported (1). Besides SCs, other interstitial cell populations are involved in myogenic differentiation, such as mesoangioblasts (MABs), vessel-associated muscle progenitors, and Fibro Adipogenic Progenitors (FAPs). Recently, we demonstrated that BMP-SMAD-signaling blockade improves MAB myogenic differentiation (2). As for FAPs, they have the potential to enhance the differentiation rate of myogenic progenitors after injury and during disease progression (3, 4), contributing to the release of cytokines able to stimulate muscle regeneration, including Interleukin 4 (IL4). In this study, we investigated how IL4 contributes to the pathogenesis of muscle wasting occurring in mice bearing the colon adenocarcinoma-C26.

METHODS

Balb/c mice were subcutaneously injected with $5x10^5$ C26 cells (C26; n=10) or PBS (C; n=10). At day 5, half of the mice from both groups were randomized to receive a daily i.p. IL4 injection (1.3µg/ mouse; IL4 n=5, C26+IL4 n=5). The animals were sacrificed 14 days after tumor implantation. Tibialis anterior (TIB) were frozen with cooled isopentane for morphological analysis. Functional experiments were performed such as forelimb grip strength, measured with Digital Grip strength meter (Columbus Instruments), and treadmill assay, motor speed set to 10 m/min, with a 1 m/min increase and an uphill inclination of 10°, till exhaustion and >10s stop. For survival experiments, mice were followed until the KU Leuven predetermined human end-point criteria were fulfilled (n=10 per group). All results were expressed as mean ± SD. When three or more groups were compared, a one-way ANOVA test was used.

RESULTS AND DISCUSSION

Body weight loss was partially rescued in C26 bearing mice daily treated with IL4 (C26+IL4) with respect to untreated C26 hosts. Functionally, C26+IL4 mice were able to perform better in terms of muscle grip and running time spent during a treadmill exhaustion assay than untreated C26-bearing animals. Consistently, C26+IL4 were able to survive longer than C26-hosts. Decreased muscle fiber CSA confirmed C26 muscle atrophy and a rescue for C26+IL4 was reported (Fig. 1 a, b). Furthermore, differently from the usual increase in cachectic conditions of SCs and FAPs, the number of SCs in C26+IL4 mice was comparable to Control levels (data not shown). Molecular analyses will be performed to understand if IL4 can induce protein synthesis, usually inhibited in C26 mice. Moreover, experiments on muscle injury will be needed to understand if IL4 can improve regeneration, which is usually impaired in cachectic conditions. These results demonstrate that the treatment with the anti-inflammatory cytokine IL4 can partially rescue cancer-induced muscle atrophy, promoting muscle performances and resulting in extended mice survival. Further experiments will be needed to understand the molecular mechanisms involved in the beneficial effect of IL4 treatment in cancer cachexia.
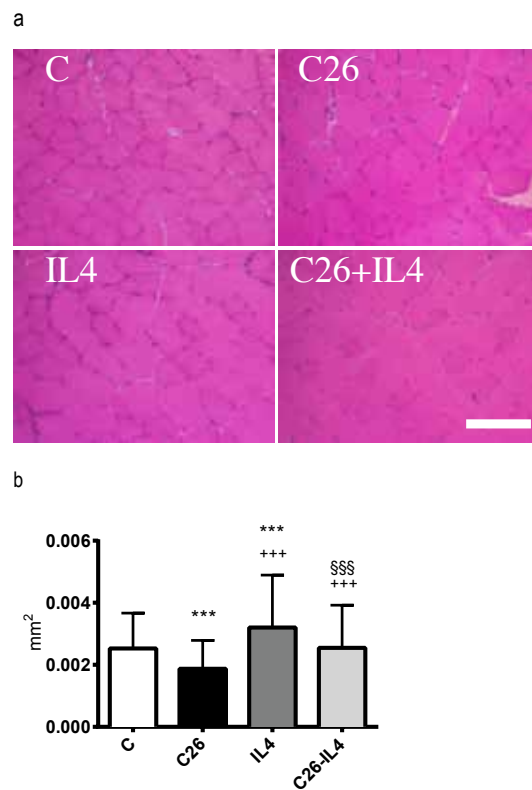
Figure 1: **a**) H&E staining and (**f**) fiber size distribution of *TIB* muscles from the different groups. Significance of the differences *p<0.05, **p<0.01, ***p<0.001, ****p<0.0001 vs C; +p<0.05, ++p<0.01, +++p<0.001, ++++p<0.0001 vs IL4; $p<0.05, $$p<0.01, $$$p<0.001, $$$$p<0.0001 vs C26. Scale bar: 50µm.

REFERENCES

[1] Penna et al., 2010; *PlosOne*; **5**: e13604.
[2] Costamagna et al., 2016; *J Mol Cell Biol*; **8**(1):73-87.
[3] Joe et al., 2010; *Nat Cell Biol*; **12**: 153-63.
[4] Mozzetta et al., 2013; *Embo Mol Med*; **5**(4): 626–639.

Poster Session 2:

Emma Hodson-Tole

Liliam Oliveira

Hoshizora Ichinose

Neale Tillin

Brent Raiteri

Wolfgang Seiberl

Marco Vaz

Carlos Cruz-Montecinos

Robert Griffiths

Brian MacIntosh

Jaqueline Lourdes Rios

Fransiska Bossuyt

Ultrasound Derived *in vivo* Measures of Skeletal Muscle Vibration during Locomotion in Humans

[1]**Emma F. Hodson-Tole**, [2]Adrian K.M. Lai

[1]Musculoskeletal Science & Sports Medicine Research Centre, Manchester Metropolitan University, Manchester, UK
[2]Dpt. Of Biomedical Physiology & Kinesiology, Simon Fraser University, Burnaby, BC, Canada
corresponding author: e.tole@mmu.ac.uk

INTRODUCTION

During locomotion impact force and energy are generated when the foot contacts the ground. Soft tissues in the body, such as skeletal muscles, have been suggested to contribute to the damping of these impact forces and energy. Direct measurement of in-vivo skeletal muscle vibrations have not however been made.

B-mode ultrasound imaging provides a non-invasive means of measuring dynamic in-vivo muscle behaviour. Computational methods of analysing collected images can be used to measure the behaviour of the aponeurosis [1] and this could be used to provide direct measurement of the vibrations that travel through a muscle.

Here we therefore exploit computational image analysis techniques to quantify the behaviour of the deep and superficial aponeurosis of the human soleus muscle (SO) during walking and running at different speeds. The aims were to: i) evaluate the use of ultrasound imaging to quantify in-vivo muscle vibrations; and ii) determine changes in muscle vibration characteristics resulting from different impact forces.

METHODS

Ten participants walked and ran on an instrumented treadmill at a range of steady-state locomotion speeds: walk at 0.7, 1.4 and 2.0 m s^{-1} and run at 2, 3, 4, and 5 m s^{-1}. Each participant gave informed written consent and the study was approved by the relevant ethics committees.

Ground reaction forces (2000 Hz) were recorded during each 15 s trial. B-mode ultrasound image sequences (80 fps) were also recorded from the mid-belly region of lateral gastrocnemius (LG), providing a clear view of the deep and superficial aponeurosis of SO. The transducer was firmly secured in place using elasticated bandage.

Ground reaction forces were filtered (fourth-order, low pass Butterworth, 60 Hz cut-off) and used to identify timing of stance phase of each stride. In addition, the input signal frequency to the body during ground impact was estimated from the vertical component of the ground reaction force [2].

Ultrasound images were analysed using an active shape model approach [1] that enabled the position of the deep and superficial SO aponeuroses to be identified (Figure 1). To quantify in-vivo muscle vibrations, 20 point landmarks were defined along each aponeurosis based on the location of the shape model fit (Figure 1). A power-frequency of the displacement of the points was used to quantify the transverse vibrations in each trial (deep-superficial direction). Prior to calculation, the mean time-varying displacement of each landmark was subtracted from each displacement value for that landmark, to minimize low frequency movement related characteristics.

RESULTS AND DISCUSSION

Incremental increases in impact forces occurred with faster walking and running speeds that were consistent with changes in measured muscle vibrations. Input signal frequencies ranged from 2 – 14 Hz for walking speeds and between 10 – 20 Hz for running. The measured frequencies of the muscle vibrations ranged from ~3 Hz during slow walking, up to ~37 Hz during fast running. These muscle vibration frequencies are similar to those previously reported from skin-mounted sensors during steady-state running [2].

With increased walking speed the power below which 99% of the landmark displacement frequencies occurred increased, on average, by ~6 Hz during stance phase. For increased running speed the increase was ~15 Hz. The vibrations were greatest during the period of initial ground contact, before being damped in the stance phase and dissipating during the swing phase.

It was anticipated that some of the vibration frequencies recorded may reflect motion artefact of the ultrasound transducer on the skin surface as the foot contacts the ground. This would lead to similar vibration frequencies being measured across all aponeuroses. However, when quantifying the frequencies of landmark displacements in the superficial aponeurosis of LG, more than 90% of the power was below 10 Hz during the first half of the stance phase. This is strikingly lower than the frequency of displacement recorded in SO aponeuroses.

Measures of vibration in deeper muscles can therefore be obtained using ultrasound data, with computational image segmentation a useful tool to extract this information.
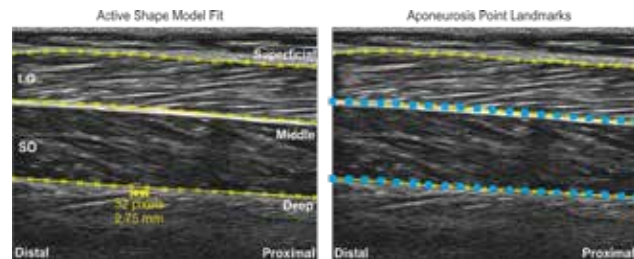

Figure 1: Example shape model fit (Left) and 20 point landmarks distributed along SO aponeuroses (Right) in one analysed image

ACKNOWLEDGEMENTS

REFERENCES

[1] Darby J et al. (2011). *J. Appl. Physiol.* **112**: 313-327.
[2] Boyer KA & Nigg BM (2004). *J. Biomech*. **40**: 1583-88.

74

SHEAR MODULUS OF THE RESTING AGONIST/ANTAGONIST MUSCLES

[1,2]**Liliam F. Oliveira**, [1]Maria Clara A. Brandão, [1]Luciano L. Menegaldo
[1]Biomedical Engineering Program, Federal University of Rio de Janeiro, RJ, Rio de Janeiro, Brazil.
[2]Physical Education and Sports, Federal University of Rio de Janeiro, RJ, Rio de Janeiro, Brazil.
corresponding author: liliam@peb.ufrj.br, liliam.oliva@gmail.com

INTRODUCTION

Shear wave elastography (SWE) has been applied to study muscle stiffness adaptation to stretching, to strengthening and to many clinical conditions (1,2). Little attention has been devoted to determining the differences in resting mechanical properties of the skeletal muscles with opposite functions around a joint (agonist/antagonist).

Free available platforms to simulate body movements are widely used for research or clinical practice, as the OpenSim (3). With these models, some mechanical relations can be estimated. The aim of this study was to test if it was possible to partially explain the shear modulus of skeletal muscle measured by SWE during rest based on the length-tension property estimated by OpenSim.

METHODS

The study was approved by the University Hospital Ethics Committee (nº 570.945 and 519.230). The sample was composed of 35 healthy individuals (30,11 ± 7,07 years old, 70,21 ± 18,28 kg and 1,67 ± 0,15 cm). Elastographic images from nine resting muscles were acquired with an Aixplorer ultrasound (Supersonic Image, v.9, linear transducer 10-2MHz): medial and lateral gastrocnemius and semitendinosus (lying pronated), vastus lateralis and medialis, rectus femoris, tibialis anterior and biceps brachii (lying supinated). For the lateral triceps brachii, the volunteer was seated, 90º elbow flexion, resting forearm.

A circular ROI was selected in the elastographic color map and the mean shear modulus (μ) was calculated through a custom routine, dividing each matrix value by 3.

The normalized fibre-length for these muscles at the same joint position was estimated by the OpenSim 4.0 (arm 26, 3Dgait2392 models), with no activation (a=0), (Figure 1).

Paired t-test or ANOVA one way were used to test for significant differences among muscles shear modulus, that act at each joint (elbow, knee and ankle).
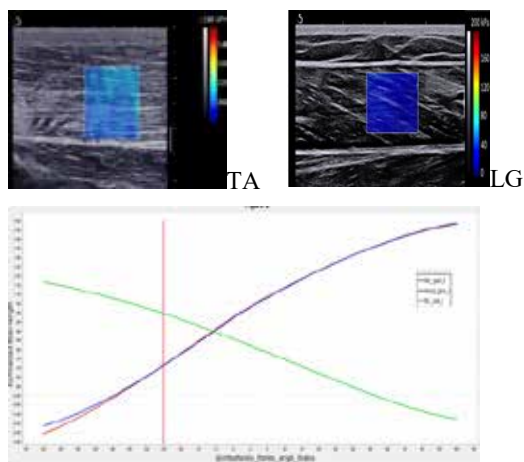

Figure 1: SWE of the TA and LG. Normalized fibre length curves from TA, LG and MG. Ankle angle around 25º. plantar flexion.

RESULTS AND DISCUSSION

Table 1: Shear modulus and normalized fibre length for the muscles at pronated or supinated lying positions.

Muscle	μ (kPa)	Norm. fiber length
Biceps Brachii (BB)	9.2±3.57*	1.29
Triceps Brachii (TB)	4,5±2,34	0.62
Semitendinosus (ST)	5,3±1,86**	1.04
Rectus Femoris (RF)	4,6±1,43	0.97
Vastus Lateralis (VL)	3,5±1,20	0.53
Vastus Medial (VM)	3,9±1,37	0.53
Tibialis Anterior (TA)	11,4±3,86***	1.00
Medial Gastrocnemius (MG)	5,06±1,4	0.72
Lateral Gastrocnemius (LG)	4,74±2,03	0.72

*$p<0.05$, **$p<0.05$ VL and VM, *** $p<0.05$ Mg and LG

The results (table 1) show that flexors muscles (pronated or supinated relaxed positions) with higher normalized fibre lengths (BB, ST and TA), showed greater shear modulus. This is in accordance with the force-length relationship where, at these lengths, passive force is already present on the curve descend phase. The slack lengths for flexors would configure more flexed joint positions. There are many other variables that have to be considered in the SWE measures; the neural contribution to tonus, the pennation angle of the fibres, although it seems not influencing significantly the shear modulus measures in vivo (4) and the tension of other passive structures as connective tissue sheaths and the extracellular matrix, which has been showed to be greatly responsible for muscle bundles stiffness (5).

CONCLUSION

The flexors are stiffer than the extensors for the respective joints when the body is lying relaxed, which can be partially explained by intrinsic muscle mechanics. The SWE has the potential to measure the resting muscle stiffness and can be applied to study altered mechanical properties conditions as delayed muscle soreness and spasticity. Additionally, it can be used to test for muscle passive stiffness increasing after eccentric contractions, as is already described for cat muscles (6).

ACKNOWLEDGEMENTS

REFERENCES

[1] Creze M et al. (2017). *Skeletal Rad.*, online.
[2] Mannarino P et al. (2019). *PlosOne*, 0205782.
[3] Delp SL et al.(2007).*IEEE Trans BiomEng*,**54**:1940-50.
[4] Lima KL et al. (2019). *J. Ultras. Med*, **38**: 81-90.
[5] Meyer GA & Lieber RL (2011). *J.Biomech*,**44**:771-773.
[6] Herzog W at al. (2003) *J.Exp.Biol*.,**206**:3635-3643.

75

Contractile and non-contractile tissues in the midthigh of the elderly and younger athletes: Inter-individual differences and relationships with body composition and muscle function

[1]**Hoshizora Ichinose**, [1]Pavlos Evangelidis, [1]Takaki Yamagishi, [2]Fumiko Tanaka,
[3]Shigenobu Shibata, [4]Munekazu Naito, [1,2]Yasuo Kawakami
[1] Graduate School & Faculty of Sport Sciences,
[2] Organization for University Research Initiatives,
[3] School of Advanced Science and Engineering, Waseda University, Tokyo, Japan
[4] Department of Anatomy, Aichi Medical University, Aichi Medical University, Aichi, Japan
Email: momiji728@akane.waseda.jp

INTRODUCTION

Skeletal muscles are comprised of contractile and non-contractile tissues, the latter of which include neurovascular, adipose and connective tissues. Non-contractile tissues (NCTs) can accumulate beneath the deep fascia lata and between (InterNCT) and within (IntraNCT) muscles [1]. These NCTs might make a functional difference between people who have a similar muscle cross-sectional area [2]. However, the extent of the individuality and the relationships with contractile tissue and muscle function still remain unclear. Moreover, these tissues are negatively associated with obesity [3]. It can be strongly related with some adipose tissues. Therefore, this study aimed to evaluate Inter- and Intra-NCT of the midthigh, and to investigate the relationships between these tissues and muscle function, contractile and adipose tissues. We targeted on the elderly individuals and younger adults who demonstrate substantial differences in their exercise habits.

METHODS

Participants were 59 healthy older adults (30 males and 29 females: aged 64-84 years) and 59 younger adults (26 males and 33 females: aged 14-28 years). Axial scanning of the right leg was performed with MRI, and cross-sectional areas (CSA) of 12 muscles (mCSA; total of contractile tissue and IntraNCT) and femur were measured. InterNCT was calculated by subtracting mCSAs and femur from the whole CSA within the fascia lata. The CSAs of Intra-NCT and contractile tissues of the quadriceps femoris (QF) and hamstrings (HAM) were also measured. Isometric knee extensor and flexor strength were measured as an index of muscle function. Body fat mass was determined by bioelectrical impedance analysis, and the CSAs of visceral and subcutaneous adipose tissues at the L4 level were measured.

RESULTS AND DISCUSSION

CSA of the Inter- and Intra-NCT of the midthigh were significantly larger in older adults than younger adults. The relative IntraNCT within mCSA (%IntraNCT) was significantly higher in HAM than QF in older adults, while there was no difference between muscles in younger adults. A previous research [4] reported higher %IntraNCT in HAM than QF both in older and younger individuals. These findings suggest that IntraNCT tends to accumulate more in HAM than QF, and that less accumulation of IntraNCT in HAM is a specific characteristic of active younger adults.

In older males, contractile tissue CSA rather than mCSA was correlated with the torque. This suggests IntraNCT as a confounding factor to the relationship between muscle mass and strength.

The CSA of InterNCT was not significantly correlated with CSA of the contractile tissue. However, significant negative correlations between CSAs of IntraNCT and contractile tissue were observed in total of older and younger groups while these correlations were positive within individual groups (Figure 1). These results suggest two factors for the IntraNCT, i.e., increase of adipose tissue with aging and that of the contractile tissue associated with muscle size.

There were significant correlations between body fat mass and Inter- and Intra-NCT. Moreover, IntraNCT showed a stronger correlation with visceral adipose tissue than InterNCT. Addison et al. [5] speculated that the Inter- and Intra-NCT is an ectopic fat depot similar to visceral adipose tissue. These NCT could be a measure of the whole body and visceral adiposity.
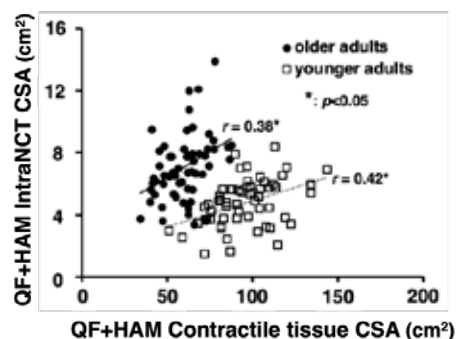
Figure 1: The relationship between contractile tissue CSA and IntraNCT CSA of the midthigh.

REFERENCES

[1] Ogawa et al. (2017). *Neural Regen Res*, **12**: 2100-2105.
[2] Maughan et al. (1983). Eur J Appl Physiol Occup Phisiol, **50**: 309-318.
[3] Goodpaster et al. (2000). *Am J Crin Nutri*, **71**: 885-892.
[4] Akima et al. (2015). *Eur J Appl Physiol*, **115**: 1627-1635.
[5] Addison et al. (2014). *Int J Endocrinol*, **309570**, 1-11.

The influence of residual force depression on torque during shortening contractions without- relative to with- pre-load

Neale A. Tillin[1], Shaun X.T. Ang[1,2]
[1]Department of Life Sciences, University of Roehampton, London, UK;
[2]National Junior College, Singapore
Email: neale.tillin@roehampton.ac.uk

Introduction

Active muscle shortening causes residual depression in steady-state isometric force (rFD), which is proportional to the work done during shortening; but, there is limited understanding of the effects of rFD on force during the shortening [1]. We recently compared torque recorded during shortening MVCs with and without a pre-load prior to shortening, in slow- and fast-velocity conditions [2]. Pre-loaded torque was achieved earlier and exceeded in the MVCs without pre-load of the fast-velocity condition, which may have been due to rFD, as the work done and thus rFD induced would have been greater in the MVCs with, compared to without pre-load. However, the effects of rFD could not be isolated from those of neural activation because contractions were voluntary. Furthermore, it was unclear why the effects of rFD were noticeable in the fast-velocity condition only. Theoretically, the effects of rFD should be greatest in conditions with a smaller proportion of work done in the contractions without- relative to with pre-load, irrespective of velocity. We aimed to investigate the influence of rFD on torque during involuntary shortening contractions (which ensure constant activation) without- relative to with- pre-load, at different iso-velocities.

Methods

Seventeen participants completed involuntary contractions (100 Hz) of the knee extensors in an isokinetic dynamometer at iso-velocities of 40, 80, 120, 160, and $200°.s^{-1}$. In each condition the knee was passively extended from 75 to 180° (full extension), and two different involuntary contractions were evoked: (1) without pre-load, 250-ms in duration, commencing at 100°; and (2) with pre-load, 1250 ms in duration, commencing 1000 ms prior to 100° being reached. Data were corrected for passive torque contributions, and torque-time in contractions without pre-load were aligned with- and divided by- torque-time in contractions with pre-load (Figure 1A). rFD was estimated as a function of work, based on the differences in both work and torque at 250 ms, between contractions with and without pre-load, in the $200°.s^{-1}$ condition. Torque data was corrected for estimated rFD and relative torque-time curves re-calculated (Figure 1B).

Results and Discussion

The torque recorded in contractions without pre-load exceeded pre-loaded torque in all conditions, and to greater extents as velocity increased (Figure 1A). Likewise, the relative torque-time curves steepened with increased velocity (Figure 1A; Table 1). After correcting for estimated rFD, pre-loaded torque was no longer exceeded in contractions without pre-load, but relative torque-time remained steeper with increased velocity, suggesting a different contractile mechanism for this phenomenon (Figure 1B; Table 1). Furthermore, the ratio of work done up to 250 ms in contractions without- relative to with- pre-load increased with velocity, suggesting a reduced influence of rFD on the relative torque-time curves with increased velocity.
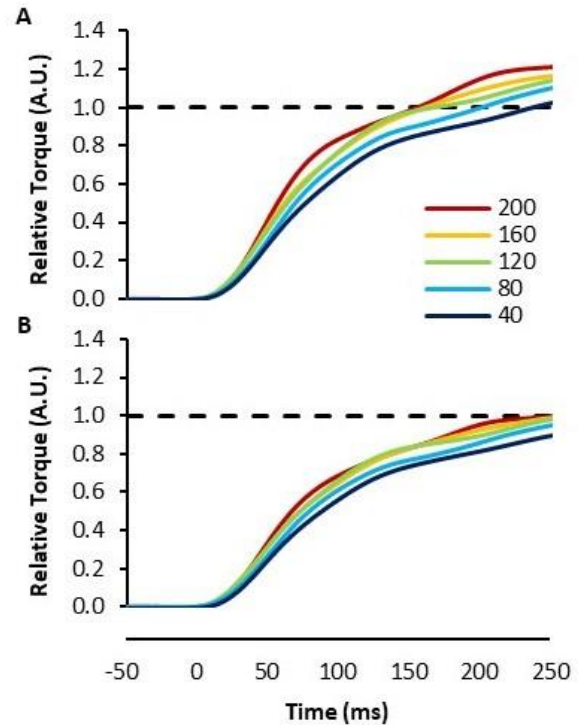
Figure 1: Torque-time at different velocities in contractions without- relative to with- a pre-load, before (A) and after (B) rFD correction.

Table 1. Time (ms) to 75% of pre-loaded torque in contraction without pre-load, before and after rFD correction.

	$40°.s^{-1}$	$80°.s^{-1}$	$120°.s^{-1}$	$160°.s^{-1}$	$200°.s^{-1}$
Before	125 ± 31	113 ± 29	99 ± 23	99 ± 25	89 ± 26
After	165 ± 44	140 ± 34	124 ± 29	126 ± 27	119 ± 29

Conclusions

These results provide novel evidence of rFD in shortening contractions, which caused earlier achievement, and exceedance, of pre-loaded torque in contractions without pre-load at all measured velocities. However, rFD did not explain the shorter time to pre-loaded torque with increased velocity.

References

[1] Chen et al., (2019). *J Appl Physiol*, **126**: 1066-1073.
[2] Tillin NA et al. (2018). *J Exp Biol*, **221**, jeb193367.

77

ECCENTRIC HAMSTRING FASCICLE BEHAVIOR OCCURS DURING THE NORDIC HAMSTRING EXERCISE

[1]**Brent J. Raiteri**, [1]Ronja Beller, [1,2]Daniel Hahn
[1]Faculty of Sport Science, Ruhr University Bochum, Bochum, NRW, Germany
[2]School of Human Movement and Nutrition Sciences, The University of Queensland, Brisbane, QLD, Australia
Corresponding author: brent.raiteri@rub.de

INTRODUCTION

Hamstring muscle strain injuries are the most common injuries among high-speed running athletes with ~80% of such injuries involving the biceps femoris long head (BFlh) [1]. The BFlh has been suggested to be at increased risk of injury because of its higher muscle-tendon unit strain relative to the other biarticular hamstring muscles during the late swing phase of high-speed running [2]. As low eccentric knee flexor strength and short BFlh fascicles have been shown to increase the relative risk of sustaining a hamstring muscle strain injury [3], eccentrically-biased hamstring exercises have been recommended to increase both eccentric strength and hamstring fascicle lengths. One such exercise, the Nordic Hamstring Exercise (NHE), has received considerable attention because of its reported ability to increase BFlh muscle fascicle length by 21% following ten weeks of training [4] and reduce hamstring injury incidence by >60% [5]. Both findings indicate that the NHE is an eccentric exercise, however, whether BFlh muscle fascicles undergo active stretch during the NHE (as opposed to the tendinous tissues alone) has yet to be investigated and this formed the aim of the current study.

METHODS

Following fixed-end maximum voluntary knee flexion contractions (MVCs) in a prone position and familiarization with the NHE exercise, 14 recreationally-active males performed at least two sets of three repetitions of the NHE, which involved lowering their torso as slowly as possible from 90-0° of knee flexion while maintaining an extended hip. At least two minutes of rest was provided between NHE sets and MVC contractions to minimize fatigue effects and the trials with the largest peak knee flexion forces were later analyzed.

All trials were performed on a custom-built apparatus, which allowed knee flexion forces and knee angles from the left leg to be respectively measured via a strap around the ankle in-series with a load cell and a goniometer at the knee. The force and goniometer signals were previously calibrated and sampled at 1 kHz using a 16-bit Power1401-3 and Spike2 data collection system (CED, Cambridge, UK).

BFlh, BF short head (BFsh) and semitendinosus (ST) muscle activities during the NHE and MVC trials were collected according to SENIAM guidelines using surface electromyography (EMG). EMG signals were amplified 1000 times and band-pass filtered between 10 and 500 Hz (AnEMG12, OT Bioelettronica, Torino, Italy), prior to being sampled at 2 kHz using the acquisition system already described.

Muscle fascicles within the superficial compartment of the BFlh were visualised with B-mode ultrasound using a 128-element, 60 mm linear transducer operating at 60 Hz with an image depth of 50 mm (Telemed, Vilnius, Lithuania). BFlh fascicle lengths were later determined in Matlab around the plateau of peak knee flexion force in seven participants (MathWorks, MA, USA) using the methods described in [6].

RESULTS AND DISCUSSION

Mean peak knee flexion forces (n=14) were greater (P=0.02) during the NHE (430±47 N) than during the fixed-end MVCs (395±56 N). This was despite shorter ($P<0.01$) mean BFlh fascicle lengths (n=7) and greater ($P<0.01$) mean knee flexion angles at peak knee flexion force in the NHE (70±11 mm and 41±9°) compared with the MVCs (83±12 mm and 12±6°). The shorter fascicle lengths at peak knee flexion force during the NHE indicate that the BFlh operated further down the ascending limb of its force-length relation where it would have a reduced isometric force capacity compared with the MVCs, so this data provides indirect evidence that the BFlh acted eccentrically during the NHE. Indeed, ultrasound imaging confirmed that the BFlh muscle fascicles were actively stretched during peak muscle activities of BFlh, BFsh and ST and at the plateau of peak knee flexion force during the NHE. The mean fascicle stretch magnitude at peak force production during the NHE was 7±4 mm and ranged from 3-14 mm across participants.

BFlh fascicle lengths at rest could not be accurately determined due to the limited field of view of the ultrasound transducer and therefore fascicle strains were not calculated. The amount of BFlh muscle fascicle shortening and the fascicle behavior at peak force in seven participants could also not be quantified due to substantial out-of-plane motion of the muscle fascicles with respect to the ultrasound imaging plane. Finally, the relationship between knee flexor strength and BFlh muscle fascicle behavior was not quantified due to the low sample size. We were careful to analyze fascicle behavior around the plateau of peak knee flexion force to ensure that hamstring muscle deactivation did not contribute to the fascicle lengthening that we observed. Whether the BFlh fascicles are stretched as much in individuals accustomed to the NHE remains to be tested. We recommend that further ultrasound imaging studies on the BFlh are conducted to determine which exercise results in the greatest active fascicle strain and to confirm whether this subsequently results in longer fascicle lengths post-training.

REFERENCES

[1] Verrall GM et al. (2003). *Am J Sports Med (AJSM)*, **31**: 969-973.
[2] Schache AG et al. (2012). *Med Sci Sports Exerc*, **44**: 647-658.
[3] Timmins RG et al. (2015). *Br J Sports Med (BJSM)*, **50**: 1524-1535.
[4] Bourne MN et al. (2017). *BJ SM*, **51**: 469-477.
[5] Petersen J et al. (2011). *AJSM*, **39**: 2296-2303
[6] Farris DJ & Lichtwark GA (2016). *Comput Methods Programs Biomed*, **128**: 111-118.

78

ELECTRICALY VERSUS VOLUNTARILY ACTIVATED STRETCH-CONTRACTIONS: IS THERE A TRUE NON-RESPONDER?

[1,2]**Wolfgang Seiberl,** [1]Anna Arlt, [1]Denis Holzer, [1]Florian K. Paternoster
[1]Biomechanics in Sports, Technical University of Munich, Munich, Germany
[2]Human Movement Science, Bundeswehr University Munich, Neubiberg, Germany
wolfgang.seiberl@unibw.de

INTRODUCTION

The phenomenon of residual force enhancement (rFE) is generally accepted to be part of the human muscle function. Furthermore, this increased force after active lengthening compared to purely isometric muscle action was found across all structural levels from muscle fiber to in vivo multi-joint leg extensions [1]. Nevertheless, several studies reported non-responder behaviour for voluntary human stretch-contractions, meaning that not all subjects showed increased residual forces after lengthening compared to isometric reference contractions [1]. The question arises, if this is related to individual's structural muscle function, or merely due to insufficient voluntary control of eccentric and post-eccentric contractions. If so, we were additionally interested in if being a non-responder changes after familiarization.

METHODS

11 subjects were invited to 5 consecutive sessions (at least 1 day rest between) to test their isometric and isometric-eccentric-isometric plantar flexion torque using a motor driven isokinetic dynamometer (IsoMed 2000, D&R Ferstl GmbH, Germany). On each test session, 3 maximum voluntary isometric (15° dorsi flexion) and 3 isometric-eccentric-isometric (10° plantar flexion - 15° dorsi flexion) contractions were performed and voluntary activation (VA) was tested using the twitch interpolation technique (supramaximal doublets). Additionally, the same contraction types were induced by means of tetanic electrical nerve stimulation (tibial nerve, ~50% [MVC]).

Data of torque, muscle activation and angular displacement were recorded (1kHz), and further processed by means of software (matlab R2019). Parameters of interest were peak eccentric torque at the end of stretch, steady-state isometric torque after lengthening and pure isometric reference torque, giving estimates for force enhancement (FE) and rFE during and after stretch, respectively. Repeated measures ANOVA (factors: voluntary vs stimulation; steps: 1st and last test session) was used to identify differences in rFE between voluntary and electrical muscle activation at beginning and end of 5 familiarization sessions. Students ttests were used to identify differences in muscle activation and VA between isometric and stretch-contractions.

RESULTS AND DISCUSSION

Abstract results are based on n=7 subjects due to ongoing data collection. For electrical stimulation, all tested subjects showed significant FE and rFE at begin and end of familiarization. There was no significant FE and rFE for voluntary activation trials independent of 1st or last session. We did not see differences in normalized EMG and VA between trials and sessions in respective steady-state phases.

From a muscle structural point of view, the results clearly show that none of our subjects can be considered a non-responder to stretch-induced FE and rFE. At 1st and last session, electrical stimulation led to significantly enhanced toque of about 15%.

Therefore, it seems self-evident that neural mechanisms cause changes in responses to stretch [2, 3]. However, we did not see differences in VA and muscle activation in steady-state phases after stretch. There might be inhibitory mechanisms counteracting eccentric maximum torque generation that explain most of the results, as we found huge differences in normalized peak torques at the end of stretch.
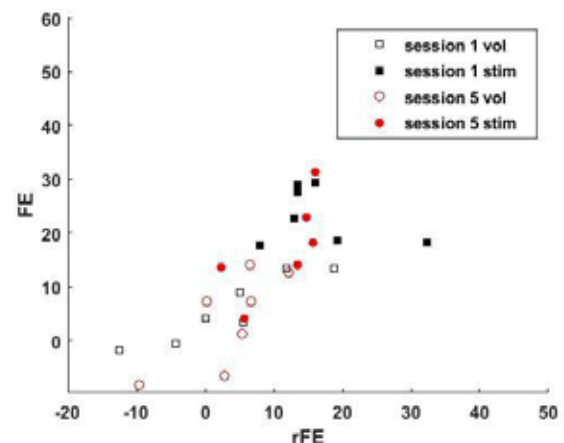
Figure 1: Relation of voluntary (vol) and stimulated (stim) Force enhancement (FE) at the end of stretch and after stretch (rFE) at 1st and 5th session.

In vivo rFE is highly accepted in literature and there seems no doubt that rFE is part of human muscle function. In contrast, our work shows that this might only be the case if there is artificial muscle activation. Even after 5 sessions of familiarization, not all subjects could show rFE. Further, rFE during voluntary contractions never reached comparable levels as seen in stimulated stretch trials. This seems to be directly related (r=.83) to the torque generated in the lengthening phase (Figure 1) where FE and rFE mechanisms a thought to be triggered. To conclude, even after 5 sessions voluntary eccentric contractions not always led to FE during stretch, and thus, did not result in rFE.

REFERENCES

[1] Seiberl W, et al. (2015). *J Electromyogr Kinesiol* ,**4**:571–80.

[2] Hahn D, et al. (2012). *PloS one* ,**11**:e49907.

[3] Sypkes CT, et al. (2018). *PeerJ*:e5421.

79

INFLUENCE OF NMES FREQUENCY AND WAVEFORM ON TORQUE PRODUCTION, STIMULATION EFFICIENCY AND DISCOMFORT IN HEALTHY SUBJECTS

[1]Rodrigo Rabello da Silva, [1]Matias Fröhlich, [2]Danton Pereira da Silva Júnior, [2]Paulo Roberto Stefanni Sanches, [1]Graciele Sbruzzi, [3]Nicola Angelo Maffiuletti, **[1]Marco Aurélio Vaz**

[1] Laboratório de Pesquisa do Exercício, Escola de Educação Física, Fisioterapia e Dança, Universidade Federal do Rio Grande do Sul, Porto Alegre, RS, Brasil, [2] Departamento de Engenharia Biomédica, Hospital de Clínicas de Porto Alegre, Porto Alegre, RS, Brasil, [3]Human Performance Laboratory, Schulthess Clinic, Zurich, Switzerland

Corresponding author: marco.vaz@ufrgs.br

INTRODUCTION

Neuromuscular Electrical Stimulation (NMES) is a widely used technique, especially for the purpose of muscle strengthening and rehabilitation [1,2,3]. NMES parameters have a great influence on torque production, stimulation efficiency and perceived discomfort during muscle stimulation [4]. However, it is not clear how NMES frequency and waveform affect these parameters.

METHODS

Twenty-four healthy male subjects volunteered for the study. Participants were positioned on an isokinetic dynamometer, and their knee extensors were stimulated using a combination of three frequencies (60, 80 and 100 Hz) and two waveforms (symmetrical - S and asymmetrical - A) at two intensity levels (20% of maximal voluntary isometric contraction - $NMES_{20\%}$, and maximum tolerated intensity - $NMES_{MAX}$). Current intensity, evoked torque, stimulation efficiency (evoked torque/current intensity) [5] and discomfort were compared between all parameters' combinations. A repeated measures two-way (factors: frequency and waveform) ANOVA with a Bonferroni post hoc test were used to identify specific differences ($p<0.05$). Effect sizes (ES, Cohen's "d") were calculated to assess the magnitude of the differences, and were classified as small if =0.2, medium if =0.5 and large if ≥ 0.8 [6].

RESULTS AND DISCUSSION

At $NMES_{20\%}$, 80 Hz showed higher stimulation efficiency than 60 Hz ($p=0.003$), while the S waveform showed higher stimulation efficiency than A at all frequencies ($p=0.003$; ES=0.44-0.54) (Figure 1). At $NMES_{MAX}$, the A waveform showed a higher current intensity ($p<0.001$; ES=0.25-0.52), but a lower evoked torque ($p=0.036$; ES=0.26-0.37) and lower stimulation efficiency ($p=0.001$; ES=0.58-0.67) than the S waveform (Figure 1). Discomfort was similar for all conditions at both $NMES_{20\%}$ ($p>0.134$) and $NMES_{MAX}$ ($p>0.614$).

Despite the similarity in discomfort, the S waveform showed higher stimulation efficiency, producing more torque with a lower current intensity. The negative triangular phase of A seems to reduce muscle force production. A frequency of 80 Hz seems to be more efficient at lower stimulation intensities, but no difference between NMES frequencies was found for stimulation efficiency at the maximum tolerated current intensity.
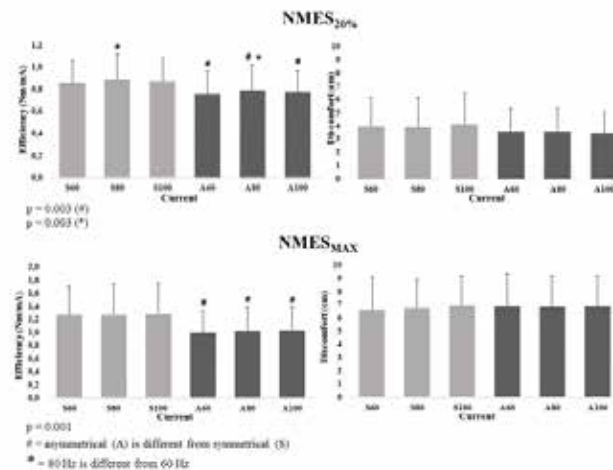
Figure 1: Mean (SD) values for stimulation efficiency and discomfort for $NMES_{20\%}$ and $NMES_{MAX}$. Stimulation frequencies = 60, 80, 100 Hz; S = Symmetrical waveform; A = Asymmetrical waveform.

REFERENCES

[1] Maffiuletti NA (2010). *Eur J Appl Physiol,* **110**:223-234.
[2] Maffiuletti et al. (2011). *Eur J Appl Physiol*, **111**:2391-2397.
[3] Salvini et al. (2012). *Rev Bras Fisioter*, **16**:175-83.
[4] Robinson AJ & Snyder-Mackler L (2008). *Clinical Electrophysiology : Electrotherapy and Electrophysiologic Testing*. Wolters Kluwer Health /Lippincott Williams & Wilkins, Philadelphia.
[5] Lieber & Kelly (1991). Phys Ther, **71**: 725-723.
[6] Cohen J (1988). *Statistical Power Analysis for the Behavioral Sciences*, Erlbaum, Hilllsdale, NJ.

ACKNOWLEDGEMENTS

Adaptations in intermuscular coordination of the triceps surae muscles in people with haemophilic arthropathy

Carlos Cruz-Montecinos [1,2,3], Sofia Pérez-Alenda [1], Mauricio Cerda [4], Huub Maas [2].
1. Department of Physiotherapy, University of Valencia, Valencia, Spain.
2. Department of Human Movement Sciences, Vrije Universiteit Amsterdam, Amsterdam, Netherlands.
3. Laboratory of Clinical Biomechanics, Department of Physical Therapy, University of Chile, Santiago, Chile.
4. SCIAN-Lab, Programme of Anatomy and Developmental Biology, ICBM, University of Chile, Santiago, Chile
Email: carcruz2@alumni.uv.es

INTRODUCTION

Haemophilic arthropathy is the result of repetitive intra-articular bleeding and synovial inflammation, resulting in severe joint damage. In people with haemophilic arthropathy (PWHA), the knee and ankle joints are commonly affected. This is accompanied by a reduced range the motion, muscle size, muscle force capacity and tendon stiffness, as well as impaired proprioception and altered neuromuscular control [1,2,3,4]. However, little is known about the coordination between synergistic muscles. In a recent study on rats, a shift from preferential recruitment of soleus (SOL) muscle to preferential recruitment of gastrocnemius (GA) muscle during locomotion in response to increased stiffness of intermuscular connective tissues was reported [5]. Intra-articular and intra-/intermuscular bleedings in PWHA may result in scar tissue formation and, hence, intermuscular connectivity [4,6]. The aim of this study was to compare the EMG activity patterns of triceps surae muscles between PWHA and healthy controls during gait at the same velocity. The hypothesis of this study was that the intermuscular coordination of triceps surae muscles during gait in PHWA is different than that in controls.

METHODS

Thirteen control subjects (CG) and fourteen PWHA walked overground on a 30 m walkway at the same velocity (1 m/s) twice. The inclusion criteria for PWHA were: positive radiological signs of haemophilic arthropathy (in knee and/or ankle), over 18 years of age and under 45 years and passive range of motion of the knee > 60 degrees and > 20 degrees in the ankle.

To assess the neural drive to the triceps surae muscles, surface electromyography (EMG) signals were collected from: Medial Gastrocnemius (MG), Lateral Gastrocnemius (LG) and Soleus (SOL). In each subject, a total of twenty cycles were used for the analysis. First, a bandpass filter (20-500 Hz, Butterworth, fifth order) was applied. To assess EMG amplitudes, the EMG signals were rectified by Hilbert-transform and smoothened by a moving average of 350 ms. To determine the amplitude ratio between synergistic muscles, the envelope of muscle activation averaged over time-normalized strides was used [5]. The amplitude ratio between pairs of muscles (SO-LG, SO-MG, and LG-MG) was calculated through the slope of the EMG-EMG loop during the stance phase [5].

Two-way ANOVAs (muscle pairs × group) were performed. If a significant interaction was found between factors, post hoc t-tests with Bonferroni correction for multiple comparisons were applied. Cohen's (d $\geq$ 0.2, d $\geq$ 0.5, d $\geq$ 0.8) were calculated, to indicate small, moderate or large effects, respectively.

RESULTS AND DISCUSSION

Two-way ANOVA indicated a significant difference between groups ($p = 0.042$), but no significant difference for muscle pairs ($p = 0.247$) were found. A significant interaction between muscle pairs and group ($p < 0.001$) was found. Post-hoc comparisons revealed for PWHA compared the CG a lower slope for SOL-LG ($p = 0.029$) and a higher slope for LG-MG ($p<0.001$), but no significant difference for SOL-MG slope ($p = 0.052$).

These results are consistent with the above described previous study during locomotion in the rat [5]. The lower slope in PWHA between SOL-MG could be interpreted as an adaptation of locomotor neural drive in response to enhanced intermuscular connectivity between the triceps surae muscles [5]. If the connectivity between SO and GA is changed in PWHA is currently unknown, but considering the fact that scar tissue is often formed after intramuscular bleedings [6], this appears likely.

These results suggest that connectivity between SOL and LG is enhanced in PWHA. It is possible that this neural adaptation is due newly formed connective tissues between SOL and GA, as a result of repetitive intramuscular bleeding [5,6,7]. Future studies are needed to confirm changes in the mechanical coupling between SOL and GA in PWHA.

Table 1: The amplitude ratio between two pairs of muscles. Abbreviation: Effect size (ES).

Pairs	CG	PWHA	p-value	ES
SOL-LG	1.20 (0.30)	0.99 (0.20)	0.026	0.83
SOL-MG	0.94 (0.16)	1.13 (0.31)	0.054	0.76
LG-MG	0.80 (0.10)	1.16 (0.32)	<0.001	1.49

REFERENCES

[1] Lafeber, F. et al (2008). Haemophilia, 14, 3-9.
[2] Hilberg, T. et al (2001). *Haemophilia*, 7, 582-588.
[3] Cruz-Montecinos, C et al (2019). *Haemophilia*. 2019; 25: e69– e77.
[4] Cruz-Montecinos, C et al (2019). *Haemophilia*, 25, e27-e29.
[5] Bernabei, M et al (2017). *Journal of neurophysiology,* 118, 1677-1689.
[6] Ribbans et al (1999) *Haemophilia*, 5, 46-52
[7] Maas, H et al (2018). *Exerc Sport Sci Rev*, 46, 26-33

Muscular and Non-Muscular Contraction in the Mammalian Diaphragm

[1]**Robert I. Griffiths**, [1]Ziad Abusara, [1]Venus Joumaa, [2]Philip J. Berger, [1]Timothy R Leonard, [3,1]Salvatore Federico.
[1]Faculty of Kinesiology, The University of Calgary, Calgary, AB, Canada
[2]Hudson Institute of Medical Research, Monash University, Clayton, VIC, Australia
[3]Mechanical and Manufacturing Engineering, The University of Calgary, Calgary, AB, Canada
corresponding author: Robert.Griffiths@UCalgary.CA

SUMMARY

The Costal muscle and the elastin rich, highly biaxial diaphragmatic ligament are in parallel on the mammalian diaphragm and both tissues can contribute to ventilatory forces and shortening.

INTRODUCTION

Our aim was to investigate these two parallel structures of the diaphragm in order to understand how they each contribute to diaphragm shortening and lung inflation.

METHODS

Costal muscle sarcomere length was calculated with the lungs at functional residual capacity (FRC) to provide Length at Functional Residual Capacity (LFRC) in four species: Sheep, Horse, Rabbit and Kangaroo with n=5 for each species.

Freshly killed specimens were placed supine with the thorax intact and the diaphragm exposed from the abdominal surface. Costal muscle fascicle lengths were measured directly with silk suture placed along fascicles and then measured with callipers. Fascicles were removed and placed fresh on a confocal microscope. The average sarcomere length over 20 sarcomeres was measured at 5 locations along the fascicle. Total number of sarcomeres in a fascicle was determined by dividing fascicle length by average sarcomere length. Measures of fascicle length at FRC were then divided by number of sarcomeres to give average sarcomere length at LFRC.

RESULTS AND DISCUSSION

The costal muscle of the diaphragm begins all contractions in quiet breathing starting with the lungs at FRC at a long sarcomere length of;

Sheep	$3.5\mu m \pm 0.16$
Horse	$3.2\mu m \pm 0.18$
Rabbit	$3.1\mu m \pm 0.08$
Kangaroo	$3.2\mu m \pm 0.29$

During physical exertion the lungs start at Residual Volume, which is less than FRC. This necessitates that the costal muscle will be stretched to even longer length before starting contraction, by active exhalation using **internal** intercostal muscles which compress the chest wall.

The muscle becomes intrinsically stronger during the breath as it shortens up the descending limb of the L:T curve. Lung volume during inspiration is inversely proportional to intrapleural pressure, which means that volume increases as intrapleural pressure becomes more negative.

The costal muscle must both shorten and produce greater force at the same time in order to further inflate the lungs.
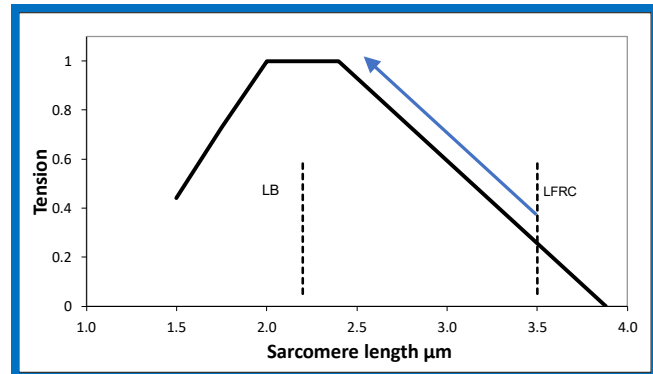

Figure 1: Sheep sarcomere length change during inspiration starting at LFRC.

The sarcomere L:T curve (Figure 1) predicts that maximal inspiration would have to stop as soon as the muscle reached the L:T plateau. However, we also need to consider the inspiratory action of the passive diaphragmatic ligament on the thoracic surface of the costal muscle. This ligament provides the pressure barrier between the thorax and abdomen as well as setting LFRC in the costal muscle as its elasticity matches the elastic recoil in the lungs [1].

The diaphragmatic ligament is highly biaxial [2] and redirects active force from the **external** intercostal muscles, that are expanding the chest wall, into passive force in the shortening direction of the fibres of the costal muscle which are perpendicular to the expansion.

Functionally, mammals can breathe quietly using costal muscle alone, or deeply by adding external intercostal breathing where the rib cage expands. Expanding the rib cage will stretch the diaphragmatic ligament perpendicular to the costal muscle fibres, and result in increased force and shortening in parallel with those muscle fibres.

We propose that the passive properties of the diaphragmatic ligament will provide the force differential above the plateau of the LT curve to enable further inflation of the lungs.

ACKNOWLEDGEMENTS

REFERENCES

[1] Griffiths,R.I. et al. (1992) *Proc.R.Soc.Lond.B,* **249**: 199-204.
[2] Griffiths,R.I. et al. (2018). *8th WCB* P4052

Force-Frequency Relationship during Fatiguing Contractions of Rat Medial Gastrocnemius Muscle

[1]**Brian R. MacIntosh,** [2]Anders M. Kristensen, [3]Andrea N. Devrome and [1]Keenan B. MacDougal
[1]Faculty of Kinesiology, University of Calgary, Calgary, Alberta, Canada
[2]Dept Public Health, Aarhus University, Aarhus C, Denmark
[3]School of Medicine, University of Calgary, Calgary, Alberta, Canada
Corresponding Author: brian.macintosh@ucalgary.ca

INTRODUCTION

Intermittent contractions causing skeletal muscle fatigue change the expression of fundamental contractile properties including: force-velocity, force-length, force-pCa^{2+} and force-frequency relationships. Our awareness of the changes in the force-frequency relationship is primarily based on measurements obtained during recovery following fatiguing contractions. During recovery, impairments of low-frequency contractions predominate this relationship. Maximal force impairment is limited or absent [1].

However, we have little knowledge of the changes in the force-frequency relationship during the contractions that are causing fatigue. This study addressed the question: what are the consequences of fatigue with respect to the force-frequency relationship during the time when fatigue is developing? Considering that fatigue results from both changes in $[Ca^{2+}]$ and Ca^{2+} sensitivity [2], it was hypothesized that low-frequency fatigue would be observed.

METHODS

The in situ rat medial gastrocnemius muscle was used for this study, with approval by the local Animal Care Committee. Rats were anesthetized with isoflurane (2%) and the left medial gastrocnemius muscle was surgically isolated and the Achilles tendon connected to an isometric force transducer. The sciatic nerve was cut and the distal stump was stimulated with supramaximal square pulses, 50 s in duration. All nerve branches to other muscles were cut so only the medial gastrocnemius muscle was contracting. The muscle was set at optimal length. A control force-frequency relationship was obtained with stimulation at: 20, 40, 60, 80, and 100 Hz.

Intermittent contractions were obtained at 50 Hz for 300 ms. Initially, contractions were every 4 s. Once a plateau in active force was achieved, the frequency was changed every few contractions to obtain contractions at the frequencies as above. This sequence was repeated during contractions every 2 s and every s. In this way, force-frequency data were obtained at 3 levels of fatigue and after 30 min of recovery.

RESULTS AND DISCUSSION

Active force decreased to a relatively constant level at each of the fatiguing frequencies of activation to 69±17, 38±13 and 28±10 % of initial active force (mean±SD). Therefore, the force-frequency curves obtained represent different levels of fatigue while the fatiguing contractions continued. The force-frequency curves obtained during intermittent contractions are illustrated in Figure 1. Active force actually decreased more at high frequencies of stimulation than at low frequencies. This is more clearly illustrated in Figure 2 where active force is expressed relative to the control value.
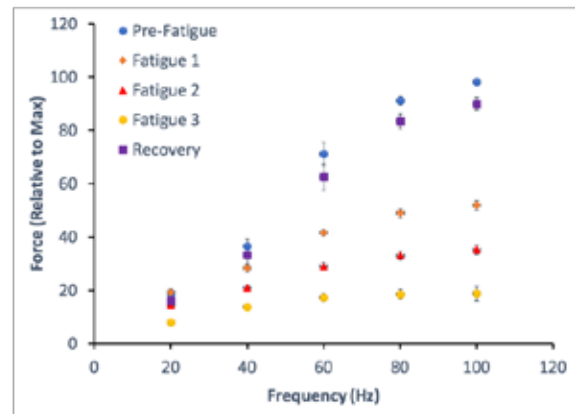
Figure 1: Force-frequency relationship for control, 3 levels of fatigue and after 30 min of recovery. Mean ± SEM.
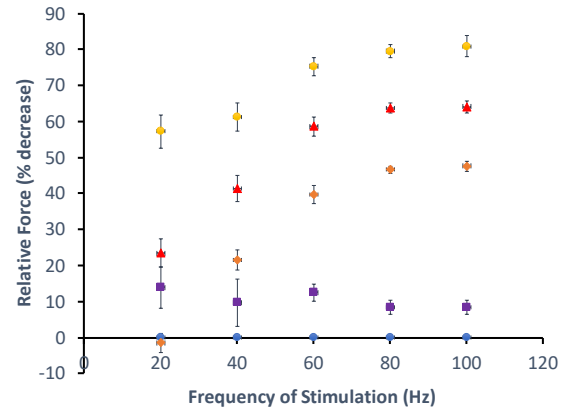
Figure 2: Active force expressed as % decrease: (initial-steady state)/initial *100. Note that active force decreased more at low frequencies than at high frequencies at any level of fatigue. Symbols are as Fig 1. Mean ± SEM

In contrast with recovery, where force is impaired more at low frequencies than with high frequency stimulation, force during fatiguing contractions is impaired more at high frequencies than at low frequencies. Potential mechanisms include decreased force per cross-bridge in conjunction with regulatory light chain phosphorylation.

ACKNOWLEDGEMENTS

REFERENCES

[1] Devrome, AN et al. (2007). J. Appl. Physiol. 102: 2294-2300.
[2] Glass, L. et al. (2018) Pflügers Archiv 470: 1243-1254.

83

rMMs

Protective effect of moderate exercise and prebiotic fibre supplementation on vastus lateralis muscle in a rat model of obesity

[1] **Jaqueline L. Rios**, [1]Venus Joumaa, [1]John Michaiel1, [1]Raylene A. Reimer, [1]David A. Hart, [1]Walter Herzog
[1]Faculty of Kinesiology, University of Calgary, Calgary, AB, Canada
corresponding author: jaquelinelourdes.rio@ucalgary.ca

INTRODUCTION

Using a Sprague-Dawley rat model, it has been shown that a high-fat/high-sucrose (HFS) diet-induced obesity leads to infiltration of fat, collagen, and macrophages cells into skeletal muscles within 12 weeks [1]. Prebiotic fibre supplementation and aerobic exercise are thought to prevent changes normally observed with obesity [2]. However, it is not known whether obesity, and associated morphological changes in skeletal muscles, affect the contractile properties of muscles at the level of the muscle fiber, and if prebiotic fibre supplementation and moderate aerobic exercise can mitigate these morphological changes and prevent contractile impairment.

Therefore, the purpose of this study was to determine the effects of a HFS diet on muscle integrity and the contractile properties of single muscle fibers, and whether prebiotic fibre supplementation and moderate aerobic exercise can mitigate the deleterious effects typically observed with obesity in this pre-clinical model.

We hypothesize that prebiotic fibre supplementation and moderate aerobic exercise regime prevent muscle morphological changes and contractile impairment.

METHODS

Twelve-week-old male Sprague-Dawley rats fed a HFS diet (40% fat, 45% sucrose) were randomized into a sedentary group (n=12), or a HFS diet combined with prebiotic fibre supplementation (10% oligofructose; n=12), or a moderate aerobic exercise group (progressive treadmill training for 30 min, five days per week; n=12) [2]. Eight chow-fed, age-matched animals, were included as lean controls.

Following the 12-week intervention period, vastus lateralis (VL) muscles were harvested. Single skinned VL muscle fibers were isolated and tested for maximal active isometric stress, unloaded shortening velocity (V0) and calcium sensitivity at a mean sarcomere length of 2.4µm. A colorimetric assay was performed to quantify triglyceride content in VL, and histological sections were stained with Picrosirius Red for quantifying intramuscular collagen content. Immunostaining for CD68+ cells was performed for quantifying macrophage density. Kruskal-Wallis testing was performed using Mann-Whitney post hoc testing to determine differences in outcome variables between groups ($\alpha \leq 0.05$).

RESULTS AND DISCUSSION

Animals in the HFS group showed a reduction in single muscle fiber maximal active isometric stress, and no changes in V0 and calcium sensitivity at an average sarcomere length of 2.4µm compared to chow group rats. Intramuscular triglycerides, collagen, and CD68+ cells were increased in the HFS group animals compared to the chow-fed animals (Figure 1).

Prebiotic fibre supplementation, but not moderate aerobic exercise, prevented the loss in muscle fiber maximal isometric stress. (Figure. 1). Prebiotic fibre supplementation and aerobic exercise prevented the increase in collagen deposition and CD68+ cells seen in HFS rats but did not prevent increases in intramuscular triglycerides in VL.

Diet-induced obesity leads to degenerative changes in muscle structure and impedes force production. The reduction in force in HFS muscle fibers cannot be explained by fat accumulation in the muscle fibers since prebiotic fibre supplementation effectively prevented force reduction without affecting the fat content in VL.

Prebiotic fibre supplementation and moderate aerobic exercise were effective in preventing muscle fibrosis and inflammation (CD68+ cells), factors known to have a detrimental effect on muscle [3]. Muscles have a high capacity to store and utilize fat, and fat accumulation in muscles might point to important adaptations to dietary lipid/carbohydrate overload.
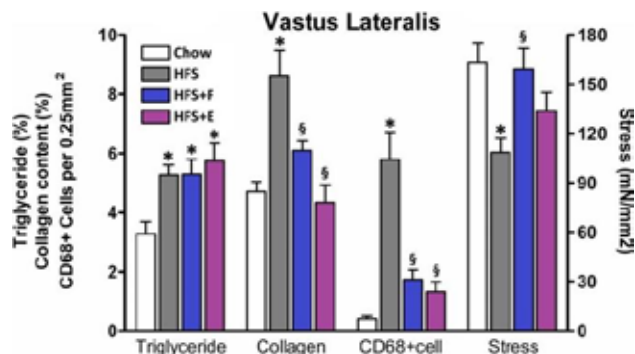
Figure 1: Mean (± 1SEM) VL triglyceride, collagen and macrophage content, and single muscle fiber maximal active stress. * indicates difference from chow group. § indicates difference from HFS group.

In conclusion, a HFS diet led to degenerative changes in muscle structure and reduced muscle force capacity. Prebiotic fibre supplementation and moderate aerobic exercise prevented collagen and macrophage infiltration, but did not prevent fat accumulation in VL, suggesting that increases in muscular fat may be an adaptive response to the HFS diet.

ACKNOWLEDGEMENTS

REFERENCES

[1] Collins KH et al. (2016). *J Orthop Res*, **34**: 2069-2078.
[2] Rios JL et al. (2019). *Sci Rep*, **9:** 3893.
[3] Mann CJ et al. (2011). *Skelet Muscle*, **1:** 1-21.

84

Supraspinatus tendon changes with repetitive wheelchair propulsion are associated with fatigue, sex, and body weight

[1,2]Fransiska M. Bossuyt, [3,4]Michael L. Boninger, [5,6]Ann Cools, [1,2]Ursina Arnet
[1,2]Swiss Paraplegic Research and University of Luzern, Lucerne, Switzerland
[3,4]Department of Veterans affairs and University of Pittsburgh, Pittsburgh, PA, USA
[5,6]University of Ghent, Ghent, Belgium and University of Copenhagen, Copenhagen, Denmark
Email: Fransiska.Bossuyt@paraplegie.ch

INTRODUCTION

The supraspinatus tendon is among the most common structures subject to subacromial impingement, tendon degeneration and pain in wheelchair users [1]. The supraspinatus, which is highly active and prone to fatigue during wheelchair propulsion, counteracts the activity of the pectoralis during the push phase and externally rotates the shoulder to bring the hand back during the recovery phase [2]. Changes in the tendon with repetitive activity provides information about the etiology of tendon degeneration.

The aims are to identify changes in the supraspinatus tendon after repetitive wheelchair propulsion and to determine the association with susceptibility to fatigue, the acromio-humeral distance (AHD), subject- and injury characteristics.

METHODS

This quasi-experimental study, with a pre-test post-test design, includes 50 wheelchair users with spinal cord injury (78% males, 50.5 ± 9.7 years of age, 26.6 ± 11.6 years since injury, 78% incomplete lesion). All participants performed a propulsion task of 15 minutes propelling as fast as possible along a figure 8-shaped course including complete stops and rest periods. Before and after the propulsion task, quantitative ultrasound protocols of the supraspinatus tendon were used to define tendon thickness (average distance in mm between top and bottom border of the tendon), echogenicity ratio (mean pixel grayscale of the tendon divided by mean pixel grayscale of the muscle above the tendon), and contrast (intensity difference between a pixel and its neighbour in the vertical direction perpendicular to expected direction of collagen fibres) from the region of interest (Figure 1) [3]. The dependent variables are the changes in tendon characteristics (post result – pre result). Co-variables include fatigue, defined by a significant increase in perceived fatigue (rate of perceived exertion) and performance (heart rate) after the task [4], sex, the AHD defined with ultrasound during 0° abduction and 90° elbow flexion [5], activity level defined with the physical activity scale for individuals with physical disabilities, time since injury, and body weight. Linear regression analyses were used to address the research questions ($\alpha=0.05$).

Figure 1: Transverse ultrasound image of supraspinatus tendon with region of interest between red vertical lines, selected based on the interference pattern ( ) from a metal marker taped to the skin.

RESULTS AND DISCUSSION

There was a significant reduction in supraspinatus tendon thickness after the propulsion task when controlling for all co-variables ($p = 0.003$; $B_0 = -1.39$ mm, SE = 0.44, 95% CI [-2.27;-0.51]). This may be caused by alignment and increased density of collagen fibres or creep. From all participants, 25 were identified as being fatigued. While fatigue did not affect the change in tendon thickness after the propulsion task in males, fatigued females had a greater reduction after the propulsion task as compared to those who did not fatigue (Figure 1) ($p = 0.044$). Also, persons who were heavier displayed a greater increase in tendon thickness after the propulsion task ($p = 0.019$; B = 0.01, SE = 0.00, 95% CI: [0.00;0.02]). There were no significant changes in echogenicity ratio or contrast after the propulsion task, suggesting the task did not affect the fluid content or the organisation of the collagen fibres within the tendon respectively ($p > 0.05$).
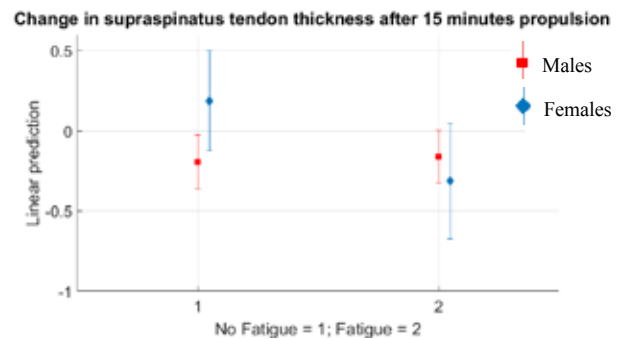
Figure 2: Predictive margins with 95% confidence intervals of change in supraspinatus tendon thickness in mm after 15 minutes propulsion. The interaction effect for fatigue (fatigued and not fatigued) and sex (male and female) is presented.

REFERENCES

[1] Brose SW et al. (2008). *Arch Phys Med Rehabil*, **89**: 2086-93.
[2] Mulroy SJ et al. (1996). *Arch Phys Med Rehabil*, **77**: 187-93.
[3] Collinger JL et al. (2010). *PM R*, **2**: 920-5.
[4] Enoka RM et al. (2016). *Med Sci Sports Exerc*, **48**: 2228-38.
[5] Mackenzie TA et al. (2016). *PM R*, **8** : 629-34.

85

A

Abbott, Emily M	46
Abusara, Ziad	82
Adkins, Amy N	53,62
Adler, Maya	24
Agten, Anouk	70
Ang, Shaun XT	77
Arlt, Anna	79
Arnet, Ursina	85

B

Bar-On, Lynn	57,65,68
Bell, Kaylyn M	33,37
Beller, Ronja	78
Berger, Philip J	82
Bernstein, Sanford I	33
Biewener, Andrew A	25
Binder-Markey, Benjamin I	47
Blemker, Silvia S	39,55
Blum, Kyle P	61,69
Boldt, Kevin	65
Bong, Sistania M	67
Boninger, Michael L	85
Bossuyt, Fransiska M	85
Broda, Nicole	47
Brandao, Maria Clara A	75
Brown, Stephen HM	40
Brynnel, Ambjorn	24

C

Campbell, Kenneth S	69
Cenni, F	64
Cerda, Mauricio	81
Cools, Ann	85
Cope, Timothy C	46,69
Corr, David T	36
Corvelyn, M	38
Costamagna, Domiziana	39,71
Costelli, Paola	71
Cruz-Montecinos, Carlos	81

D

Daley, Monica A	25
De Beukelaer, Nathalie	57,68
de Brito Fontana, Heiliane	50
de Campos, Daiani	50
De Groote, Friedl	67
Desloovere, Kaat	38,57,64,68
Devrome, Andrea N	83
Dewald, Julius PA	53,62
Duelen, Robin	71
Dutta, Samrat	30

E

Evangelidis, Pavlos	54,76

F

Federico, Salvatore	82
Franklin, David	31
Fröhlich, Matias	80
Fukutani, Atsuki	66

G

Gage, Matthew J	30
Garmirian, Lindsay	62
Gayan-Ramirez, G	38
Glasheen, Bernadette M	63
Gordon, Joanne C	25
Granzier, Henk	24
Griffiths, Robert I	82
Guo, Yiming	33

H

Hahn, Daniel	52,78
Han, Seong-won	32,50,64
Hanssen, Britta	57,64
Hart, David A	84
Hernandez, Yaeren	24
Herzog, W	28,31,32,34,41,50, 56,60,64,66,84
Hessel, Anthony L	29
Higuchi, Hideo	23
Hisada, Toshiaki	23
Hodson-Tole, Emma F	74
Holzer, Denis	79
Horslen, Brian C	69
Huang, Alice	33
Hwang, Yongtae	23

I

Ichinose, Hoshizora	76
Irving, Thomas C	29

J

Javidi, Mehrdad	49
Jinha, Azim	32
Joumaa, Venus	28,29,32,34,64,82,84

K

Kawakami, Yasuo	26,54,76
Kaya, Motoshi	23
Kiss, Balazs	24
Koppes, Ryan A	36
Knaus, Katherine R	55
Kristensen, Anders M	83
Kronert, William A	33

L

Lai, Adrian KM	74
Larkin-Kaiser, Kelly	34

86

Lee, Sabrina SM	44
Leonard, Timothy R	28,34,41,60,82
Lieber, Richard L	22,47
Lin, David C	45,49
Loya, Amy K	63

M

Maas, Huub	81
MacDougal, Keenan B	83
MacIntosh, Brian R	83
Maes, K	38
Maffiuletti, Nicola Angelo	80
Martino, Giovanni	67
Mazara, Nicole	40
McGowan, CP	45,49
McKay, J Lucas	67
Menegaldo, Luciano L	75
Michaiel, John	84
Millard, Matthew	31,60
Miller, Mark S	37
Mishra, Dhruv	29
Monroy, Jenna A	31
Moo, Eng Kuan	41
Murray, Wendy M	53,62

N

Naito, Munekazu	76
Nardelli, Paul	46,69
Nelson, Brent	30
Nelson, Christa M	62
Nishikawa, Kiisa C	29,30
Noonan, Alex M	40

O

Oldshue, Ashley H	61
Oliveira, Liliam F	75
Onasch, Franziska	57
Otsuka, Shun	26,54

P

Papgeorgiou, Eirini	64
Paternoster, Florian K	79
Peeters, Nicky	57,64
Penna, Fabio	71
Pereira da Silva Junior, Danton	80
Perez-Alenda, Sofia	81
Prinsen, S	38
Power, Geoffrey A	40
Punith, Laksh K	61

R

Rabello da Silva, Rodrigo	80
Raiteri, Brent J	52,78
Rao, Deepti	33
Reimer, Raylene R	84
Rios, Jaqueline Lourdes	84

S

Sahani, Rihani	39
Sampaolesi, Maurilio	37,71
Sawatsky, Andrew	50
Sawicki, Gregory S	46,61
Sbruzzi, Graciele	80
Schwaner, MJ	45
Seiberl, Wolfgang	79
Shan, Xiyao	26,54
Shibata, Shigenobu	76
Siebert, Tobias	48
Slosberg, Jared N	37
Smith, Ian C	56
Stefanni Sanches, Paulo Roberto	80
Stevens, S	70
Straight, Chad R	37
Swank, Douglas M	33,36,37,63

T

Tanaka, Fumiko	76
Tillin, Neale A	77
Timmermans, A	70
Ting, Lena H	61,66,68

V

Van Campenhout, Anja	38,57,64,68
Vandenabeele, F	70
van der Pijl, Robbert	24
Vaz, Marco Aurelio	80
Verbrugge, J	70

W

Washio, Takumi	23
Weersink, Erin	40

Y

Yamagishi, Takaki	54,76
Yang, Chi	54

Z

Zwambag, Derek P	40

rMMs

MEETING ROOM B

ANNOUNCER

OUTDOOR BALCONY

STAIR DN

LOBBY

WOMENS W/C

MENS W/C

STAIR DN

CAFÉ SOÚTH (below)

BALCONY

STAIR

BANQUET ROOM

STORAGE

PRE-FUNCTION AREA

ELEVATOR

WOMEN'S WASHROOM

MEN'S WASHROOM

KITCHEN

STAIR

MECHANICAL

OFFICE

OFFICE

STORAGE

STORAGE

STORAGE

JANITOR

NO PUBLIC ACCESS

MEETING ROOM A

UP

STAIR

NO PUBLIC ACCESS

MENS W/C

WOMENS W/C

OFFICE

OFFICE

ADMINISTRATION OFFICE

FIRST AID ROOM

MAINTENANCE

UP

STAIR

MAIN ENTRANCE

CAFÉ SOUTH

FIREPLACE

STAIR

EXTERIOR PATIO

CAFÉ NORTH

ELEVATOR

OFFICE

WOMEN'S WASHROOM

MEN'S WASHROOM

CAFE

KITCHEN

WOMEN'S WASHROOM SHOWER

STAIR
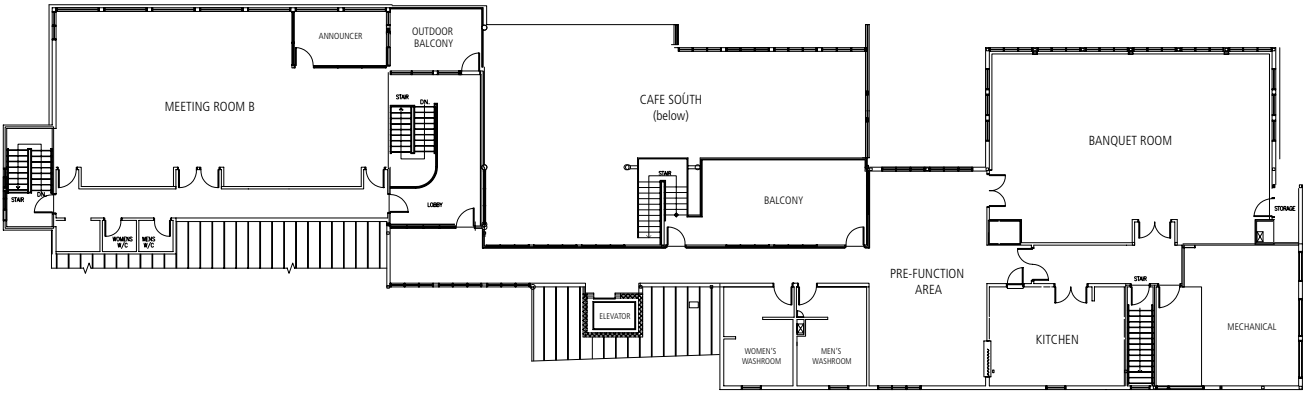
MEN'S WASHROOM SHOWER
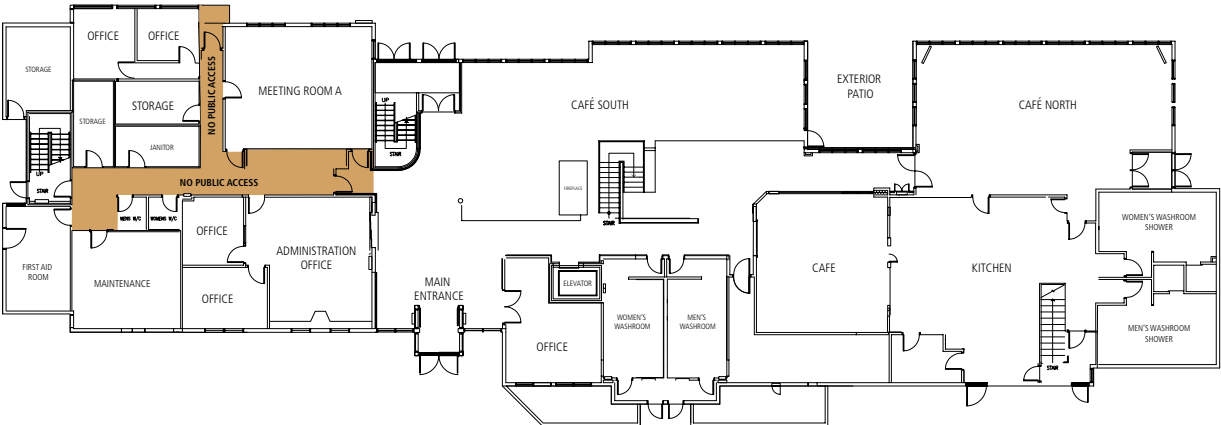
Schedule at a Glance

Time	Saturday, July 27	Sunday, July 28	Monday, July 29
08:00 - 08:24		Coffee	Coffee
08:24 - 10:00		Session: Molecular Muscle Mechanics	Session: Animal muscle function in vivo
10:00 - 10:30		Coffee Break	Coffee Break
10:30 - 11:30		Keynote Lecture	Keynote Lecture
11:30 - 12:42		Session Cellular Muscle Mechanics	Session: Human muscle function in vivo
12:42 - 14:00	Registration	Lunch	Lunch
14:00 - 15:00	Registration	Keynote Lecture	Keynote Lecture
15:00 - 16:30	Disc Golf at Canmore Nordic Centre / Free Time	Poster Session 1	Poster Session 2
16:30 - 17:00	Reception	Grassi Lakes Hike	Mountain Biking at Canmore Nordic Centre / Free Time
17:00 - 17:30	Keynote Lecture	Grassi Lakes Hike	Mountain Biking at Canmore Nordic Centre / Free Time
17:30 - 18:30		Grassi Lakes Hike	Mountain Biking at Canmore Nordic Centre / Free Time
18:30 - 19:00	Social	Dinner for Keynote & Invited Presenters	Social
19:00 - 19:30	Social	Dinner on your own	Social
19:30 - 20:00		Dinner on your own	Banquet Dinner
20:00 - 21:00			Banquet Dinner